(Annual Report) 2000-2001

1. Physiological Changes in Remote Action Experiment

Weizhong Chen, Hideyuki Kokubo, Hirotaka Nakamura, Masataka Tanaka, Suzue Haraguchi, Tong Zhang, Tomoko Kokado, Mikio Yamamoto, Kimiko Kawano [1] and Takao Souma[2]([1] Nippon Medical School, Tokyo, [2] Tokyo Metropolitan College)

***Keywords*:** *direct mental interaction with living system (DMILS), remote action, laogong point, skin temperature of palm, qi, to-ate*

In this experiment, which is one of a series of remote action experiments, two to-ate practitioners were placed in separate rooms with normal communication deprivated. We measured physiological changes of one of the two who acted as a Receiver, when the other who acted as a Sender, attempted to give "remote influence" to the Receiver at a distance. These subjects had shown statistically significant coincidences of the time of their apparent motions in previous similar experiments we had carried out.The Receiver was seated in an electromagnetic shielding cage and the Sender performed only one "sending" motion during each 80-second trial in double blinded and randomized conditions. The Receiver's skin temperature of the left palm was sampled at a rate of 200Hz by a thermistor. The Sender or Receiver pushed the switch of an event marker when they sent or received a qi of to-ate. The output signals were recorded as the sending time or the response time, along with EEG and other physiological data, by a recorder.We analyzed the Receiver's skin temperature changes [^{O}C] in the period of 10 seconds before and after sending /receiving time. The difference of sending and receiving time was within 10 seconds, and the average of the finite difference of skin temperature from -10.0 sec is shown in Fig.1. Trace B showed some fluctuations from -5 sec to +4 sec during receiving time (0 sec) that were considered due to pushing and wanting to push the event marker switch, while trace A also showed a fluctuations at five seconds before sending time.In conclusion, fluctuation of the Receiver's skin temperature during sending time was observed. We considered it to be caused by remote influences or the motion of pushing the switch since it was near the receiving time. But the analysis after that showed that the fluctuation during sending time was largely contributed by one trial.

Publications:

Chen, W., Kokubo, H., Nakamura, H., Tanaka, M., Haraguchi, S., Zhang, T., Kokado, T., Yamamoto, M., Kawano, K. and Souma, T.: *J. Intl. Soc. Life Info. Sci*., 19(1): 179- 186, 2001.

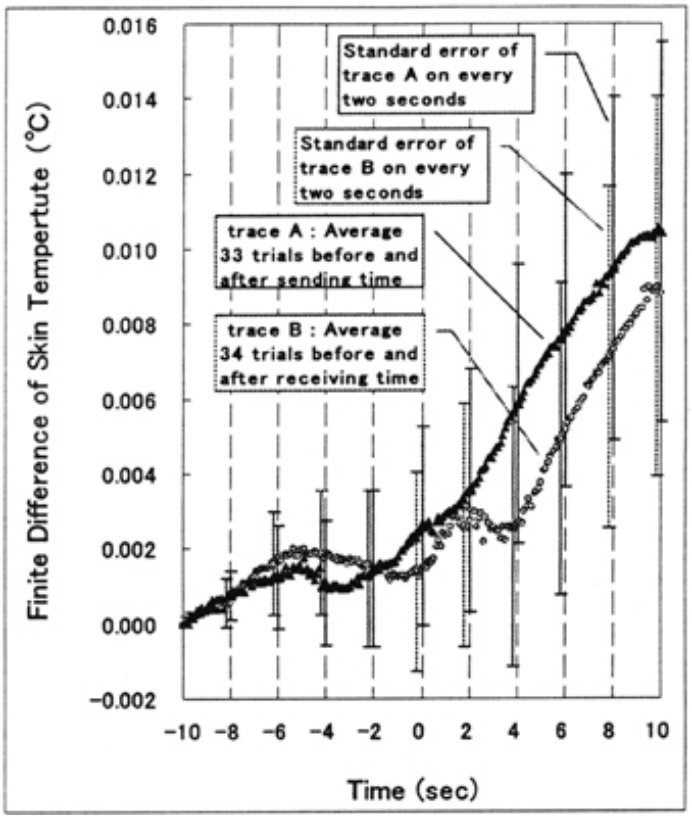

Fig.1. Finite difference of skin temperature change of receiver's left palm before and after (+10.0 sec) receiving

/sending time (0.0 sec)

2.Effects of External End-Shields for Positron Emission Tomography

Tomoyuki Hasegawa and Hideo Murayama

Keywords**:** *radiation shields, Monte Carlo simulation, positron emission tomography, nuclear medicine*

Radiation from outside the field-of-view of a PET system operating in the 3D data collection mode increases the single event count rates of the system, which produces an increase in the accidental count rate. These accidental coincidences can be measured and subtracted from the image data, however the process adds statistical noise to the data and causes deterioration in the quality of the images. The effectiveness of an end- shield depends on its diameter, thickness and composition, and the distribution of the sources of radiation.

The system employed in this work was an ECAT EXACT HR+ (CTI/Siemens produced), operating in the 3D data collection mode with the standard data collection parameters (span 9 and maximum ring difference 21). Each end-shield was a circular slab of lead mounted on a steel plate for strength and rigidity. The sides employed were 10 or 20 mm thick lead, 3.2 or 6.4 mm thick steel, 300 or 350 mm inner diameter, and 550 mm outer diameter. The end-shield was mounted on the gantry just outside the first detector.

The standard uniform cylinder phantom (20 cm inner diameter and 18.5 cm inner length) containing ^{18}F dissolved in water was placed 34 cm from the center of the axial field-of-view of the scanner. By using the Monte Carlo code based on GEANT 3.21, the single event and accidental count rates were obtained. 100 million events were simulated for each condition under study. It was confirmed that the simulated sensitivity and scatter fraction agreed with phantom measurement to be better than 5 %.

The measured accidental count rates versus the Monte Carlo results for each configuration are plotted in fig. 2. The lightest end-shield (t10-d350) reduced the accidental count rate to about 3 % of the count rate without end-shields (no e-sh). The rate was slightly better with the thicker end-shield of the same diameter (t20-d350). A somewhat larger drop in count rate was noted with the shield with the smaller inner diameter (t10-d300). These results indicate that 10 mm of shielding is adequate and that larger reductions in background are caused by blocking line-of-sight access of the radiation to the detector.

Physical measurements and Monte Carlo simulation results confirm that even relatively thin lead shielding can dramatically reduce the count rates for activity originating outside of field-of-view of the PET system. Users should be aware of the possibility that scatter in the shielding or support material can lead to significant background rates.

Publication:

Hasegawa, T., Michel, C., Kawashima, K., Murayama, H., Nakajima, T., Matsuura, H. and Wada, Y. : IEEE Trans. Nucl. Sci., 47, 1099-1103, 2000.

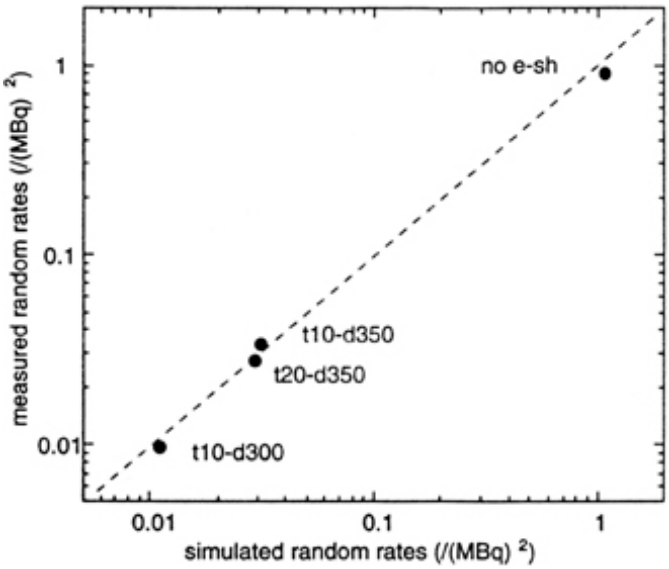

Fig.2. Measured random count rates in comparison with Monte Carlo calculations.

3.A Fast Algebraic Image Reconstruction Method for a Clinical PET Scanner

Taiga Yamaya, Takashi Obi*, Masahiro Yamaguchi*, Nagaaki Ohyama* and Hideo Murayama

(*Imaging Sci. & Eng. Lab., Tokyo Inst. of Tech.)

***Keywords*:** *image reconstruction, positron emission tomography (PET), nuclear medicine*

Algebraic reconstruction methods, such as natural pixel decomposition (NPD), have been successfully used to improve quality of positron emission tomography (PET) images by accurate modeling of the measurement system, while the conventional filtered backprojection (FBP) method is based on an inaccurate system model. These algebraic methods, however, require extensive computation since they deal with a large matrix of the same dimension as that of the measurement data.We proposed a fast image reconstruction method based on an algebraic technique using approximation and pre-processing. The proposed method estimates each element of the sampled image using a subset of measurement data, while conventional algebraic reconstruction methods use all the data. For each image point to be reconstructed, the subset contains the measurement data that contribute significantly to the image point.Consequently the dimension of the matrix becomes small, and operators to obtain the PET image directly from subsets of measurement data are pre-computed and stored for each image point. In addition, the constraint that ensures quantitative reconstruction, which NPD does not deal with, is easily installed in the proposed method because of the element-by-element implementation. Since image reconstruction in PET is usually an ill- conditioned inverse problem, the constraint effectively improves image quality. At this stage, we suppose that scatter coincidences, random coincidences and attenuation are corrected completely.After optimizing the size of the subset using numerical simulation, we applied the proposed method to experimental data for the ECAT EXACT HR+ (Siemens/CTI) scanner operating in 2D mode. The phantom, placed at the center of the scanner, consisted of a cylindrical vessel (200 mm in diameter and 190 mm in length) with 1.42 mCi ^{18}F activity water and two rods with water and air respectively. After the normalization and attenuation correction, the reconstructed images were obtained using the proposed method, NPD and FBP. Here the scatter correction was not implemented. Two FOMs, cold contrast recovery (cCR) and the normalized standard deviation (NSD), were used to evaluate the image quality. The trade-off between the NSD and the cCR is shown in Fig. 3, using the proposed method and NPD with different values of regularization parameters and FBP with a ramp filter of different cut-off frequencies. In order to evaluate the effect of the constraint, the proposed method with no constraint was also applied. We clearly see that the proposed method has a higher cCR value for any particular value of background noise level. The result also shows that the constraint corrects the contrast recovery loss caused by the selection of the measurement data. The averaged calculation time on an Alpha 500MHz PC to reconstruct one image slice using the proposed method is 4.7 sec., while NPD requires 28 min. and FBP requires 2.8 sec. The proposed method has an advantage in calculation time over NPD and has a similar time to FBP. In summary, our proposed method produces images with almost the same or superior quality to the conventional algebraic methods and has a similar computation time to FBP.

Publication:

Yamaya, T., Obi, T., Yamaguchi, M., Kita, K., Ohyama, N. and Murayama, H.: *IEEE Trans. Nucl. Sci.*, 47, 1670-1675, 2000.

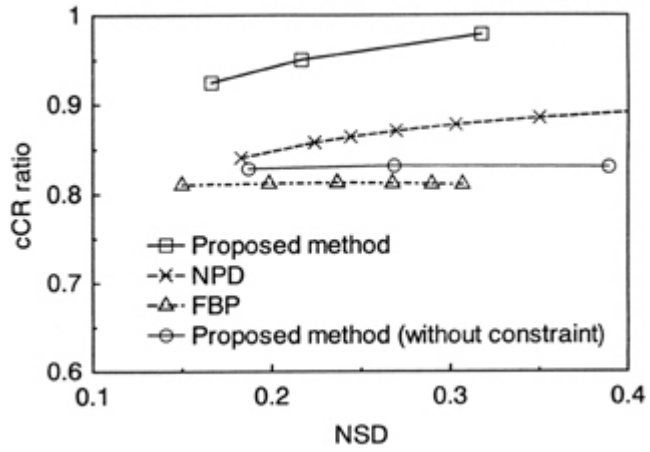

Fig.3. Graph showing the trade-off between background noise (NSD) and contrast (cCR) using real PET data.

4. Spot Scanning Using Radioactive ^{11}C Beams for Heavy-Ion Radiotherapy

Eriko Urakabe, Tatsuaki Kanai, Mitsutaka Kanazawa, Atsushi Kitagawa, Koji Noda, Takehiro Tomitani, Mitsuru Suda, Yasushi Iseki[1], Katsushi Hanawa[1], Kohsuke Sato[1], Munefumi Shimbo[2], Hideyuki Mizuno[3], Yoichi Hirata[4], Yasuyuki Futami[5], Yoshihisa Iwashita[6] and Akira Noda[6] ([1]Toshiba Co.; [2]Nat. Cancer Center; [3]Saitama Cancer Center; [4]AEC Co.; [5]Shizuoka Pref.; [6]Kyoto Univ.)

***Keywords*:** *spot scanning, heavy-ion radiotherapy, 3-D conformal irradiation, radioactive beam, positron emitter, momentum spread*

A scheme for therapeutic irradiation with ^{11}C beams has been developed in order to form and verify a three-dimensionally (3-D) conformal irradiation field for cancer radiotherapy. The stopping points of positron emitter, such as ^{11}C can be directly measured after irradiation using a positron emission tomography (PET). Yield of ^{11}C beams through projectile fragmentation process is less than 1% of the primary beams and is considerably low. We have adopted a spot scanning method, which provides high beam-utilization efficiency.

The spot scanning method at HIMAC uses no ridge filter, which is an insertion device controlling the momentum distribution, and supress the further growth of the beam size inducing the scattering at devices located in the beam line. This method adopts spot beams whose dose distributions are 3-D localized around their Bragg peak. The spot beam is scanned stepwise over the tumor region in the direction lateral to the beam by horizontal and vertical scanning magnets. In parallel to the beam direction, the range is adjusted by inserting PMMA plates (range shifter). Thus we can form a 3-D conformal irradiation field. One of the features of the scanning system is that the beam delivery is stopped during the transition time between spots for precise dosecontrol.

Produced ^{11}C beam has a momentum spread of a few %, and picking out its momentum can control the depth profile of spot beam. Since a wide momentum gives high beam intensity and a wide distal falloff, we compromised yield and momentum spread. The selected momentum spread between 97.5% and 99.5% gives a distal falloff of 3mm. The beam-utilization efficiency is 0.4% of the primary ^{12}C beam.

An irradiation field of 35 x 35 x 43 mm^3 was optimized and spot scanning using ^{11}C beams was carried out. The dose distribution was measured as shown in Fig. 4. by a multi-strip parallel-plate ionization chamber (MuSIC) and acrylic plates. The flatness of $\pm$ 2.3%, including an error of 1% in the detector resolution, could be obtained.

In spot scanning, it is essential to estimate the 3-D dose distribution of each spot beam. In contrast to the primary beam, estimating the dose distribution is complicated because of the wide momentum spread of ^{11}C beams. A spot beam with a wide momentum spread is considered to consist of monochromatic beam fractions of various momenta, which lead to various ranges in the human body. Each beam fraction has a different lateral beam size because of the chromatic aberration of the lens

system used in beam delivery. Based on a measurement of the beam size at each momentum, we estimate the lateral and depth-dose distributions of the spot beam. The reconstructed dose distribution of the irradiation field was in good agreement with the experimental results, i.e., within + 0.2%.

Publications:

Urakabe, E., Kanai, T., Kanazawa, M., Kitagawa, A., Noda, K., Tomitani, T., Suda, M., Iseki, Y., Hanawa, K., Satoh, K., Shimbo, M., Mizuno, H., Hirata, Y., Futami, Y., Iwashita, Y., and Noda, A.: *Jpn. J. App. Phys.*, 40, 2540-2548, 2001.

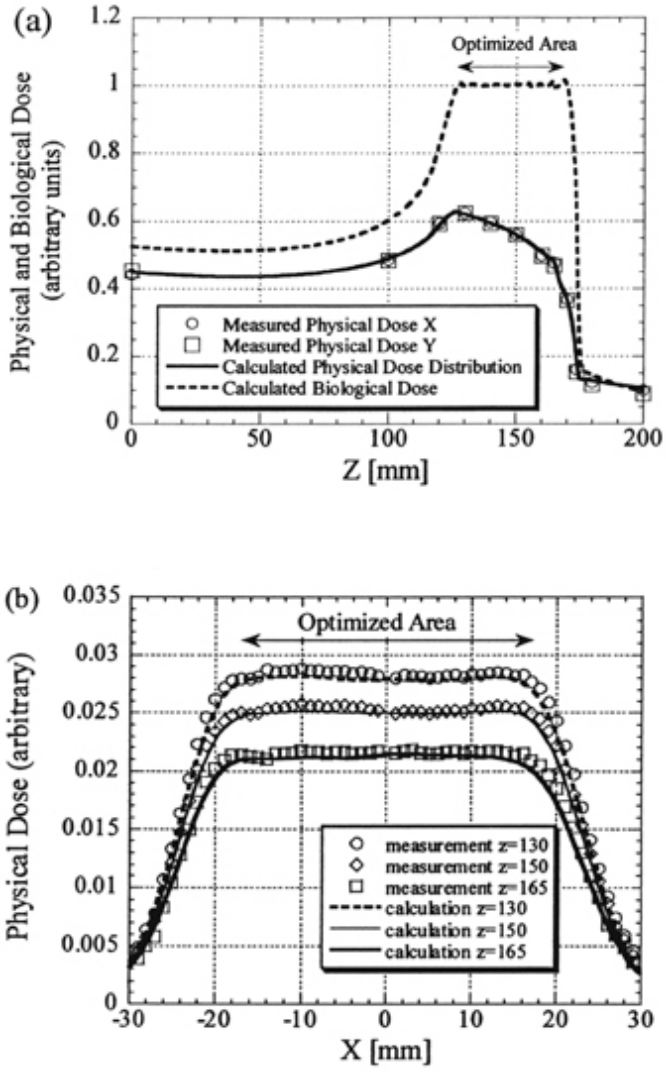

Fig.4. Dose distributions of the irradiation field. (a) Calculated physical and biological ones in the depth direction. Physical ones measured by the X and Y electrodes of MuSIC. (b) Physical one in the lateral directions measured at 0, 150 and 245 mm-depth in acrylic phantom by MuSIC.

5. First Observation of Ion Pumping Effects in a Pulsed Penning Source

Yukio Sato and Atsushi Kitagawa

***Keywords*:** *Penning source, ion pumping, low gas pressure, gas pulsing, multiply-charged ions*

It is empirically and theoretically known that a high yield of multiply-charged ions can be obtained under a low gas pressure in Penning sources (PIGISs). One of the main reasons for this is the long lifetime of fast electrons in the plasma, which allows the trapped ions to be highly ionized through a step-by-step ionization process. In the PIGIS of the HIMAC, the gas flow is not being pulsed, but there is a transient pressure response in the source when the arc is pulsed that permits the production of the high-charge state ions. This report describes the first observation of an ion pumping mechanism (gas pulsing phenomenon) in a pulsed PIGIS and its application to the production of multiply-charged ions for the heavy ion synchrotron (HIMAC) at NIRS.

Considering the low repetition cycle (< 1 Hz) and the short arc pulse width (< 10 ms) in the pulsed PIGIS, outgassing from the surface of the chimney may also be periodic. Since the temperature of the chimney is not high due to the low arc power (< 50 W on average) and direct water cooling, the adsorption of neutral atoms on the surface of the chimney during the long arc-off time (1 s) and the rapid desorption by pulsed discharge would be periodic in an equilibrium state under constant gas flow. It is thus possible to roughly predict an ion- pumping process according to the following (for the case of Ar): (1) The number of Ar atoms involved in the PIG chimney (volume,10 cm^3) is calculated to be 3.5x 10^{14} which corresponds to the initial atom density {*n(0)*}, when the average vacuum in the chimney is considered to be 1x10^{-3} Torr with a gas flow of 0.2 cm^3/min. (2) When the arc current (I_{arc}) is 5 A (typical value), the ion current (I_i) into the cathode is about 1.0 A, because around 20 % of I_{arc} is I_i. (3) Since the average charge state of Ar ions in the plasma is probably 2+ or more, I_i should be at least 3x10^{15} ions per 1.0 ms, suggesting that, in several ms, a large number of neutral atoms (10^{16} ions) including both *n(0)* and outgas is evacuated from the chimney by ion pumping. (4) On the other hand, the outgassing should dry up quickly due to such fast pumping, while the time constant of gas flow into the chimney is very long and is on the order of 100 ms based on a geometrical consideration.

(5) The neutral atom density {*n(t)*} in the chimney should therefore be rapidly decreased due to this fast ion pumping and the lack of gas supply. (6) In about 10 ms, *n(t)* becomes very small and the arc operation becomes unstable. (7) During the short time before such unstable operation, a high yield of Ar^{8+} can be obtained under a reasonably low gas pressure.

The estimated *n(t)* and the measured beam waveform (Ar^{8+}) are given in Fig.5, and this *n(t)* agreed basically with the vacuum pattern measured at the head of the pumping system. Thus an ion-pumping device originally equipped in a low-duty pulsed PIGIS has been observed. No additional apparatus was necessary, except pulsing the source. Compared with the cw PIGISs, this pulsed PIGIS could produce a high yield of Ar^{8+} ions by a factor of 100-1000 under a similar design and power (peak). As can be seen

in Fig.5, the beam waveform for multiply-charged ions was generally triangular. The best record for Ar^{8+} so far was 700 e A and its time width was on the order of ms, which is long enough for the injection time (100-200s) of the synchrotron.

Publications:

Sato, Y., Kitagawa, A., Miyata, T., Sakamoto, H. and Yamada, S.: *Nucl. Instrum. and Meth*., A450, 231-234, 2000.

Sato, Y., *et al*.: *Proc. 20th Int. Conf. Linac*, Monterey, CA, 654-656, 2000. 3) Miyata, T., et al.: *Rev. Sci. Instrum*., 71, 972-974, 2000.

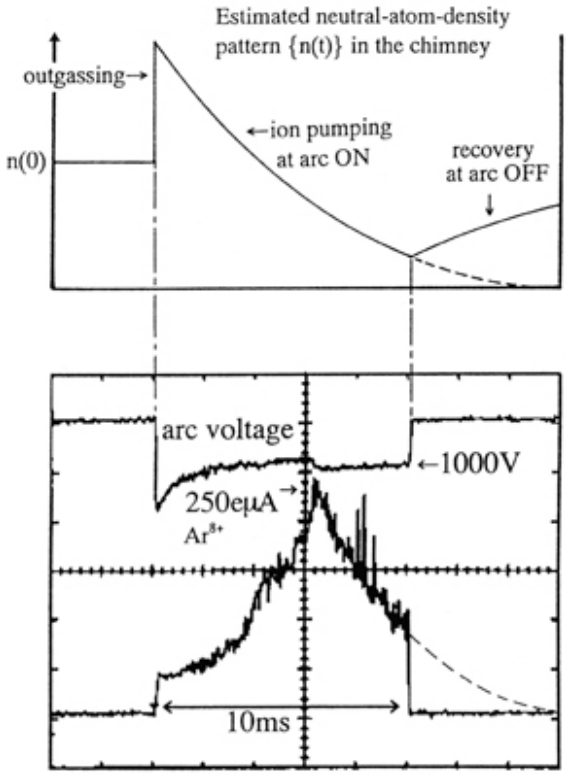

Fig.5. Measured pulse patterns of the arc voltage and typical beam waveform of Ar^{8+}, and the estimated neutral atom density {*n(t)*}. A rising time of outgassing was assumed to be similar to the speed of the plasma production (order of s), and seemed negligibly small in the time scale of the figure. The yield of Ar^{8+} gradually increased through a step-by-step ionization process and reached the maximum under a low gas pressure in 6-7 ms, then rapidly decreased due to a lack of neutral atoms.

6. Simultaneous Measurement of Coming Directions and Energies of Gamma-rays Using a Tandem Detector

Yoshiyuki Shirakawa

Keywords**:** *gamma-ray, NaI(Tl) scintillator, BGO scintillator, photomultiplier, photopeak, coming direction, energy*

A tandem detector, which positively raises directional dependence for coming gamma-rays, has been produced experimentally to measure directions and energies of coming gamma-rays simultaneously. In the tandem detector, a cylindrical NaI(Tl) scintillator, the same sized BGO scintillator, and a fitted photomultiplier tube are combined optically in this order. Since the lengths of crossing each scintillator are changed according to coming directions of gamma-rays, the directions can be recognized by counting photopeaks on a spectrum made by the NaI(Tl) and the BGO scintillators and by obtaining the ratio of photopeak counts.

This procedure is given by the form of

R = peak counts by BGO / those by NaI(Tl)= f (θ) (1)

where θ is a coming direction from 0 to 90 degrees.

Experiments were carried out using the tandem detector: (1) to confirm the measurement principle and (2) to the performance. A ^{137}Cs source of 3.7MBq was put in front 20cm of the detector (θ =0). Coming gamma-rays were counted for 60 seconds and the counting ratio was calculated from the spectrum (Fig.6) . The source was moved in10-degree intervals on the side of the detector through 90 degrees (θ =90). Then the similar experiments were repeated. Next, the experiments were repeated with the distances between the source and the detector as 30cm, 100cm and 200cm. From the results of the experiments, it was proven that the counting ratio R changed from approximately 1.7 to 3.0 when the direction θ was changed from 0 to 90 degrees. The relation between R and θ is expressed approximately by

$R(\theta) = (R(0)+R(90))/2 + (R(90)-R(0)) \sin(\theta)$ (2)

or obtained by the polynomial form of

$R(\theta) = 4x10^{-6}\ \theta^3 + 6x10^{-4}\ \theta^2 - 7.3x10^{-3}\ \theta + 1.69$ (3)

where Eq.(2) was derived using a sine form and Eq.(3) was given by a fitting method. This means that the coming direction can be decided when the counting ratio is known. At the same time, it was confirmed that the energy characteristics of the tandem detector were the same as those of conventional NaI(Tl) and BGO scintillators.

As a result, it has been shown that the tandem detector has a possibility of measuring the coming directions and the energies of gamma-rays simultaneously.

Publications:

1) Shirakawa, Y.: Radioisotopes, **50**, 4, 117-122, 2001.

2) Shirakawa, Y.: *JASP*, *Radiation Science*, **26**, 4 67-73 ,2000.

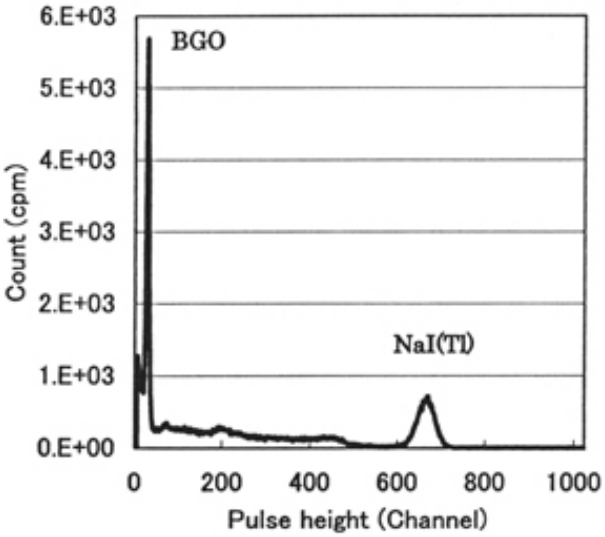

Fig.6. Typical spectrum of Cs-137 as recorded by the tandem detector (source-detector: 20cm, =0)

7. Phenolic Compounds Catalyze the Conversion of Singlet Oxygen into Hydroxyl Radical in the Presence of DMPO

Jun-ichi Ueda and Toshihiko Ozawa

Keywords**:** *singlet oxygen, spin trap, ESR, phenolic compounds*

The relationship between the activities of phenolic compounds to quench singlet oxygen ($^1O_2$) and their oxidation potentials was investigated by electron spin resonance (ESR) spectroscopic and cyclic voltammetric methods. $^1O_2$ was generated by UVA (> 330 nm)-irradiation of hematoporphyrin (HP) and detected as an oxidative product, 2,2,6,6-tetramethyl-4-piperidone-1-oxyl (TEMPON), of 2,2,6,6-tetramethyl-4- piperidone (TEMPD). Phenolic compounds used here were the following ten compounds: isoeugenol, *p*-eugenol, guaiacol, phenol, *p*-methoxyphenol, Trolox C, dopamine, 2,6-dimethoxyphenol, 4-hydroxybenzoic acid, and hydroquinone. The ESR measurements indicated that Trolox C quenched $^1O_2$ more than other phenolic compounds at physiological pH, whereas phenol and 4-hydroxybenzoic acid quenched it only slightly. Since the oxidation potential of Trolox C is lower than those of phenol and 4-hydroxybenzoic acid, these results suggested that quenching activity of phenolic compounds against $^1O_2$ was closely related to their oxidation potentials.

To investigate what kind of reactive oxygen species were generated during the reaction of $^1O_2$ with phenolic compounds, the compounds were added to this $^1O_2$- generating system in the presence of two spin traps 5,5-dimethyl-1-pyrroline *N*-oxide (DMPO) and the derivative 5-(diethoxyphosphoryl)-5-methyl-1-pyrroline *N*-oxide (DEPMPO), and the spin adducts of reactive oxygen species were measured by ESR. As a consequence, the formation of DMPO adduct of hydroxyl radical (˙OH) (DMPO/˙OH) was observed, whereas no DEPMPO/˙OH was produced. This result suggested that no phenolic compound used here reacted with $^1O_2$ to generate reactive oxygen species.

Furthermore, the relationship obtained between the amounts of DMPO/˙OH produced and oxidation potentials of phenolic compounds indicated that phenolic compounds with lower oxidation potentials may efficiently accelerate the conversion of $^1O_2$ to .OH compared to those with higher oxidation potentials, although the formation of DMPO/˙OH was dependent on the initial reaction of DMPO with $^1O_2$. On the other hand, in the absence of phenolic compounds, DMPOX was observed, and the signal intensity was dependent on both irradiation time and DMPO concentration.

8. Induction of Superoxide in Glioma Cell Line U87 Stimulated with Lipopolysaccharide and Interferon Gamma: ESR Using a New Flow-type Quartz Cuvette

Hidehiko Nakagawa, Nobuo Ikota, and Toshihiko Ozawa

Keywords**:** *superoxide, nitric oxide , U87 glioma cell, flow-type quartz cuvette, TEMPOL , lipopolysaccharide , interferon-*

Superoxide and nitric oxide are endogenous radical species, which are considered to play important roles not only in inflammation as protective factors, but also in signal transduction and in neurodegenerative diseases. Just like immune cells such as macrophages in peripheral tissues, glial cells in the brain are considered to play a role in protecting against infection and oxidative stress. The production of nitric oxide and superoxide is suggested to be induced by treatment with cytokines or endotoxic reagents in several glioma cell lines. However, there have been only a few attempts to measure the induction of superoxide and nitric oxide. In this study, the lines. However, there have been only a few attempts to measure the induction of superoxide and nitric oxide. In this study, the production of superoxide and nitric oxide induced in U87 glioma treated with lipopolysaccharide (LPS) and interferon- (IFN-) was examined by ESR spectroscopy using a newly designed flow-type quartz cuvette without detaching the cells from the culture plate (Fig. 7A,B). ESR spectra of 2,2,6,6-tetramethyl-4- hydroxy-1-piperidinyloxy (TEMPOL) with U87 cells on a quartz culture plate were measured at 15-min intervals and signal intensity was quantified. Without U87 cells, the signal did not decay. The observed rate constant of the signal decay was increased in the case of U87 cells pretreated with LPS and IFN- (Fig.7C). The observed pseudo-first rate constants were calculated to be 3.05 x 10^{-3} /min/10^{6} cells and 6.14 x 10^{-3} /min/10^{6} cells in the case of non- treated cells and LPS/IFN- -pretreated cells, respectively. This increase of the rate constant by LPS/IFN- -pretreated U87 cells was inhibited in the presence of superoxide dismutase (SOD) and catalase (Cat). The observed pseudo-first rate constant was calculated to be 3.39 x 10^{-3} /min/10^{6} cells in the case of LPS/IFN- -pretreated cells with SOD and catalase. From the difference of the observed rate constants in the presence and absence of both SOD and catalase, the signal decay of TEMPOL with superoxide was calculated to be 2.75 x 10^{-3} /min/10^{6} cells. Since the reaction rate constant of TEMPOL with superoxide has been calculated to be 3.90 x 10^{7} $M^{-1}min^{-1}$, the concentration of superoxide in LPS/IFN- -treated U87 cells was estimated to be 70.5 pM/10^{6} cells.

An ESR spin trapping method using *N*-dithiocarboxy- sarcosine (DTCS, Fig.7D)-iron complex was ewmployed to measure nitric oxide from U87 cells pretreated with LPS/IFN- for 24 h, but only a weak signal of NO adducts was detected. Furthermore the nitrite and nitrate levels in the medium, measured with a fluorometric detection kit, did not increase for 24 h.

The results obtained in this study suggested that superoxide production by U87 cells was induced by

treatment with LPS/IFN- for 24 h. Nitroxide spin probes have been reported to act as a superoxide scavenger or a SOD-mimic. TEMPOL, one of the nitroxide spin probes, was considered to act as a SOD-mimic in the redox mechanism, that is, TEMPOL was readily which was essentially spent only in the reaction with TEMPOL. The reaction of the oxoammonium cation with superoxide was considered to be negligible as long as the concentration of TEMPOL was high enough in the system.

In conclusion, it was found that treatment with LPS/IFN- for 24 h induced production of superoxide, but not nitric oxide in a glioma cell line, U87. The work was done by ESR using a superoxide-sensitive spin probe, TEMPOL, and spin-trapping reagent for nitric oxide, Fe-DTCS. The use of the new cuvette designed for adhesive cells and quartz culture plates will be an effective way to measure glioma cells by ESR without their detachment from the plates.

Publications:

Nakagawa, H., Moritake, T., Tsuboi, K., Ikota, N. and Ozawa, T. : *FEBS Lett*.., 471, 187- 190, 2000.

Nakagawa, H. , Sumiki, E. , Takusagawa, M., Ikota, N., Matsushima, Y. and Ozawa, T.: *Chem. Pharm. Bull*., 48, 261-265, 2000.

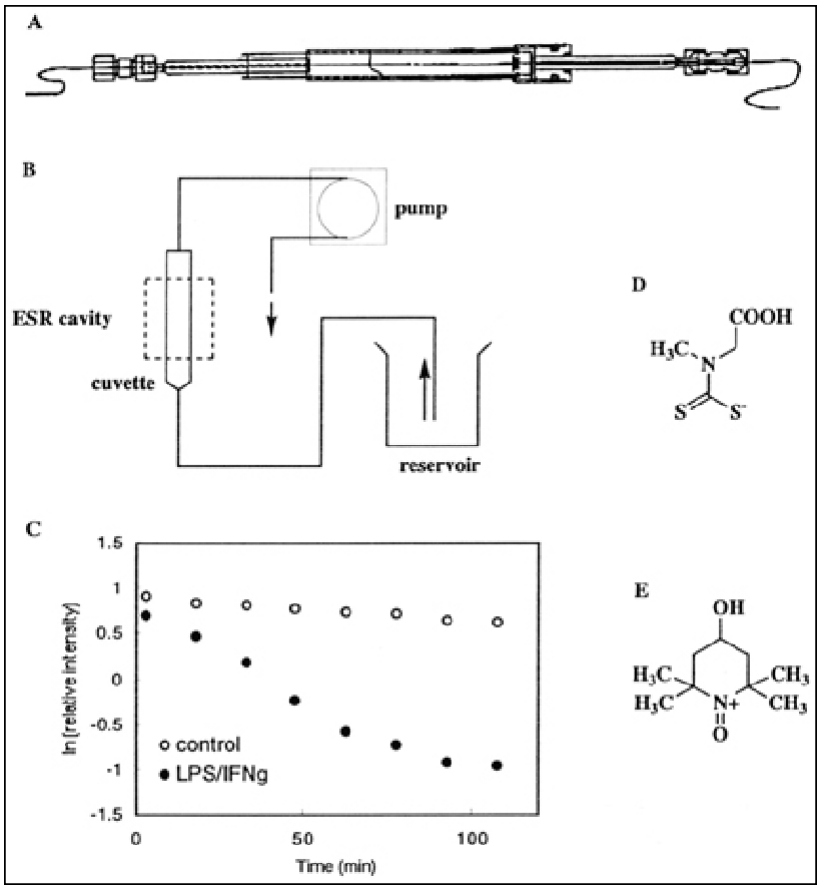

Fig.7. The structure of the new flow-type quartz cuvette (A); a diagram of the ESR measurement system (B); and ESR signal decay of TEMPOL with U87 glioma cells (C, the time course of the relative signal intensity measured at 15-min intervals). Chemical structures of *N*-

9. Improved Synthesis of 5-tert- Butoxycarbonyl 5-methyl-1-pyrroline N-oxide

Masaaki Sato, Kazunori Anzai, Nobuo Ikota, and Toshihiko Ozawa

Keywords: *ESR spin trapping 5, 5-dimethyl-1-1-pyrroline N-oxide, superoxide, 5-tert-butoxycarbonyl 5-methyl-1-pyrroline N-oxide, improved synthesis*

The spin trapping method is a useful method for the detection of unstable radicals. Radicals are trapped by non-radical spin trapping reagent and converted to stable radical adducts which can be observed with an ESR spectrometer. DMPO (1, 5,5-dimethyl-1-1-pyrroline *N*-oxide) has been widely used to trap superoxide and hydroxyl radical. A major disadvantage of DMPO is that the DMPO-superoxide adduct (DMPO-OOH) spontaneously decays to the DMPO-hydroxy adduct (DMPO-OH). The phosphorylated analog, DEPMPO (2, 5-(diethoxyphosphoryl)-5-methyl-1-pyrroline *N*-oxide), has been reported recently. In contrast to DMPO- OOH, DEPMPO-OOH does not decompose to DEPMPO-OH. However, ESR spectra of DEPMPO adducts are complicated due to the hyperfine coupling from an additional ^{31}P and the existence of diastereomers.

Substitution of the 5-methyl group in DMPO with an electron-withdrawing group increases the stability of superoxide adduct and has led to the synthesis of a carboxylated analogs. More recently, a new analog, BMPO (3, 5-*tert*-butoxycarbonyl 5-methyl-1-pyrroline *N*-oxide) has been reported. However, synthetic procedures for BMPO were not well established. Here, we describe an improved synthesis of BMPO.

The synthetic route for the preparation of (3) is illustrated in Fig. 8. The cyclic nitrone spin trap, BMPO, was prepared starting from 2-bromopropionic acid (4), which was converted to the corresponding *tert*-butyl ester (5) by treatment with isobutene in the presence of sulfuric acid in dioxane (yield 90%). This ester was also obtained from 2-bromopropionyl bromide and *tert*-butyl alcohol in the presence of silver cyanide in benzene at reflux temperature in comparatively low yield (30 %). Teatment of 5 with sodium nitrate and phloroglucinol in dimethylformamide at room temperature afforded *tert*-butyl 2-nitropropionate (6) in 56% yield. The nitro compound (6) was then treated with acrolein in the presence of triethylamine in acetonitrile under Ar atomosphere at 10 ^{o}C to give the desired Michael adduct, i.e. nitro aldehyde (7), almost quantitatively (99 %). Reduction of the nitro aldehyde (7) with zinc powder in MeOH-H_2O (1:1, v/v) in the presence of ammmonium chloride gave the BMPO (3) in 66 % yield as white needles (mp 97-98^{o}C) after purification by column chromatography and recrystallization from hexane-dichloromethane.

The BMPO superoxide (BMPO-OOH) adduct was about 10 times more stable than DMPO-OOH in the spin trapping of superoxide anion generated by the hypoxanthine-xanthin oxidase system.

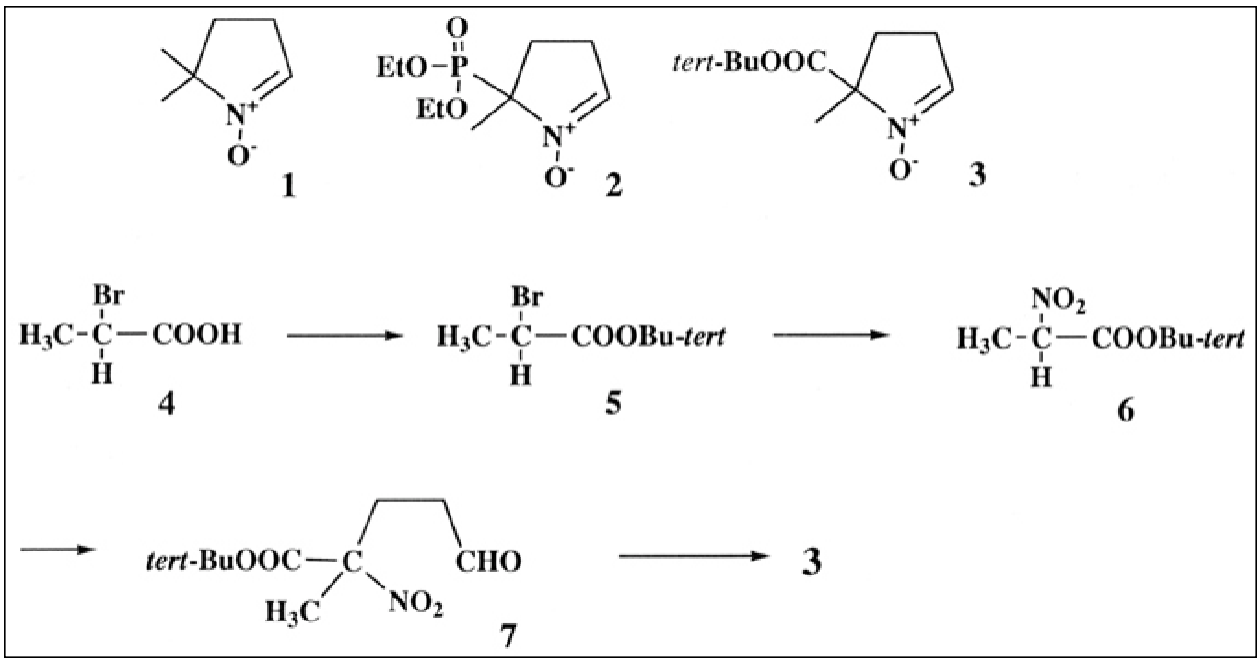

Fig.8.Synthetic scheme for the preparation of BMPO.

10. Potent Preventive Action of Curcumin on Radiation-induced Initiation of Mammary Tumorigenesis in Rats

Hiroshi Inano and Makoto Onoda

***Keywords*:** γ-rays, mammary tumor, curcumin, anti-initiation, chemoprevention

Tumor initiation by radiation in mammary glands is dependent upon the cell-stage, because estrogen is a direct or indirect sensitizer for tumor initiation by radiation. Previous studies in our laboratory have demonstrated that administration of WR-2721 or cysteamine prior to the irradiation has a potent preventive effect at the initiation stage of mammary tumorigenesis to be due to the scavenging of free radicals. Other recent work has indicated that phytochemicals with anti-oxidant properties can inhibit tumor initiation and promotion. Curcumin, a major pigment in turmeric obtained from rhizomes of *Curcuma longa* LINN, possesses both anti-inflammatory and anti-oxidant properties and has no toxicity. We have found that when administered orally for a long period after the whole body irradiation, curcumin has potent preventive activity during tumor promotion in radiation- initiated mammary tumorigenesis.

Now, we have evaluated the preventive effect of curcumin on radiation-induced tumor initiation in rat mammary glands. Fifty-four female rats were mated and then divided in two groups at day 11 of pregnancy. In the first group as control, 27 rats were fed a basal diet during the experimental period, and in another one as the experimental group, 27 rats were fed a diet containing 1% curcumin between day 11 of pregnancy and parturition, day 23 of pregnancy. All rats of both groups received whole body irradiation with 1.5 Gy-rays from a ^{60}Co source at day 20 of pregnancy, and were then implanted with a diethylstilbestrol pellet. Rats were examined for palpable mammary tumors for 1 year. A high incidence (70.3%) of mammary tumorigenesis was observed in the control group. The tumor incidence (18.5%) was significantly reduced in the rats fed curcumin during the initiation stage (Table 1). In the curcumin-fed group, the appearance of the first palpable tumor was delayed by 6 months and the average latent period until the appearance of mammary tumors was 11.2 months, i.e. 2.5 months longer than in the control group. Histological examination showed the proportion of adenocarcinoma (16.7%) in total tumors in the curcumin-fed rats was half of that (32.1%) in the control group. At the time of radiation, curcumin did not have any effect on organ weight or on the development and differentiation of mammary glands of pregnant rats. Also, no change in litter size and body weight of pups born from curcumin-fed rats indicated curcumin had no toxicity. These results suggest that curcumin does not have any side effects, and is an effective agent for chemoprevention acting at the radiation-induced initiation stage of mammarytumorigenesis.

Publications:

Inano, H., Onoda, M., Inafuku, N., Kubota, M., Kamada, Y., Osawa, T., Kobayashi, H. and Wakabayashi, K.: Carcinogenesis, 20, 1011-1018, 1999.

Inano, H., Onoda, M., Suzuki, K., Kobayashi, H. and Wakabayashi, K.: Radiat. Res. 153, 68-74, 2000.

Inano, H., Onoda, M., Suzuki, K., Kobayashi, H. and Wakabayashi, K.: Intl. J. Radiat. Biol.,76, 1113-1120, 2000.

Inano, H., Onoda, M., Suzuki, K., Kobayashi, H. and Wakabayashi, K.: Carcinogenesis,21, 1043-1050, 2000.

Inano, H., Onoda, M., Inafuku, N., Kobayashi, H. and Wakabayashi, K.: Carcinogenesis,21, 1835-1841, 2000.

Onoda, M. and Inano, H.: Nitric Oxide: Biol. Chem. 4, 505-515, 2000.

Table 1. Development of mammary tumors in irradiated rats fed curcumin during the initiation stage.

Diet	No. of rats used	Rats with tumors (Incidence,%)	No. of mammary tumors[a]			Multiplicity[b]	Latency period[b] (months)	Iball's index
			FA (%)	AC (%)	Total			
Control	27	19 (70.3%)	19 (67.9%)	9 (32.1%)	28	1.5±0.2	8.7±0.4	26.5
Curcumin	27	5 (18.5 %)[c]	5 (83.3%)	1 (16.7%)	6	1.2±0.2	11.2±0.2[d]	5.0

a FA; fibroadenoma; AC: adenocarcinoma.

b Number of mammary tumors/tumor-bearing rat, mean+ SE.

c Significant difference ($P<0.0001$) from the control group by the X^2 test.

d Significant difference ($P<0.005$) from the control group by Student's *t*-test.

11. A Possible Mechanism of Inactivation of C17-C20 Lyase in Rat Ovary by a Single Injection of hCG

Keiko Suzuki

Keywords**:** *P450, down-regulation, cholesterol, StAR, ROI*

The activity of C17-C20 lyase in immature rat ovary which had been pretreated with PMSG was down-regulated completely in 6 h by a single injection of hCG. Since cycloheximide and actinomycin D prevented the decrease to some extent, the transcription of genes and newly protein syntheses were supposed to be involved in the process. At first testosterone in the ovary was measured by radioimmunoassay. In the experiment, testosterone increased 30 min after hCG treatment, but decreased to the basal level at 1 h. Lyase is a P450 enzyme and has a heme at the active center. Therefore heme oxygenase was investigated, because the enzyme destroys heme. At first the transcriptional level of heme oxygenase-1 was examined by northern blot analyasis.

However, it did not change until 6 h after the injection of hCG . And although zinc protoporphyrin, an inhibitor of heme oxygenase, was injected to the rat 1 and 3 h after hCG treatment, the down- regulation of lyase was not prevented. Therefore heme oxygenase was not involved in the down- regulation. Next the transcription of steroidogenic acute regulatory protein (StAR) was examined similarly. The level of mRNA of StAR increased 20 min after the injection of hCG, and increased further until 2 h. Finally, to examine the possible involvement of reactive oxygen intermediates (ROI) in this process, rats were consecutively pretreated with dimethyl sulfoxide at 12 and 3 h before the injection of hCG. As a result, the down-regulation of lyase at 6 h after hCG injection was protected to some extent in these animals. Therefore ROI was possibly involved in the down- regulation.

In this system, a huge amount of cholesterol is supplied to the cholesterol side chain cleavage enzyme (SCC) transiently by hCG injection as shown by the transient increase of testosterone. And the transcriptional increase of StAR indicates cholesterol might have been supplied further continuously. It is known that P450 enzymes such as lyase generate ROI in this process and thus microsomal enzymes are destroyed by the ROI. This mechanism is possibly working in the down- regulation of lyase.

12. Low-Dose Irradiation Influences Ca^{2+} Signaling in Cultured Rat Hepatocytes

Tetsuo Nakajima, Bing Wang, Masako Nose, Hiromi Itsukaichi, Harumi Ohyama and Osami Yuakawa

Keywords**:** *rat hepatocytes, low-dose effect, Ca^{2+} signaling, adaptive response*

We have already demonstrated that radiation induces diacylglycerol(DAG) production by phosphoinoside-specific phospholipase C(PI-PLC) and protein kinase C activation in cultured rat hepatocytes. Since DAG production by PI-PLC is accompanied by the production of inositol 1,4,5- trisphosphate(IP_3), which works in Ca^{2+} signaling, radiation might influence Ca^{2+} signaling in the cells. On the other hand, we have previously reported that, in cultured rat hepatocytes, low-dose irradiation (0.05-0.1 Gy) induces the increase of intracellular radical scavenging ability in relation to adaptive response. In this study, the effect of low-dose irradiation on Ca^{2+} signaling in rat hepatocytes was investigated as compared with the effect of high-dose irradiation on it. No change in the cytosolic Ca^{2+} concentration ($[Ca^{2+}]$i.) was observed after irradiation of hepatocytes with
0.1 Gy of X-rays. However, the irradiation prolonged the time for restoration of ATP-induced $[Ca^{2+}]$i uptake to the basal $[Ca^{2+}]$i level in the cells compared with that in non-irradiated cells. High-dose irradiation with 10 Gy did not have any effect on the time for the restoration of ATP- induced $[Ca^{2+}]$i uptake to the basal level in the cells, but reduced the level of the ATP-induced $[Ca^{2+}]$i uptake. In contrast, low-dose irradiation with 0.1 Gy did not change the level of the ATP- induced $[Ca^{2+}]$i uptake. The prolonged time in ATP-induced $[Ca^{2+}]$i uptake suggests that low-dose irradiation might specifically influence Ca^{2+} signaling and induce adaptive response.

13. X-ray or Heavy Ion Radiation-induced Chromosome Damage on an Ionizing Radiation Sensitive Mutant Mouse Cell Line as Analyzed by Atomic Force Microscope

Masahiro Murakami, Masako Minamihisamatsu, Hiromi Itsukaichi, Koki Sato*, and Isamu Hayata(* Kinki Univ.)

***Keywords*:** *chromosome damage, X-rays, heavy ion radiation, atomic force microscope*

Ionizing radiation induces chromosome damage. Low linear energy transfer (LET) radiation, such as X-rays, ionize sparsely. On the other hand, heavy ion radiation (classified as high LET radiation), which densely deposits its energy along the path of particle radiation, causes clustered DNA breaks. It is unclear whether or not there is any structural difference in chromosome damage induced by low LET radiation or high LET radiation.

We applied an AFM for nanometer-level structural analysis of chromosome damage induced by X- rays or heavy ion irradiation. An X-ray-sensitive mutant mouse cell line, SL3-147, was exposed to radiation by X-rays or heavy ions [neon ions (initial energy of 400 MeV/n) and carbon ions (initial energy of 135 MeV/n)] and then the fine structures of chromosome aberrations were visualized by AFM. After irradiation, the cells were kept under 5% CO_2 at 37^{o}C- in a culture medium containing

0.05 μg/ml of colcemid for 1.5h or 20h, and then collected. The cells were treated with a hypotonic solution of 0.075M KCl, fixed with methanol-acetic acid (3:1), and then air-dried slides were prepared. The AFM can visualize detailed structure of the chromosomes. The structure of the break point induced by X-rays or neon ions (LET=100keV/ μm, 1.5Gy) or carbon ions (LET=100keV/ μm, 1.5Gy) radiation was imaged by AFM. A fibrous structure was observed in these break points. This fibrous structure is considered to correspond to the 30 nm fiber of chromatin structure. We could not recognize any difference in structure of X-ray and heavy ion radiation induced chromosome damage at this resolution of AFM.

14. Reactivity of Nitroxyl Spin Probes with Reactive Oxygen Species

Keizo Takeshita, Keita Saito and Toshihiko Ozawa

Keywords**:** *superoxide anion radical, hydroxyl radical, nitroxyl radical, reaction rate constant*

Nitroxyl radical has been reported to react with hydroxyl radical (·OH) resulting in loss of an ESR signal, and it also loses the ESR signal by reaction with superoxide anion radical ($O_2^{\cdot -}$) in the presence of thiol or NADH. This suggests that spin probes carrying nitroxyl radical should be useful to monitor *in vivo* detection of reactive oxygen species by using ESR spectroscopy operating at low microwave frequency. However, little is known about details of ESR signal-loss caused by these oxygen radicals. In this study, the signal decay rates of structurally different spin probes were examined with ·OH-, $O_2^{\cdot -}$-, and singlet oxygen ($^1O_2$)-generating systems, and apparent reaction rate constants for the reaction between spin probes and these oxygen radicals were determined.

·OH, $O_2^{\cdot -}$, and $^1O_2$ were generated with the UV-H_2O_2 system, hypoxanthine/xanthine oxidase system, and thermal decomposition of 3-(1,4-epidioxyl-1,4-dihydro-1-naphtyl) propionic acid, respectively. Spin probes used were derivatives of pyrrolidine nitroxyl (PROXYL) and piperidine nitroxyl (TEMPO). Decay rate caused by ·OH varied depending on both ring structures and substituents of spin probes. Loss of the ESR signal was the most rapid with TEMPO, while oxo- TEMPO and amino-TEMPO were relatively resistant to ·OH. The rate for PROXYL derivatives was moderate. The apparent rate constants estimated were 4.3×10^9 $M^{-1}s^{-1}$ for carbamoyl-PROXYL and 4.8×10^9 $M^{-1}s^{-1}$ for hydroxy-TEMPO, using mannitol as a competitive standard. Signal decay of TEMPO, hydroxy-TEMPO, carboxy-TEMPO, and amino-TEMPO was relatively rapid in the $O_2^{\cdot -}$- generation system in the presence of cysteine, although the decay of oxo-TEMPO and PROXYL derivatives was slow. Apparent rate constant of the reaction between hydroxy-TEMPO and $O_2^{\cdot -}$ was estimated to be 1.8×10^4 $M^{-1}s^{-1}$ in the presence of cysteine. No signal decay was observed for the reaction of any spin probes with $^1O_2$. These observations suggest that PROXYL derivatives should be useful to probe *in vivo* generation of ·OH, because it has been reported that PROXYL derivatives were more stable than TEMPO derivatives in various biological reduction systems.

15. The Preliminary Experiments for Clinical Multi Nuclei MRS Using a Commercial MRI System.

Hiroo Ikehira, Franck Girard, Takayuki Obata, Tetsuya Suhara, Shuji Tanada and Yasuhito Sasaki

***Keywords*:** ^{19}F, ^{7}Li *, magnetic resonance spectroscopy, chemical shift imaging*

The study of dynamic natural abundance ^{19}F-magnetic resonance spectroscopy (^{19}F-MRS) on 5-FU based medicines was performed in the human liver using commercial 1.5T MRI equipment. A single tuned custom-made circular shape surface coil with a diameter of 15 cm operating at 60 MHz was used for the ^{19}F-MRS study. Localized proton shimming with a whole body coil was performed with an adequate volume to include the observing area of the surface coil, and the line width of the water signal was less than 20 Hz. The normal clinical dose of oral fluorine anticancer medicine should be too small to detect a sufficient signal for ^{19}F-MRS using commercial MRI equipment. But we can observe very different spectroscopic appearance patterns of 5-FU. We examined whether the pharmacokinetics in the liver of orally administered 1-hexylcarbamoyl-5- fluorouracil (HCFU) differs from that of orally administered 5'-deoxy-5-fluorouridine (5'-DFUR).

This preliminary study indicated ^{19}F-MRS technique should be very useful method to evaluate *in vivo* 5-FU based medicine metabolism.

In another experiment ^{7}Li 2D-CSI (two dimensional chemical shift imaging) of human brain was also performed. Lithium salts have been widely used in the treatment of mood disorders, but their mechanism of action is still not clear. In this work, a methodology for two-dimensional lithium-7 imaging in clinical systems is presented. The data were acquired using a phosphorus volume head coil that was re-tuned for the lithium-7 frequency. A spectroscopic sequence was used to acquire the free induction decay (FID) after volume excitation using a hard pulse. The results obtained on the head of patients undergoing lithium treatment (n=7, 0.6 mEq/l average serum level) demonstrate that images of adequate signal to noise ratio (100:1) can be obtained in acceptable imaging times (55 min) using the proposed methodology. The distribution of ^{7}Li appears uniform in the brains of the patients studied.

Publications:

Ikehira H, Girard F, Obata T, Ito H, Yoshitomi H, Kamei H, Kanazawa Y, Tanada S, Sasaki Y, Miyazaki M, Nakajima N, Takano H, Ito H: British Journal of Radiology 72 , 584-589, 1999

Girard F, Suhara T, Sassa T, Okubo Y, Obata T, Ikehira H , Sudo Y, Koga M, Yoshioka H, Yoshida K: MAGMA 13 (1) , 1-7, 2001

16. Effects of Antibodies of Growth Factors and Cytokines on the Proliferation of Cultured Epidermal Melanoblasts and Melanocytes Derived from Skins of UVB-Induced Pigmented Spots in Mice

Tomohisa Hirobe

Keywords**:** *melanoblast, melanocyte, antibody, UVB, proliferation*

Long-term exposure to ultraviolet radiation B (UVB) induced pigmented spots in the dorsal skin of hairless mice. It has been shown that the proliferation of epidermal melanoblasts and melanocytes derived from skins of UVB-induced pigmented spots is greatly stimulated by using a serum-free culture system supplemented with dibutyryl adenosine 3':5'-cyclic monophosphate (DBcAMP) and basic fibroblast growth factor (bFGF). In this study, to understand what factors are involved in regulating the proliferation of cultured epidermal melanoblasts and melanocytes, numerous antibodies against growth factors and cytokines were added in the serum-free medium from the initiation of primary cuture. Results showed that antibodies against endothelin-1, -2, -3, granulocyte macrophage colony stimulating factor (GMCSF), stem cell factor (SCF) inhibited the proliferation of cultured mouse epidermal melanoblasts and melanocytes derived from skins of UVB-induced pigmented spots. These results suggest that numerous factors are involved in regulating the proliferation of melanoblasts and melanocytes from skins of UVB-induced pigmented spots.

Publications:

T. Hirobe and H. Abe: J. Exp. Zool., 286, 632-640, 2000.

T. Kunisada, H. Yamazaki, T. Hirobe, S. Kamei, M. Omoteno, H. Tagaya, H. Hemmi, U. Koshimizu, T. Nakamura, and S. Hayashi: Mech. Dev. 94, 67-78, 2000.

17. Regulation of the Catalase Gene Promoter in Hydrogen Peroxide-Resistant HP100 Cells

Mitsuru Nenoi, Sachiko Ichimura, Kazuei Mita, Osami Yukawa, and Iain L. Cartwright

***Keywords*:** catalase, hydrogen peroxide, apoptosis, transcription, promoter

Reactive oxygen species (ROS) play a critical role in the onset of apoptosis induced by various extracellular stimuli, including ionizing radiation. Therefore active regulation of ROS- metabolizing enzymes may be one response to an apoptotic stimulus. In this regard HP100 cells, H_2O_2-resistant variants derived from human leukemia HL60 cells, display an interesting phenotype wherein the activity of catalase is constitutively high, while its mRNA is reduced after X ray-irradiation. In the present study, we investigated the molecular mechanisms underlying this phenomenon. By combining analyses from nuclear run-on, reporter gene transient transfection, genomic footprinting, site-directed mutagenesis, EMSA, and Western blotting experiments, we found the following. (i) The expression of catalase is primarily regulated at the transcriptional level. (ii) The GC-box which is located - 70 bp from the major transcriptional start site of the catalase gene functions as the core promoter element. (iii) Much higher levels of Sp1 are expressed in HP100 than in HL60, associating with the overlapping Sp1/Egr-1 recognition sequence in the GC-box at -70 bp. (iv) A WT1/Egr-related factor is induced in response to 20 Gy of X rays and it associates with the overlapping Sp1/Egr-1 sequence in the GC-box at -70 bp. (v) The CCAAT element at - 92 bp strongly enhances transcription in HP100. (vi) Higher levels of NF-Y are expressed in HP100 than in HL60, associating with the CCAAT element at -92bp. (vii) Both the inverted CCAAT sequence at - 42 bp and the CCAAT sequence at - 121 bp regulate transcription negatively in HL60 and positively in HP100.
Based on these findings, we suggest that a mechanism such as that shown in Fig. 9 could be the means by which promoter regulation of the catalase gene occurs. Fig. 9A illustrates the catalase gene promoter in HL60, where the transcription initiation complex containing RNA polymerase II may not be very effectively recruited to the transcriptional start site because of the low nuclear content of Sp1 and NF-Y in HL60. In HP100, on the other hand, binding of Sp1 to the overlapping Sp1/Egr-1 sequence in the GC-box at -70 bp (EgrSp-70) might now result in an assemblage of factors that allows efficient entry of the initiation complex at the transcriptional start site (Fig. 9B). NF-Y bound to the CCAAT sequence at -92 bp (CCAAT-92) may cooperatively stimulate this process. When HP100 is irradiated with X rays, induced binding of the WT1/Egr-related factor (Egr) to the EgrSp-70 element may somehow lead to complex disassembly, resulting in the initiation complex being inhibited from entry (Fig. 9C). The identification and precise characterization of factors postulated in Fig. 9 remains the subject of future study. In particular, identification of the WT1/Egr-related factor is of great interest in relation to the potential involvement of catalase in ionizing radiation-inducible apoptosis.

Publication:

Nenoi, M., Ichimura, S., Mita, K., Yukawa, O., and Cartwright, I.L.: *Cancer Res.* 61 5885-5894 2001.

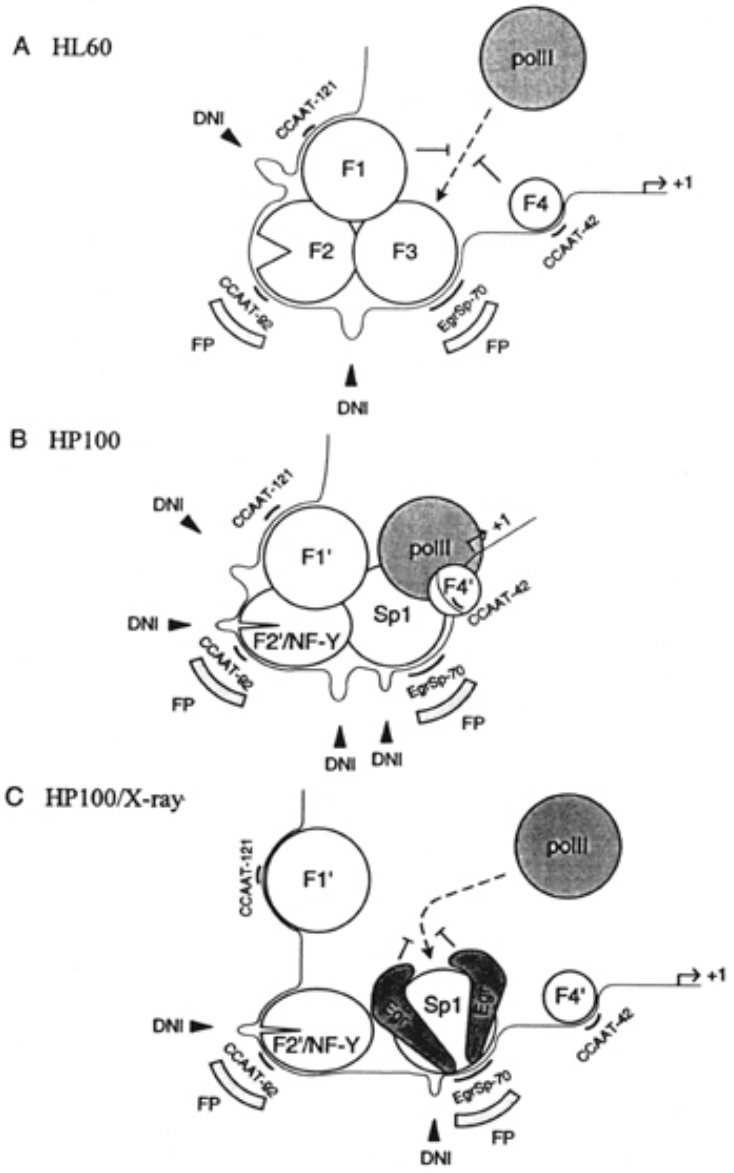

Fig.9. A possible mechanism for promoter-based regulation of the catalase gene in HL60 and HP100 cells. DNI and FP indicate DNase I- sensitive sites and footprints, respectively, which were observed in the genomic footprinting analysis. Egr represents the WT1/Egr-related factor observed in the EMSA experiment.

18. Modulation by Curcumin of NF-*k*B Activation in Cultured Rat Mammary Gland

Makoto Onoda and Hiroshi Inano

***Keywords*:** curcumin, NF-*k*B, I*k*B, mammary gland, nitric oxide, nitric oxide synthase

We found in a previous report that curcumin, a yellow pigment and a major component of turmeric, had the ability to inhibit induction of inducible nitric oxide synthase (iNOS) by lipopolysaccharide (LPS) in the rat mammary gland and to scavenge NO radicals. However, the NO-generation by iNOS within the mammary gland was not disturbed by the presence of curcumin after the pre-stimulation with LPS. It is, therefore, likely that curcumin does not affect the post-translational processes of iNOS de novo synthesis. In this context, we undertook an investigation to elucidate whether curcumin influenced the expression and translocation of NF -*k*B, the transcription factor that regulates iNOS gene transcription, and I*k*B, an inhibitory element of NF-*k*B, by using rat mammary gland tissue culture system.

Female Wistar-MS (8-week-old) rats were primed by implantation with pellets of 17β-estradiol (0.5 mg/3-week-release type) and progesterone (35 mg/3-week-release type). After 3 weeks of priming, the rats were sacrificed by carbon dioxide asphyxiation and the inguinal mammary glands were excised asceptically for organ culture. The isolated mammary glands were diced into approximately 3 mm cubes, and each cube cultured in the well of 24-multiwell plates containing 2 ml of 5% fetal calf serum (FCS)/Dulbecco's Modified Eagle's Medium (DMEM) supplemented with antibiotics and antimycotic in a mixture of 5% CO_2/95% air at 37°C for 2 days. The medium was then replaced with 5% FCS/DMEM in the presence or absence of LPS (0.1 or 0.5 μg/ml), and the culture was maintained for another 30 or 60 min. Curcumin (100-fold concentration) dissolved or suspended in absolute ethanol was added at the same time to the LPS treated cultures. At the end of the culture, the cultured mammary glands were collected and further processed for the preparation of mammary gland homogenates. The mammary glands cultured in various conditions were minced and homogenized in ice-chilled 5 mM Tris-HCl buffer (pH 7.5) containing 0.25 M sucrose, 5 mM EGTA and inhibitors (1 mM phenylmethylsulfonyl fluoride, 2 mM sodium vanadate, 10 μg/ml aprotinin, 5 μg/ml leupeptin). The homogenates were then centrifuged at 600 *xg* for 10 min at 4°C, and cytoplasmic (supernatant) and nuclear (precipitate) fractions were separately reconstituted in reducing sample buffer and loaded into the mini-gel system for SDS-PAGE. Subsequently, the separated proteins were electrotransferred to a nitrocellulose membrane. The membrane was reacted overnight with either anti-NF-*k*B p65 or anti-I*k*Bα body. NF-*k*B p65 and I*k*Bα were detected with 2nd antibody conjugated with alkaline phosphatase. The immunoreactivity was, then, visualized with nitro blue tetrazolium (NBT) and 5-bromo-4-chloro-3-indolyl phosphate (BCIP). The molecular weight of the immunoreactive bands was estimated from plots of molecular weight vs. relative mobility of rainbow marker standard proteins which were run simultaneously with the sample proteins.

The amount of NF-*k*B in the cytoplasmic fraction did not pronouncedly change after 30 and 60 min incubations with LPS (0.1 and 0.5 μg/ml), however, that of the nuclear fractions was obviously increased in the mammary gland by LPS-stimulation (Fig. 10). In addition, I*k*Bα content slightly, but clearly,

declined in cytoplasmic fractions of LPS-treated mammary gland. These indicate the degradation of I*k*Bα, NF-*k*B activation and the translocation of this transcription factor from cytoplasm to nucleus in the mammary gland in a short term after the stimulation by LPS.

On the other hand, the addition of curcumin (100 μM) with LPS (0.1 μg/ml) to the culture clearly inhibited the translocation to the nucleus of NF-kB and recovered the reduction of I*k*Bαin the cytoplasmic fraction (Fig. 10), while, curcumin at the same dose did not show any inhibitory effect on the NF-*k*B translocation and I*k*Bα degradation in the mammary gland treated with a higher dose (0.5 μg/ml) of LPS.

This may indicate a limited potential for curcumin on the iNOS inhibition under the current experimental conditions because of less solubility of curcumin in the in vitro culture system. In any event, NO produced harmfully within the mammary gland during acute and chronic pathophysiological conditions may perturb the regulation of normal mammary gland development and its function. Results shown here support the idea that curcumin possesses the ability to reduce induction of iNOS by LPS in the mammary gland.

The results also suggest that a part of the inhibitory activity of curcumin on iNOS induction in mammary gland may be due to inhibition of the NF-*k*B activation cascade following I*k*B degradation. Figure Legend.

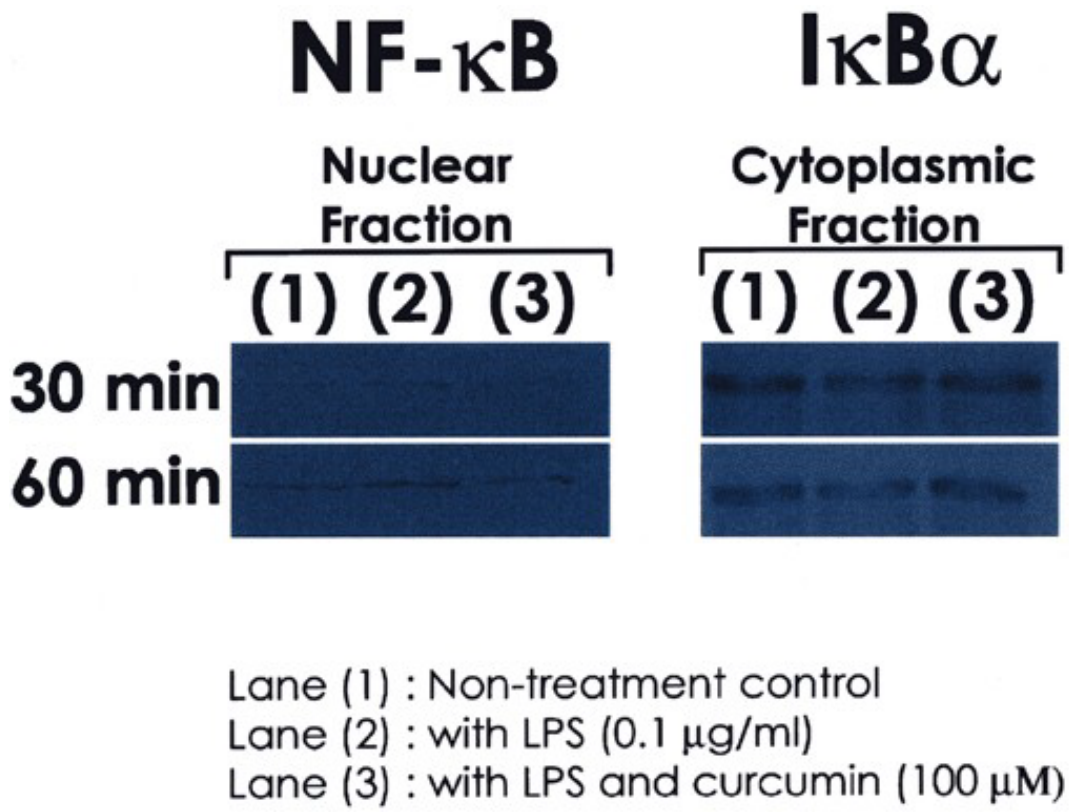

Fig.10. Immunoblot analyses of NF-kBp65 and IkB in nuclear and cytoplasmic fractions, respectively, obtained from cultured rat mammary glands. Each fraction (10 g/lane) was loaded onto the SDS-PAGE mini-gel system and the immunoreactive substances were visualized by Western blot analysis with an alkaline phosphatase-conjugated secondary antibody. Lane 1, non-treatment control; Lane 2, control + LPS (0.1 g/ml); Lane 3, control + LPS + curcumin (100 M).

19. Allocyclic X Chromosome Visualized by Drug-Induced Premature Chromosome Condensation

Reiko Kanda, Yoko Yamagishi and Isamu Hayata

***Keywords*:** calyculin A, chromosome painting, human lymphocytes, inactive X, premature chromosome condensation (PCC)

Okadaic acid and calyculin A, inhibitors of serine/threonine protein phosphatases, can induce premature chromosome condensation (PCC) at any stage of the cell cycle in human peripheral lymphocytes. Using this PCC technique, the authors previously attempted to develop a new biodosimetry for absorbed radiation dose, and they examined cytogenetical reactions of lymphocytes in different stages of the cell cycle to the phosphatase inhibitors mentioned above. In the course of PCC studies, one highly condensed chromosome per nucleus was frequently observed at early to middle S phases in female cells treated with calyculin, but not in male cells (Fig. 11). When these PCC spreads were hybridized with a whole chromosome- painting probe for the X chromosome, one FISH signal was located on the highly condensed chromosome. The other signals were diffused on the extended fibers or small particles. Judging from the Giemsa stained image, the former seemed to have finished DNA replication, while the latter was in the process of replication.

Since such a highly condensed chromosome has seldom been observed in male PCC spreads, it was considered an inactive X chromosome, which may be identical to the sex chromatin body ("Barr body") of oral mucosal cells.

The present finding appears to be inconsistent with earlier reports that the inactive X chromosome replicates later than autosomes and the active homolog. One simple explanation for this finding could be that the inactive X chromosome in human female lymphocytes might precede other chromosomes in DNA replication at the end of the S phase in the cell cycle. Another hypothesis could be that the culture conditions, such as calyculin treatment, had an effect on the cellular factor that keeps the inactive X chromosome in late replication resulting in precocious replication of the inactive X chromosome. Recently, it was found that histone macroH2A1was concentrated in the inactive X chromosome of female mammals. This new histone might cause preferential condensation of the inactive X chromosome on calyculin treatment.

Publication:

Kanda, R. and Hayata, I.: *Somat. Cell Mol. Genet*. 25*,* 173-176, 1999.

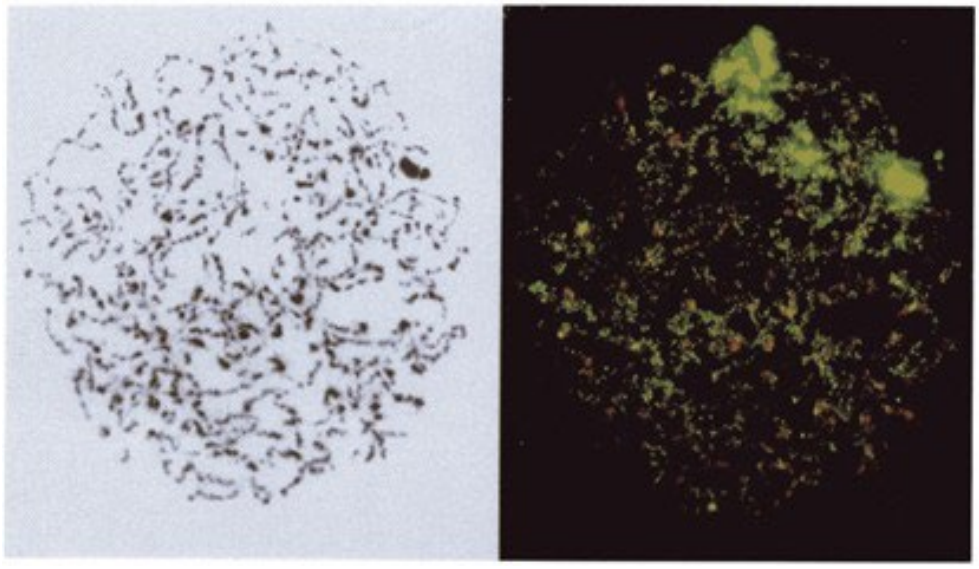

Fig.11. Prematurely condensed chromosomes (PCC) induced by calyculin A in female lymphocytes at early S phase. Cells are stained with Giemsa (left) and subsequently painted with whole chromosome painting probes for the X-chromosome (right). One hybridized chromosome was condensed to form a metaphase-like chromosome. The other hybridized signal was on the diffused fibers.

20. Relative Biological Effectiveness of the 235 MeV Proton Beams at the National Cancer Center Hospital East

Koichi Ando, Yoshiya Furusawa, Masao Suzuki, Kumie Nojima, Hideyuki Majima, Sachiko Koike, Mizuho Aoki, Wakako Shimizu, Yasuyuki Futami, Takashi Ogino, Shigeyuki Murayama, and Hiroshi Ikeda

***Keywords*: r**elative biological effectiveness, human, mouse, cell survival, crypt

A therapy-dedicated cyclotron was installed in the National Cancer Center Hospital East (NCCHE) at Kashiwa in 1997. Prior to the start of clinical use, we investigated the biological effectiveness of therapeutic proton beams for cell lethality. The proton beams accelerated up to 235 MeV were horizontally extracted from the cyclotron, and scattered by a bar-ridge filter to produce a Spread-Out-Bragg-Peak (SOBP) of 10-cm width. The biological systems used here were mouse intestinal crypt cells and three *in vitro* cell lines, including SCC61 human squamous cell carcinoma, NB1RGB human fibroblasts and V79 Chinese hamster cells. The dose responses after irradiation at either the entrance plateau or the middle portion of SOBP were compared with those after linac 6 MV X-ray irradiation. The fit of a linear quadratic model to survival curves showed that proton irradiation increased the α value of SCC61 and the β value of V79 cells with a least change for α/β ratio of NB1RGB cells. The isoeffect dose that reduced either cell survivals to 10% or mouse jejunum crypts to 10 per circumference was termed D10. The relative biological effectiveness (RBE) of protons obtained by comparing the D10 values between protons and X-rays ranged from 0.9 to 1.2. The depth distribution of cell lethality was measured by replating V79 cells after irradiation from a "cell stack chamber" that received a single dose of 7 Gy at the middle position of the SOBP. The thus-obtained cell survivals at various depths coincided well with the estimated survivals, but tended to decrease at the distal end of the SOBP. We concluded that an RBE of 1.1 would be appropriate for 235 MeV proton beams at the NCCHE.

Publication:

Ando, K., Furusawa, Y., Suzuki, M., Nojima, K., Majima, H., Koike, S., Aoki, M., Shimizu, W., Futami, Y., Ogino, Y., Murayama, S. and Ikeda, H.: J.Radiat.Res. 42, 79-89, 2001

21. Radiobiologial Effects of Heavy Ion Beams on Cells

Yoshiya Furusawa, Mizuho Aoki, Koichi Ando, Hideki Matsumoto[1], Akihisa Takahashi[2], Tetsuya Kawata[3], Kerry George[3] and Marco Durante[4] ([1]Fukui Med. Univ.; [2]Nara Med. Univ.; [3]Johnson Space Center; [4]Univ. Fedellico II.)

***Keywords*:** *heavy ion, LET, RBE, p53, apoptosis, chromosome aberration*

LET-RBE spectra of cell inactivation of aerobic and hypoxic cells from three different cell lines by accelerated 3He-, 12C- and 20Ne-ion beams were investigated to design a spread- out Bragg peak beam for cancer therapy at HIMAC, prior to clinical trials. Cells that originated from a human salivary gland tumor (HSG cells) as well as V79 and T1 cells were exposed to 3He-, 12C- and 20Ne-ion beams with an LET ranging from approximately 20-600 keV/m under both aerobic and hypoxic conditions. Cell survival curves were fitted by equations from the linear-quadratic model and the target model to obtain survival parameters. RBE, OER, alpha and D0 were analyzed as a function of LET. The RBE increased with LET, reaching a maximum at around 200 keV/m, then decreased with a further increase in LET. Clear splits of the LET-RBE or -OER spectra were found among ion species and/or cell lines. At a given LET, the RBE value for 3He ions was higher than that for the other ions. The position of the maximum RBE shifted to higher LET values for heavier ions. The OER value was 3 for X rays but started to decrease at an LET of around 50 keV/m, passed below 2 at around 100 keV/m, and then reached a minimum above 300 keV/m; however, the values remained greater than 1. The OER was significantly lower for 3He ions than the others.

The relationship between the LET values and cell death, defined as either apoptosis or loss of reproductive integrity (reproductive death), was studied using V79 cells. The cells were irradiated with X-rays or carbon-ion beams from the HIMAC. Apoptosis was defined based on the morphological change upon treating cells with caffeine. The apoptotic index, the ratio of apoptotic cells to the total, after exposure to 2 Gy of X-rays was 0.043. Upon irradiation with carbon ion beams, the index was gradually increased with increasing LET values, reaching a maximum of 0.076 at 110 keV/m, and then decreased to 0.054 at 237 keV/m. An analogous pattern of the LET dependence was observed between reproductive death and apoptotic death. The cell survival values obtained after 2 Gy exposure (SF2) were 0.64, 0.13, and 0.24, respectively. A similar trend was found for the RBE values calculated from the initial slope for both apoptosis and reproductive death. These results strongly suggested that the target for both types of cell death was the same.

The dependence of p53 on the radiation enhancement of thermosensitivity at different LET was investigated. The aim of this study was to investigate the dependence of p53- gene status on the radiation enhancement of thermosensitivity at different levels of LET. We used two kinds of human glioblastoma transfectants of A- 172 cells bearing the wild-type p53 gene, A-172/neo cells with control vector containing the neo gene and A-172/mp53 cells with both the dominant negative mutated p53 gene and neo gene. We exposed these cells to X-rays and accelerated carbon ion beams (13-200 KeV/m) followed by heating at 44 degrees C. Cellular sensitivities were determined using clonogenic assay. The radiation enhancement of thermosensitivity was LET-dependent for the A-172/neo cells, but this was not clearly

demonstrated in the A-172/mp53 cells. The supraadditive radiation enhancement of thermosensitivity was observed in A-172/neo cells at the LET range of 13 to 70 keV/m, though only an additive effect was observed at higher LET. In A-172/mp53 cells, only an additive effect was observed for all the LET examined. These results indicated that the radiation enhancement of thermosensitivity was p53- and LET-dependent. Our results suggested that the combined use of high-LET radiation and hyperthermia would provide useful applications for cancer therapeutic purposes.

Cytogenetic damage in lymphocytes in peripheral blood from cancer patients during tumor therapy X-rays and carbon ion beams was determined. Blood samples from patients diagnosed with esophageal or uterine cervical cancer were obtained before, during, and at the end of the radiation treatment. The novel technique of interphase chromosome painting was used to detect aberrations in prematurely condensed chromosomes 2 and 4. The fraction of aberrant lymphocytes was measured as a function of the dose to the tumor volume. For comparison, blood samples were also exposed in vitro to X-rays or to carbon ions accelerated at the HIMAC. The carbon ions were more efficient than X-rays in the induction of chromosomal aberrations in vitro. In patients with similar pathologies, tumor positions, and radiation field sizes, however, carbon ions induced a lower fraction of aberrant lymphocytes than X-rays during the treatment. The initial slope of the dose-response curve for the induction of chromosomal aberrations during the treatment was correlated to the relative decrease in the number of white blood cells and lymphocytes during the treatment. The carbon ions induced a lower level of cytogenetic damage in lymphocytes than X-rays, reducing the risk of bone marrow morbidity.

Publications:

Furusawa, Y., et al.: Radiat Res 154: 485-96, 2000.

Furusawa, Y.: In; Exploring Future Research Strategies in Space Radiation Sciences. Iryoukagakusha, pp.104-109, Tokyo. 2000.

Aoki, M. et al.: J. Radiat. Res. 41: 163-75, 2000.

Durante, M., et al.: Int. J. Radiat. Oncol. Biol. Phys. 47: 793-8, 2000.

Kawata, T., et al.: Int. J. Radiat. Biol. 76: 929-37, 2000.

Matsumoto, H., et al.: Int. J. Radiat. Biol. 76: 1649-57 2000.

Takahashi, A., et al.: Int. J. Radiat. Oncol. Biol. Phys. 47: 489-94, 2000.

Takahashi, A., et al.: Int. J. Radiat. Biol.76: 335-41, 2000.

Yamada, S., et al.: Cancer Lett. 150: 215-21, 2000.

George, K., et al.: Int. J. Radiat. Biol. 77: 175-83, 2001.

Kawata, T., et al.: Int. J. Radiat. Biol. 77: 165-74, 2001.

Shigematsu, N., et al.: Int. J. Mol. Med. 7: 509-513, 2001.

22. Cytogenetic and Cellular Events during Radiation-induced Thymic Lymphomagenesis in p53 Heterozygous(+/-) B10 Mice

Kaoru Tanaka, Shiro Aizawa, Keiko Watanabe, Hideo Tsuji, Masahiro Mori, Hitoko Kamisaku, Yoko Hirabayashi, and Tohru Inoue

***Keywords*:** *thymic lymphomas, p53 heterozygous mice*

Cellular and cytogenetic events in radiation-induced thymic lymphomagenesis were investigated in p53 heterozygous (+/-) mice following a single dose of whole-body irradiation. p53 heterozygous mice developed thymic lymphomas in a dose-dependent manner. The loss of wild type p53 allele (loss of heterozygosity; LOH) occurred in all/most thymic lymphomas induced in irradiated p53 heterozygous mice. Cytogenetic analysis for the mechanism of LOH indicated that the loss of wild type p53 gene in the lymphomas was caused by the duplication of the disrupted p53 gene allele through either homologous recombination or non-disjunctional chromosome duplication. The suppression of lymphoma development bythe injection of normal bone marrow cells into mice after irradiation suggested that a critical event for the development of prelymphoma cells occurred between 4 and 5 weeks after irradiation. The results suggested that theloss of wild type p53 gene in thymocytes of p53 heterozygous mice preceded the development of prelymphoma cells after irradiation and may be a valuable marker for understanding of the role of radiation in radiation-induced leukemogenesis.

Publications:

Kamisaku, H., Aizawa, S., Tanaka, K., Watanabe, K. and Sado, T.: *Int.J. Radiat. Biol.* , 76, 1105-1111, 2000.

Kitagawa, M., Aizawa, S., Sado, T.,Yamaguchi, S., Suzuki, T., Hirokawa,K. and Ikeda, H., *Leukemia* (in press).

Tanaka, K., Aizawa, S., Watanabe, K., Tsuji, H., Mori, M., Kamisaku, H., Hirabayashi, Y.and Inoue, T.: *Int. J. Radiat. Biol*. (in press).

23. Development of Thymic Lymphomas by Ionizing Radiation in Scid Mice

Toshiaki Ogiu, Hiroko Ishii-Ohba, Shigeru Kobayashi, Mayumi Nishimura, Yoshiya Shimada, Hideo Tsuji, Hideki Ukai, Fumiaki Watanabe, Fumio Suzuki, and Toshihiko Sado

***Keywords*:** Scid mice, radiation-induced thymic lymphomas, oncogenes, Ras, Notch1

The Scid mouse shows a severe combined immunodeficiency because it lacks both T- and B-cell functions caused by highly repressed V(D)J recombination in immunocyte-development due to drastic reduction of ability to rejoin coding segments by DNA-dependent protein kinase (DNA- PK). For the analysis of effects of *Scid* mutation on radiation- carcinogenesis, Scid (*Scid* homozygous), C.B-17 (wild-type) and their (C.B-17xScid)F1 hybrid (*Scid* heterozygous) were used.

Regarding acute effects of ionizing radiation, Scid mice were more sensitive than F1 and wild- type mice, not only *in vivo*, but also *in vitro*. In long-term carcinogenesis experiments, groups of Scid, C.B-17 and F1 mice were exposed to a single whole-body radiation with 1 - 3 Gy gamma rays. Most irradiated Scid mice died with thymic lymphomas 20 to 40 weeks after irradiation. By contrast, C.B-17 and F1 mice survived longer, and incidences of thymic lymphomas were low.

Oncogenes involved in thymic lymphoma development were analyzed. The possible role of *Ras* activation in spontaneous and radiation-induced lymphomas of the Scid mice was examined. However, neither activated K-*Ras* nor N-*Ras* genes were detected in spontaneous lymphomas and no N-*Ras* mutations were detected in radiation-induced lymphomas. Although K-*Ras* mutations increased as a function of dose in radiation-induced lymphomas, they were rather infrequent.

Rearrangements of *Notch1* gene were analyzed using Scid and wild-type thymic lymphoma cell lines established in this laboratory. About one third of radiation-induced Scid thymic lymphomas exhibited DNA rearrangements whereas one fifth of wild-type lymphomas displayed abnormalities. Analysis of abnormalities revealed that intragenic deletions and insertions of IAP or MuLV were observed in thymic lymphomas derived from Scid and wild-type mice. These data suggest that the defective *Scid* gene participates in the formation of DNA rearrangements in *Notch1* gene and that dysregulated *Notch1* plays a role in murine thymic lymphomagenesis.

It may be concluded that there is a close relationship between radiosensitivity and development of thymic lymphomas in *Scid* homozygotes. Development of thymic lymphomas in Scid mice may correlate with reduced DNA-PK activity that is high in the thymus as compared with other organs, and might correlate with an increase in the yield of deletion or insertion in oncogene(s) rather than point mutation

24 .Radiation-Associated Loss of Heterozygosity at Ikaros Allele and Ikaros Mutation in Murine Thymic Lymphomas

Yoshiya Shimada, Mayumi Nishimura and Shizuko Kakinuma

***Keywords*:** Ikaros, LOH, thymic lymphomas

Ionizing radiation is a potent carcinogenic agent. In order to find the tumor suppressor locus associated with radiation carcinogenesis, we determined the frequency and distribution of loss of heterozygosity (LOH) of X-ray-induced thymic lymphomas (TLs) of B6C3F1 mice using 58 microsatellite markers. We found a unique locus with frequent LOH in the centromeric region of chromosome 11 of X-ray-induced lymphomas. This locus has never been observed to be similarly altered in either *N*-ethylnitrosourea-induced or spontaneously developed lymphomas, suggesting radiation specific molecular alteration. The LOH patterns of individual TLs indicated that the common region of LOH was located within 1.6 cM between *D11Mit62* and *D11Mit204*, a region syntenic to human chromosome 7p13. Linkage analysis revealed that the markers of the common LOH region were genetically linked to *Ikaros*. *Ikaros* encodes a Krüppel-type zinc- finger transcription factor that plays a critical role in both lineage commitment and differentiation of lymphoid cells. We next aimed to delineate the *Ikaros* inactivation with special reference to the LOH status, and to determine the relative contribution of each type of *Ikaros* inactivation in radiation-induced TLs. We demonstrated that *Ikaros* was frequently altered (in 50% of TLs), and that its inactivation was caused by a variety of mechanisms, which came under one of the following four categories: (i) null expression (14%); (ii) expression of unusual dominant-negative isoforms, (11%); (iii) amino acid substitutions in the N-terminal zinc-finger domain for DNA binding caused by point mutations (22%); (iv) lack of the *Ik-1* isoform due to the creation of a stop codon by insertion of a dinucleotide in exon 3 (3%). The null expression, amino acid substitutions, and dinucleotide insertion inactivation types were well correlated with LOH at the *Ikaros* allele (86%), and were consistent with Knudson's two hit-theory. On the other hand, TLs expressing dominant-negative *Ikaros* isoforms retained both alleles. These results indicate that *Ikaros* inactivation takes place by a variety of mechanisms in radiation- induced murine TLs and is frequently associated with LOH, this association depending on the type of inactivation.

Publications:

Shimada, Y., Nishimura, M., Kakinuma, S., Okumoto, M., Shiroishi, T., Clifton, K.H. and Wakana, S.: *Radiat. Res*. 154, 293-300, 2000.

Shimada, Y., Nishimura, M., Kakinuma, S., Takeuchi, T., Ogiu, T., Suzuki, G., Nakata, Y., Sasanuma, S., Mita, K. and Sado, T.: *Int. J. Radiat. Biol*. 77, 465-473, 2001.

25. RT-Nested PCR diagnosis of Mouse Hepatitis Virus Contamination in Immunocompromised mouse Population

Hiromi Takahashi-Omoe, Satoru Matsushita and Akihiro Kawano

***Keywords*:** mouse hepatitis virus, immunocompromised mouse, RT-nested PCR

Mouse hepatitis virus (MHV) is a positive-strand RNA virus in the family *Coronaviridae* and is known to be the most prevalent virus infecting laboratory mice. MHV infection is a serious problem, because MHV is a fatal pathogen for immunocompromised mice, such as nude mice and severe combined immunodeficient (Scid) mice.

MHV infection in a mouse population is usually diagnosed serologically by such methods as enzyme linked immunosorbent assay (ELISA) and immunofluorescent staining. These methods, however, cannot be applied to the detection of MHV infection in immunocompromised mice, since they do not develop normal antibody responses. When serologic methods are not applicable, the infectious viruses or viral genes should be directly detected. Therefore, we have developed a reverse transcription plus nested polymerase chain reaction (RT-nested PCR) system combined with southern blot analysis of PCR. The first and second PCRs were designed to amplify 989 bp and 575 bp DNA fragments from the coding region of MHV mRNA7, and the southern blot was designed to confirm the specificity of the first PCR product. Using these methods, mouse samples dissected from necrotic foci on the liver of thirteen C.B-17/Icr-*scid/scid* mice and six BALB/c-*nu/nu* mice were tested. The results gained from RT-nested PCR combined with southern blot analysis demonstrated that no tested mice were infected by MHV. We suggest that the methods employed in this study are useful for MHV detection in specimens that are obtained from immunocompromised mice.

26. Comparison of Respiratory Lesions in C3H and C3H-Scid Mice Experimentally Infected with CAR Bacillus

Akihiro Kawano, Satoru Matsushita, and Hiromi Takahashi-Omoe

***Keywords*:** CAR bacillus, respiratory lesion, Scid mice

Cilia-associated respiratory (CAR) bacillus is an unclassified, gram-negative, filamentous bacterium that was tentatively designated in 1985 as one of the agents that cause chronic respiratory diseases in laboratory rodents. CAR bacillus infection is characterized by histological lesions consisting of attachment of the organisms on the ciliated epithelium of the respiratory tract and peribronchial cuffing with round cells such as lymphocytes and plasma cells, accompanied by mucopurulent exudate filling the bronchial lumen and leukocytic infiltration in the lamina propria.

To understand the mechanisms of anti-CAR bacillus host defenses, we infected C3H/He (C3H) mice and C3H/He-*scid*/*scid* (Scid) mice, which lack functional T and B lymphocytes and consequently show severe combined immunodeficiency, with the SMR strain of CAR bacillus. 18 mice of each strain were inoculated intranasally with a lung homogenate containing the SMR strain, and 18 mice of each strain were inoculated with sterile PBS. Three inoculated mice and three control mice of each group were euthanatized on days 4, 7, 14, 21, 28 and 56 postinoculation (PI). The body weight of C3H mice inoculated with the SMR strain decreased from day 28 PI as compared with that of control mice. However, the body weight of inoculated Scid mice from day 21 PI was less than that of the Scid mice on day 0 PI. Histologically, CAR bacilli were observed on the ciliated epithelial cells of trachea from day 7 PI and those of bronchi from day 14 PI in each group. Although CAR bacilli increased with time after inoculation, the number of CAR bacilli was not different between the groups throughout the experimental period. In the trachea, round cell infiltration was observed in the tracheal lamina propria of C3H mice from day 7 PI and the lesions progressed with time. Mucopururent exudate was mild in the tracheal lumen throughout the period. In Scid mice, however, mucopururent exudate became severe with time and round cell infiltration was slight. In the lungs, peribronchitis with peripheral lymphoid follicles was observed in C3H mice from day 21 PI and these lesions developed extensive mucopurulent bronchopneumonia and atelectasis with time. In Scid mice, peribronchitis was mild and peripheral lymphoid follicles were not shown.

Neutrophilic exudate in the bronchial lumen was more severe than that of C3H mice, but mucopurulent bronchopneumonia and atelectasis were intensive as compared with those of C3H mice. It is suggested that Scid mice may be affected more severely than C3H mice in CAR bacillus infection, because the body weight of Scid mice decreased markedly. The respiratory lesions of Scid mice are characterized by the following findings as compared with those of C3H mice: (i) milder peribronchitis with poor round cell infiltration, (ii) more severe neutrophilic exudate in the lamina of affected airways, and (iii) more intensive mucopurulent bronchopneumonia.

27. Therapy of Radiation Damage to Normal Tissues with Selective Inhibitors of Cyclooxygenese-2: YM177 Tends to Reduce Mouse Mortality from Haemopoietic Syndrome

Itsuro Tamanoi, Masatoshi Itoh[1], Hisamasa Joshima, Tatsuo Hayao and Adam S.Michalowski[2] ([1] Cyclotron Radioisotope Center, Tohoku Univ.; [2]8 Ollgar Close, London,U.K.)

***Keywords*:** cyclooxygenase, NSAID, COX-1, COX-2, haemopoietic syndrome

Various non-steroidal anti-inflammatory drugs (NSAID) have been successfully used in animals and humans to alleviate ionizing radiation-induced reactions in normal tissue. They act by interfering primarily with cyclooxygenase (COX)-1, a constitutive enzyme normally present in most types of cells. NSAID are less effective as inhibitors of COX-2. For this reasons the drugs, when administered repeatedly in high therapeutic doses, cause serious side-effects affecting especially the stomach. New generation NSAID selectively inhibit COX-2 while sparing COX-1 and thus exert their anti-inflammatory action without causing damage to the gastro-intestinal tract. We have begun studying therapeutic effectiveness of these highly selective COX-2 inhibitors, that is, YM-177(4-[5-(4-methylphenyl)-3-(trifluoromethyl)-1 H-pyrazole-1-yl] benzensulfonamide from Yamanouchi Pharmaceutical Co.) in reducing undesirable radiation reactions. YM-177 was administered in drinking water to C57BL/6J male mice irradiated with
5.5 to 6.5 Gy to achieve a constant level of the inhibitor while measuring its intake. The treatment was aimed at a specific humoral component of the radiation reactions only. Accordingly, it was began 24 h after whole body irradiation to avoid interference with an instantaneous reduction in the number of clonogenic cells and rapid intracellular repair process. YM-177 was given until the end of the month long observation period following radiation exposure. Mouse survival rate (LD50/30) and duration of survival of those animals which succumbed due to haemopoietic failure within the first post-irradiation month served as criteria of therapeutic effectiveness of YM-177 administered in doses ranging from 0.17 to 3.4 mg/kg· day. Only the two lowest doses of YM-177 significantly reduced mouse mortality suggesting that in whole body-irradiated mice endogenous prostanoids synthesized with the involvement of
COX-2 can contribute to death from haemopoietic syndrome.

28. The Nucleotide Sequence of Schizosaccha- romyces pombe Chromosome III

Mitsuoki Morimyo, Etsuko Hongo, Go Kenu, Tomoyasu Higashi, Yukari Ito, Yumiko Yoshida, Masahiro Ajimura, Etsuko Shiroma, Kazuei Mita, Kimihiko Sugaya, Shunichi Sasanuma and Izumi Matsumoto

Keywords**:** *S. pombe cDNA, BAC clone, shotgun sequencing, gene expression map*

In a study of the structure and function of the housekeeping genes of eukaryote, we chose *Schizosaccharomyces pombe (S. pombe)* as a model organism. It is assumed to have 6,000 genes and the genome size of 14 megabases (Mb) compared to 40,000 genes and 3,000 Mb for humans. In spite of the greater numbers for humans, *S. pombe* can be used as a model organism for humans, because its genes are similar to human genes which can be normally expressed in yeast, its housekeeping genes are conserved through eukaryotic evolution, and many of its genes have introns which make cDNA sequences essential to determine physical organization of genes from the genomic DNA sequence. Moreover, the functions of *S. pombe* genes are easily identified by disrupting them with homologous recombination.We have analyzed 12,000 cDNA clones made by mRNA prepared from late log phase cells of *S. pombe* and identified over 2,500 genes (900 similar clones with known genes and 1800 newly found clones). Among the cDNA clones, 8,118 were deposited with the DDBJ and put on the ftp site of NIRS. By using these cDNA clones mapped on the chromosome III of *S. pombe*, we made a BAC contig map of chromosome III. A minimum set of 20 BAC clones covering the whole chromosome III was selected for the shotgun sequencing. The BAC DNA was partially digested by an endonuclease, followed by the fractionation in a sucrose gradient sedimentation and DNA fragments ranging from 1 to 3 kbp were recovered for sequencing at a redundancy of 6-10. Except for the tandem repeats of rDNA regions at both ends, we determined the DNA sequence of chromosome III which was 2,482,668 bp without interruption. The centromere contained 10 repeats of 6.6 kbp unit length fragments. We identified an ORF found in the assembled DNA sequence as a gene by using the gene-finding program developed for *S. pombe* and a homology search in protein databases and our *S. pombe* cDNA database (http://133.63.36.123). In all, we found 1162 protein-coding genes on chromosome III. Therefore, average gene length was estimated to be 2137 bp. Combining the information about gene location on the chromosome obtained from genome sequencing and its relative gene expression got from cDNA analysis with the genetic map, we made the gene expression map of *S. pombe* chromosome III.

Publications

Morimyo, M., Mita, K., Hongo, E., Ajimura, M., Higashi, T., Sugaya, K., Inoue, H., Yamauchi, M., Tsuji, S., Saito, T., Ito, H., Sasanuma, S., Nohata, J., Kimura, T., Ishihara, Y., Hattori, A., Hayashi, A., Koike, Y., Shiroma, E.: *Mol. Bio. Cell*, 11 suppl., 1572(2000).

Morimyo, M.: UNESCO-EOLSS (in press).

29. A Mutation in the Largest (Catalytic) Subunit of RNA Polymerase II and Its Relation to the Arrest of the Cell Cycle in G1 Phase

Kimihiko Sugaya, Shun-ichi Sasanuma, Peter R. Cook*, and Kazuei Mita (*The Sir William Dunn School of Pathology, Oxford Univ., UK)

***Keywords*:** *RNA polymerase II, temperature-sensitive mutant, cell cycle, hemizygosity, sequencing*

Transcriptional activity of RNA polymerase II is modulated during the cell cycle. We previously identified a temperature-sensitive mutation in the largest (catalytic) subunit of RNA polymerase II (RPB1) which causes cell-cycle arrest and genome instability. We have characterized a different cell line that has a temperature-sensitive defect in cell cycle progression, and found that it also has a mutation in RPB1. The temperature-sensitive mutant, tsAF8, of the Syrian hamster cell line, BHK21, arrests at the non-permissive temperature in the mid-G1 phase. The RPB1 in tsAF8, which is found exclusively in the nucleus at the permissive temperature, is also found in the cytoplasm at the non-permissive temperature. Comparison of the DNA sequences of the RPB1 gene in the wild-type and mutant shows the phenotype results from a (hemizygous) C-to-A variation at nucleotide 944 in one RPB1 allele; this gives rise to an ala-to- asp substitution at residue 315 in the protein. Aligning the amino acid sequences from various species reveals that ala315 is highly conserved in eukaryotes.

30. Dimerization and Nuclear Localization of Ku70 and Ku80 Proteins

Manabu Koike, Tadahiro Shiomi, and Aki Koike

Keywords*: *Ku70, Ku80, dimerization, nuclear localization signal, GFP

Ku, a heterodimer of Ku70 and Ku80, plays a key role in multiple nuclear processes, e.g. DNA repair, chromosome maintenance, and transcription regulation. Heterodimerization is essential for Ku-dependent DNA repair in vivo, although its role is poorly understood. Some lines of evidence suggest that heterodimerization is required for the stabilization of Ku70 and Ku80.

Here we show that the heterodimerization of these Ku subunits is important for their nuclear entry. When transfected into Ku-deficient xrs-6 cells, exogenous Ku70 and Ku80 tagged with green fluorescent protein (GFP) accumulated into the nucleus, whereas each nuclear localization signal (NLS)-dysfunctional mutant was undetectable in the nucleus, supporting the idea that each Ku can translocate to the nucleus through its own NLS. On the other hand, the nuclear accumulation of each NLS-dysfunctional mutant was markedly enhanced by the presence of an exogenous wild-type counterpart. In Ku-expressing HeLa cells, each NLS-dysfunctional mutant, as well as wild-type Ku70 and Ku80, was still detectable in the nucleus, whereas the double mutant of each Ku subunit, with decreased functions of both nuclear targeting and dimerization, was undetectable there. Our results indicate that each Ku subunit can translocate to the nucleus not only through its own NLS, but also through heterodimerization with each other.

In conclusion, we have shown a novel role for the heterodimerization of Ku70 and Ku80. Ku70 and Ku80 appear to have multiple functions as a monomeric form and a heterodimeric form.

There are at least two nuclear translocation pathways of each Ku subunit. We speculate that the Ku subunits may use the NLS-dependent nuclear translocation pathway to perform some function(s) independent of each other and Ku subunits may use the nuclear translocation pathway through heterodimerization to perform the same functions dependent on each other.

The control mechanism for nuclear localization of Ku70 and Ku80 plays, at least in part, a key role in regulating the physiological function of Ku in vivo. Further studies to elucidate the molecular mechanisms of nuclear transport of the Ku subunits will lead to a better understanding of the regulation mechanism of nuclear proteins.

Publications:

1) Koike, M., Shiomi, T., and Koike, A.: J. Biol. Chem. 276, 11167-11173, 2001.

2) Koike, M., Kuroiwa, A., Koike, A., Shiomi, T., and Matsuda, Y. : Cytogenetics and Cell Genetics. in press.

3) Koike, M., Shiomi, T. and Koike, A. Biochem. Biophys. Res. Commun. 276, 1105-1111, 2000.

31. Phosphorylation Sites of NPAT by CyclinE/CDK2 Complex

Yasuharu Ninomiya, Akiyo Nisiyama, Masashi Sagara, Yoichi Taya* and Takashi Imai (* Natl. Cancer Center Research Institute)

***Keywords*:** *NPAT, ATM, cyclin/CDK, phosphorylation*

The characteristic most widely studied in human genetic disorder ataxia telangiectasia (AT) is hypersensitivity to ionizing radiation. AT responsible gene, ATM could enhance survival of AT cells after irradiation exposure, decrease radiation-induced chromosome aberrations, reduce radioresistant DNA synthesis, and partially correct defective cell cycle checkpoints. We identified NPAT gene from 0.5 kb upstream of ATM. Because these two genes were transcribed in opposite direction and because our reporter assay revealed that the 0.5 kb nucleotide sequence flanked by the two genes had bi-directional promoter activity, we examined a possibility that the NPAT gene is also related to cellular responses to DNA damage or cell cycle control. And by retroviral study, the NPAT gene seems to have important role at cell cycle control. To investigate relationship between NPAT function and cell cycle control after irradiation, we first analyzed mRNA- and/or protein-expression pattern of the NPAT in each stage of the cell cycle in normal human fibroblast cells after irradiation. We found that both mRNA and protein of NPAT were not induced through cell cycle after 2 Gy irradiation.

Because NPAT was predicted to have multiple phosphorylation sites by protein kinases, which are function for cell cycle control, in vitro phosphorylation sites of NPAT by cyclin/CDKs using the GST fusion protein were examined. We identified the N-terminal 126 amino acid-region of NPAT was phospholylated by mainly both cyclin A/CDK2 and cyclin B/cdc2 while Thr^{1359} at C- terminal region of NPAT was phosphorylted by three types of cyclin/CDK complexes, cyclin A/CDK2, cyclin B/cdc2 and cyclin E/CDK2. Both Ser^{775} and Ser^{779} at the central region of NPAT were phosphorylated by mainly cyclin E/CDK2. In vitro phosphorylation by cyclin D1/CDK4 was not observed at any site of NPAT. These data suggest that the each phosphorylation site of NPAT was specifically recognized by cell cycle specific cyclin/CDKs and the phosphorylation of NPAT may be regulated through cell cycle specific manners.

32. Analysis of Functional Regions for the Nuclear Localization of NPAT

Masashi Sagara, Yasuharu Ninomiya, Hiroko Ito and Takashi Imai

Keywords**:** *NPAT, nuclear localization signal, basic amino acid clusters*

NPAT plays a role in S phase entry as a substrate of cyclin E-CDK2 and activation of histone gene transcription. Although previous amino acid sequence analysis suggested that NPAT contains three clusters of basic residues, ^{1368}KKRK^{1371}, ^{1397}KKKK^{1400} and ^{1402}KKKK^{1405} at the carboxyl terminus, resembling the classical nuclear localization signal (NLS) motifs, no experimental data have showed these predictive NLS motifs are functional. To investigate whether these basic amino acid clusters are effective for nuclear transport of the protein, a green fluorescent protein-NPAT (GF-NP) was constructed. The full coding region of NPAT was amplified by PCR and fused in-frame to pCMX-SAH/Y145F to generate GF-NP. The fusion gene was transfected into cultured mammalian cells and the cells fixed with 4% paraformaldehyde.

The image of the GF-NP was obtained using a conventional microscope equipped with a fluorescein isothiocyanate filter set. After transfection of the fusion gene containing the full coding region of NPAT into the cells, the GF-NP product was detected clearly in the nucleus. When the basic amino acid clusters at the carboxyl terminus were mutated by the PCR-based site directed mutagenesis method, ^{1368}KKRK^{1371} to ^{1368}KELK^{1371}, ^{1397}KKKK^{1400} to ^{1397}KELK^{1400} and ^{1402}KKKK^{1405} to ^{1402}KLKK^{1405} respectively, most of the mutants could not be retained in nucleus. A truncated fusion protein, which lacked all of the three basic amino acid-clusters, i.e. ^{1368}KKRstop^{1371}, was also distributed throughout the cytoplasm and nucleus. These data suggest that all three clusters of basic residues in NPAT are essential for targeting the nucleus.

33. Analyses of Transcriptional Control Region of NPAT and ATM Genes

Masashi Sagara, Yasuharu Ninomiya, Hiroko Ito and Takashi Imai

Keywords**:** *NPAT, ATM, transcription, Promoter*

NPAT has been identified as a gene closely linked to the ATM gene on human chromosome 11q23. Because these two genes are transcribed in opposite directions and share a 0.5kb 5' upstream sequence, we investigated the nucleotide sequence essential for the expression of ATM and NPAT genes. Both the 5'-flanking region (approximately 2.8kb) of NPAT and that (approximately 2.2kb) of ATM were amplified with each specific primer set from human genomic DNA by PCR. The PCR-amplified DNA fragments were subcloned and the structure of the clones was confirmed by sequencing. These plasmids covered the region containing the sequence of exon from 1a to 4 and intron from 1 to 4 of the ATM gene and exon 1 and a portion of the first intron of NPAT gene. The cloned fragments were sequentially deleted and fused with the coding region of the luciferase gene in the promoterless reporter plasmid pGL3- basic. Each of these recombinant DNAs was then used for transient gene expression experiments by transfection into HeLa cells and the resultant luciferase activity was measured. The data indicated that the region from -350 to +10bp upstream of NPAT gene is essential for NPAT transcription and that the region from -709 to +11bp upstream of ATM gene is required for ATM transcription. Previous nucleotide sequence analysis showed that the region essential for both gene transcriptions contains potential binding sites for multiple transcription factors such as Sp1, CCAAT-box binding protein, E2F and CREB. To investigate the significance of the CRE-like site and two E2F-like sites, these sites were mutated and the fragments were fused to the luciferase gene in sense or antisense orientations relative to both NPAT and ATM genes. The NPAT promoter activities decreased from 100% (wild-type) to 82% (E2F-like site I), to 57% (E2F-like site II), to 42% (E2F-like site I and E2F-like site II) and to 10% (CRE-like site). The ATM promoter activities also decreased from 100% (wild-type) to 57% (E2F-like site I), to 75% ((E2F-like site II), to 47% (E2F-like site I and E2F-like site II) and to 24% (CRE-like site).
Therefore, the two E2F-like sites and the CRE-like site in the common franking region of the genes are required for both transcriptions. These results suggested that the 0.5kb nucleotide sequence flanked by the two genes has bi-directional promoteractivity.

34. Brain Structures of a Medaka Mutant, el (eyeless), in Which Eye Vesicles Do Not Evaginate

Yuji Ishikawa, Masami Yoshimoto, Naoyuki Yamamoto, and Hironobu Ito

***Keywords*:** *brain, eye, development, mutation, mutant, vertebrate, teleost fish, medaka*

Eye development and brain structures of a mutant teleost fish were investigated. The *el* (*eyeless*) mutation in medaka (*Oryzias latipes*) is recessive and affects eye formation, in the most severe cases, it results in absence of the eyes. Developmental studies revealed that normal eyeballs are not formed in the *el* mutant embryos but small optic cup-like structures differentiate *in situ* in the walls of the prosencephalon without evagination.

The anophthalmic *el* homozygous fish hatched normally, although they did not respond behaviorally to visual stimuli. A small fraction of them were grown to adulthood. In the adult anophthalmic *el* homozygous fish, the brain exhibited abnormalities in several subdivisions. A pair of small abnormal protrusions was observed on the surface of the ventral telencephalon and preoptic area. Immunocytochemistry using a rhodopsin monoclonal antibody showed that opsin-positive cells were present in the abnormal structures. Bodian staining showed that the optic nerves were present near the abnormal structures, although the number of optic nerve fibers was extremely small. The optic tectum was extremely small and the thickness of the stratum opticum and stratum fibrosum et griseum superficiale was reduced. These behavioral and morphological observations suggest that the adult anophthalmic *el* homozygous fish are functionally blind, although small retina-like structures were partially differentiated and persist in the adult fish brain. Moreover, the adult anophtalmic *el* homozygous fish were infertile, and the sizes of the hypophysis and the hypothalamus were reduced. Thus, the *el* mutation affects not only brain structures that are related to the visual system, but also those related to the reproductive system.

Publication:

Ishikawa, Y.: *Bioessays*, 22, 487-495, 2000.

35. Cryopreservation and Transport of Mouse Spermatozoa at -79°C

Masanori Okamoto, Naomi Nakagata[1], and Yutaka Toyoda[2] ([1]Kumamoto Univ.; [2]Obihiro Univ.)

***Keywords*:** *cryopreservation, in vitro fertilization, mouse spermatozoa, transport*

Since the first reports of successful mouse sperm cryopreservation, mouse spermatozoa have also been successfully stored at -196°C, as have various other species. If frozen spermatozoa can survive cryopreservation at around -80°C for relatively long periods of time, storage and transport of mouse spermatozoa can be simplified, allowing for more widespread use in biomedical research. In the present study, two experiments were carried out, i.e., we examined the fertilizing ability of frozen spermatozoa which had been maintained at -79°C for relatively long periods of time and transported by packing in dry ice.

In experiment 1, spermatozoa obtained from adult Jcl:ICR male mice were frozen and stored in an ultra-low temperature freezer maintained at -79°C from 1 week to 8 months. ICR mouse oocytes were inseminated with frozen-thawed spermatozoa. *In vitro* fertilization rates of the frozen-thawed sperm after 1 week and 4 months of storage were high at 71 and 71%, respectively. These values did not differ significantly from the value (73%) of the control stored at -196°C. In contrast, the 8-month storage rate was significantly lower at 51%. In experiment 2, frozen spermatozoa obtained from adult Jcl:BDF1 male mice were transported in a Styrofoam box packed in dry ice over a 3-days period. After transport, ICR mouse oocytes were inseminated with frozen-thawed spermatozoa. Table 2. summarizes the results for sperm motility, *in vitro* fertilization and production of normal young with frozen-thawed mouse sperm after transport at -79 and -190°C. *In vitro* fertilization rate of frozen-thawed spermatozoa after transport at -79°C was high at 88%, which was not significantly different from that (84%) of the transported control at -190°C. After transferring two-cell embryos derived from frozen spermatozoa to the recipients, 37-62% of the embryos developed into offspring in both experiments.

These results indicate that mouse spermatozoa can survive cryopreservation for 4 months in an ultra-low temperature freezer and transport by packing in dry ice at -79°C. Liquid nitrogen containers and dry shippers are not always available in all laboratories, but ultra-low temperature (-80°C) freezers and dry ice are found in most major laboratories. The results obtained for the present method demonstrate the feasibility of sperm cryopreservation and transport at -79°C. This method is simple and convenient for preserving and transporting spermatozoa. For transport at -190°C, a dry shipper has to be used to transport frozen spermatozoa and it has to be returned to the consigner. In contrast, the containers holding frozen samples do not need to be returned in cases where dry ice is used. Thus, transport by packing in dry ice at -79°C is much easier than that by a dry shipper. The storage and transport of mouse spermatozoa can be simplified, thus allowing for the wider utilization of

transgenic mice in biomedical research. We believe that the present method of transporting frozen spermatozoa will enable widespread exchange of transgenic mice between laboratories.

Publication:

Okamoto, M., Nakagata, N. and Toyoda, Y.: *Exp. Anim.,* 50, 83-86, 2001.

Table 2. Sperm motility, in vitro fertilization and production of normal young with frozen-thawed mouse spermatozoa after transport by packing in dry ice and dry shipperspermatozoa after transport by packing in dry ice and dry shipper

Temperature during transport (℃)	Sperm motility after thawing*	No. of oocytes fertilized/no. of oocytes examined# (%)	No. of oocytes developing to the two-cell stage# (%)	No. of parturition/no. of recipients	No. of live young/no. of embryos transferred# (%)
-79(Dry ice)	40-50	84/ 95 (88.4) a	84 (88.4)	4/5	52/ 84 (62.0)
-190(Dry shipper)	40-50	86/102(84.3) a	86 (84.3)	5/6	54/86 (62.7)

Cryopreserved BDF1 mouse spermatozoa were packed in straws and transported for 3 days. ICR mouse oocytes were inseminated with frozen-thawed spermatozoa. *Percentages of actively motile sperm were based on counts in the sperm suspension. # Based on data from two replicate experiments. a,Values with the same superscripts are not significantly different (P>0.05).

36. Effective Timing of Initial Administration of Ca-DTPA for Removal of Inhaled Plutonium Nitrate in Rats

Satoshi Fukuda, Haruzo Iida, Yuji Yamada, Kumiko Fukutsu and Akira Koizumi

***Keywords*:** *Ca-DTPA, plutonium nitrate, first injection time, removal effect, inhalation, rats*

The effective timing of the initial injection of Ca-DTPA and the subsequent early treatment for removal of inhaled plutonium nitrate were studied in rats. One group of rats that had inhaled plutonium nitrate received an intraperitoneal injection of Ca-DTPA at a daily dose of 150 μmol/kg for 3 days, beginning at 0.5, 1, 2, 6, or 12 h after inhalation of plutonium; a second group received an injection at a daily dose of 30 μmol/kg (the daily recommended dose for humans), beginning 1h after plutonium inhalation. A third group served as the control with no treatment. During the experiment, the urine and feces were collected every day; on day 4, the rats were sacrificed and dissected to measure plutonium concentration in blood and various organs.

The first administration of Ca-DTPA (150 μmol/kg) at 1-6 h after inhalation initiated an increase in urinary plutonium excretion during the first 24 h following inhalation and also resulted in significant increases of urinary plutonium excretion for up to 3 days following the treatment (Fig.12). The increase was measured in comparison to the urinary levels of the rats that had treatment initiated at 0.5 h or 12 h. In the group that was given 30 μmol/kg Ca-DTPA, higher urinary plutonium excretion was found, compared to the control group; however, these levels were lower than those of the group that was administered a dose of 150 μmol/kg. Although the retention rates in various organs of the Ca-DTPA treatment groups varied compared to the corresponding organs in the control group, the changes were very slight. The results indicate that Ca-DTPA administration within 1-6 h after exposure to plutonium is effective to increase the urinary excretion of plutonium in rats

Publication:

Fukuda, S., Iida, H., Yamada, Y., Fukutsu, K. and Koizumi, A.: *J. Health Phys.*, 36, 25-30, 2001.

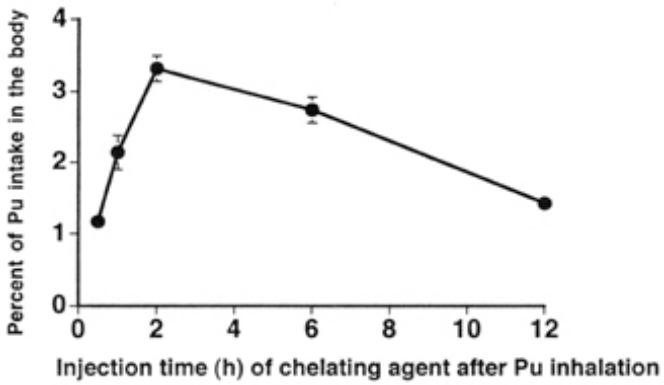

Fig.12. Amount of plutonium excreted in the urine for 3 days after Ca-DTPA injection. Each vertical bar represents the mean ± 1SE.

37. Serotonin 5-HT2 Receptors in Schizophrenic Patients as Studied by Positron Emission Tomography

Yoshiro Okubo, Tetsuya Suhara, Kazutoshi Suzuki, Kaoru Kobayashi, Osamu Inoue, Omi Terasaki, Yasuhiro Someya, Takeshi Sassa, Yasuhiko Sudo, Eisuke Matsushima, Masaomi Iyo, Yukio Tateno and Michio Toru

Keywords**:** *5-HT_2 receptors, positron emission tomography, [^{11}C]N-methylspiperone, schizophrenia, prefrontal cortex*

Using positron emission tomography (PET) and [^{11}C]N-methylspiperone (NMSP), we examined 5-HT_2 receptors in the cortex of schizophrenic patients in whom we had previously observed decreased prefrontal D1 receptor binding. The subjects were 10 neuroleptic-naive schizophrenic patients, 7 schizophrenic patients who were drug-free but had previously been treated with neuroleptics, and 12 normal controls. A non-significant trend towards decreased prefrontal [^{11}C]NMSP binding was observed in the neuroleptic- treated patients, suggesting a possible effect of previous neuroleptic treatment on the alteration in cortical 5-HT_2 function. However, the neuroleptic-naive patients showed no noticeable difference in cortical [^{11}C]NMSP binding compared to the controls. Our results do not rule out the role of 5-HT_2 function as a crucial site of therapeutic activity of schizophrenia, but they do suggest that cortical 5-HT_2 receptors might not be primarily involved in the pathophysiology of schizophrenia.

The possible role of 5-HT dysfunction in the pathophysiology of schizophrenia has gained considerable attention over the last several years. This is partly due to the clinical efficacy of atypical antipsychotic drugs with relatively weak dopamine D2 antagonistic potency but high affinity for 5-HT_2 receptors. Further, it has been hypothesized that dopamine receptor blockade would reduce positive symptoms in schizophrenia, while blockade of 5-HT_2 receptors would reduce negative symptoms and decrease extrapyramidal side effects. In addition, postmortem studies have reported decrease 5-HT_2 receptor densities in the prefrontal cortex of schizophrenic patients.

Several radioligands have been proposed for PET for the examination of 5-HT_2 receptors in the living human brain. Recently, two PET studies used [^{18}F]setoperone to investigate the cortical 5-HT_2 receptors in schizophrenic patients and found no difference compared to controls. These findings are in contrast to those of the postmortem studies and need to be replicated with other PET radioligands for 5-HT_2 receptors.

In our previous study on dopamine D1 and D2 receptors in schizophrenic patients, we used [^{11}C]NMSP for striatal D2 receptors and [^{11}C]SCH23390 for striatal and cortical D1 receptors. Although D1 and D2 receptors showed no changes in the striatum, D1 receptor binding in the prefrontal cortex of schizophrenic patients decreased compared to controls.

We have evaluated only the striatal [^{11}C]NMSP binding which represents dopamine D2 receptors. However, NMSP has a high affinity not only for D2 receptors, but also for 5-HT$_2$ receptors. Since the cortical D2 receptor density is very low , the cortical binding of [^{11}C]NMSP has been assumed to represent the binding to 5-HT$_2$ receptors. Thus [^{11}C]NMSP has been extensively used as a PET radioligand to investigate the cortical 5-HT$_2$ receptors.

Publication:

Okubo, Y., *et al*.: Life Sci., 66, 2455-2464, 2000.

38. Brain Cholinergic Function in Dementia with Lewy Bodies and Alzheimer's Disease as Measured by Positron Emission Tomography

Hitoshi Shinotoh, Kiyoshi Fukushi, Noriko Tanaka, Akiyo Aotsuka, Tsuneyoshi Ota, Shin-ichiro Nagatsuka, Shuji Tanada, Toshiaki Irie

Keywords**:** *positron emission tomography, cholinergic function, acetylcholinesterase, ^{11}C-MP4A, dementia with Lewy bodies, Alzheimer's disease*

Postmortem studies have demonstrated more extensive loss of cholinergic function in the cerebral cortex in dementia with Lewy bodies (DLB) than in Alzheimer's disease (AD). In the present study, we measured brain regional acetylcholinesterase (AChE) activity, an index of cholinergic function in patients with DLB and AD by positron emission tomography (PET) and a radiotracer, N-[^{11}C]methylpiperidin-4-yl acetate (MP4A).

Seven patients with DLB (4 men and 3 women; 75±6 years; NNMS score: 13±7), 36 patients with AD (17 men and 19 women; 62±8 years; NNMS score: 17±5) and 14 normal controls (NC) (9 men and 5 women; 67±10) participated in this study. A sequence of 16 PET scans was acquired covering 40 minutes after intravenous injection of ^{11}C-MP4A (approximately 20 mCi) in each subject. Arterial blood samples were collected 24 times in 15 minutes after tracer injection for measurement of total radioactivity and metabolite analysis. For quantification of AChE activity, a three-compartment kinetic model was employed to yield estimates of K_1 (transport into tissue), k_2 (tissue clearance of unchanged tracer into blood), and k_3 (hydrolysis rate of [^{11}C]MP4A by AChE, i.e. AChE activity) using the time-radioactivity curve in regions of interest in the brain and metabolite corrected arterial plasma input function.

The k_3 values in the cerebral cortex were remarkably reduced by 37% in the 7 patients with DLB ($p<0.001$ with Bonferroni correction compared with NC), and moderately reduced by 20% in the 36 patients with AD ($p<0.0001$ compared with NC). The reduction of cortical k_3 values in DLB patients was more severe than that in the AD patients ($p<0.001$).

The results suggest that the ascending cholinergic systems from the basal forebrain are more severely impaired in DLB than AD. The severe loss of cholinergic function may be related to typical symptoms such as visual hallucinations.

39. Development of an Automated System for the Quick Production of ^{13}N-labeled Compo- unds with High Specific Activity Using Anhydrous [^{13}N]NH_3

Kazutoshi Suzuki and Yuichiro Yoshida

Keywords*:*n*itrogen-13, anhydrous [^{13}N]NH_3, ^{13}N-labeled compounds, specific activity, automation*

N-13 (half-life: 9.965 min; 100% +decay) is one of the most important of all positron emitters. It has been used mostly in the chemical form [13N]NH3 or as enzymatically synthesized 13N-labeled amino acids in the field of nuclear medicine. However, in clinical applications, N-13 is of limited use compared to other positron emitters such as C-11 and F-18, mainly due to its short half-life which causes difficulties both in the synthesis of 13N-labeled compounds and in their clinical applications. N-13 may be used more widely if more 13N-labeled compounds are made available. High specific activity may also increase the applicability of 13N-labeled compounds for receptor studies with PET.

We developed an automated system (Fig.13) to realize: 1) production of an aqueous solution of [13N]NH3; 2) concentration and desiccation of the [13N]NH3 solution; 3) reaction of anhydrous [13N]NH3 with substrate; 4) purification and formulation. A 10 mM ethanol solution was saturated with pure O2 gas and then loaded into the target chamber (1.9 ml). The solution was irradiated at 17 A for 25 minutes with 18 MeV protons (15.7 MeV on target). The [13N]NH3 generated directly in the target chamber by the 16O(p,)13N reaction was concentrated on the preconditioned cation exchange column and then eluted with 30 l of 2N KOH under a He gas flow and desiccated through the small column filled with 250 mg of CaO (3 mm i.d. X 30 mm, kept at 150 oC), and introduced into a cooled reaction vessel (-20oC) containing substrate and Na2CO3 in 0.6 ml THF. The mixture was allowed to react for 30 seconds under a hot air flow (70 oC). The reaction mixture was then purified with a Sep PAK silica cartridge. The effluent was introduced into the flask of a specially designed rotary evaporator and evaporated to dryness by heating with hot air (80 oC) under reduced pressure. An i.v. injectable solution of [13N]p-nitrophenyl carbamate (as a model compound) was obtained by dissolving it in 8 ml of physiological saline solution and by filtrating the solution through a 0.22 m Millex filter into a sterilized vial. The product was analyzed by radio-HPLC using a Finepak SIL C18 column with CH3CN/0.1M-CH3COONH4/CH3COOH= 100/300/5.

In summary, we established an automated production method for the quick synthesis of 13N-labeled compounds with ultra-high specific activity using anhydrous [13N]NH3 as a synthetic precursor for practical use in PET studies. Using this system, we could obtain [13N]p-nitrophenyl carbamate ([13N]NPC) ready for i.v. injection in 5.1 + 0.1 minutes at the yield of 3.5 + 0.4 GBq, specific activity 1800 + 200 GBq/mol, and radiochemical purity >99 % (n = 3).

Publications:

Suzuki, K., Yoshida, Y., Shikano, N. and Kubodera, Y.: Applied Radiation and Isotopes, 50, 1033 - 1038, 1999.

Suzuki, K. and Yoshida, Y.: Applied Radiation and Isotopes, 50, 497-503, 1999.

Sasaki, M., Haradahira, T. and Suzuki, K.: Radiochimica Acta. 88, 217-220, 2000.

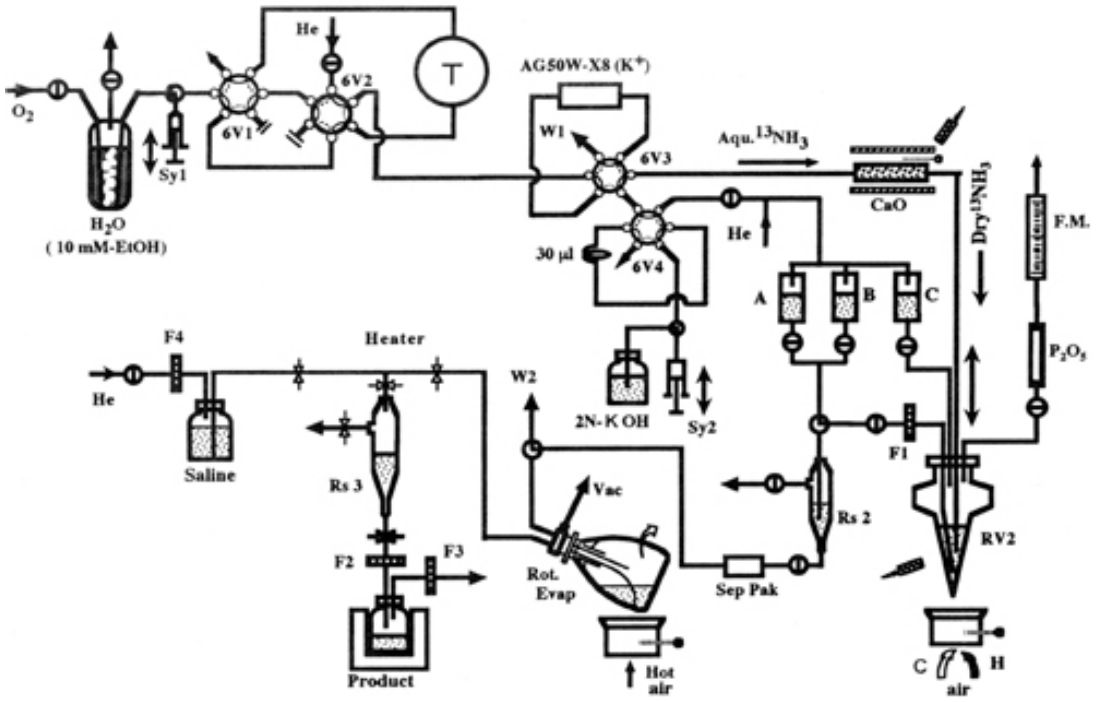

Fig.13. System diagram for the automatic production of i.v. injectable ^{13}N-labeled compounds. (Suzuki K. et al.)

40. Co-operative Study to Establish a Lung Cancer Screening System using CT Units

Toru Matsumoto, Tadaaki Miyamoto, Susumu Kandatsu, Kyosan Yoshikawa, Kiminori Suzuki[1], Yuko Sunami[1], Keiichi Nagao[2], Yoshiaki Masuda[2], Hisao Itoh[2], Hidemi Oowada[2], Takayuki Kuriyama[2], Takehiko Fujisawa[2], Takaichiro Suzuki[3], Chikazumi Kuroda[3], Hiroyuki Tajima[4], Akinobu Yoshimura[4], Tsuyoshi Yano[5], Mitsuomi Matsumoto[6], Toru Nakagawa[7], Yukinori Kusaka[7], Shinnji Yamamoto[9], Yuichi Fujino[10], Kenichi Kaneki[11],([1]Chiba Anti-TB Association; [2] Chiba University; [3] Osaka Medical Center for Cancer and Cardiovascular Diseases; [4] Nippon Medical School; [5] Arakawa City Cancer Prevention Center; [6] Tokyo Metropolitan University of Health Sciences, [7] Hitachi Health Care Center; [8] Fukui Medical School; [9] Toyohashi University of Technology; [10] NTT Cyber Solution Laboratories; [11] Hitachi Medical Corp.)

***Keywords*:** *lung cancer, CT, cancer screening*

In 1998, the total number of deaths from lung cancer in Japan (50,867) exceeded that (50,662) from stomach cancer, which was until then the most common cause of death in Japan. In this abstract, we introduce research activities concerning lung cancer screening using CT units.

Rolled chest radiophotographs or conventional chest X-rays have generally been the most common imaging means for lung cancer screening. Since it is considered difficult to identify lung tumors smaller than 2 cm in diameter without metastasis in 1990, we suggested detecting small tumors at an early stage by lung cancer screening CT (LSCT). In 1992, we developed a low-dose CT unit (tube current: 3mA - 140mA) for LSCT. In 1994 and 1996, we developed two vehicles equipped with an LSCT and initiated a study on a lung cancer screening system using two mobile CT units and two LSCTs in two cooperating institute. Approximately 23 regular researchers and 16 cooperative members have joined this research project, including experts from both medical and engineering fields.

The main aim was to establish an LSCT system that allows efficient early detection of lung cancer. At present, pilot studies of lung cancer screening using CT units are going on for the future development of a thoracic CT screening system by examining the popuation living in the Kanto and Kansai regions. Step-1 is an aplication for the secondary screening with an LSCT following mass screening with rolled chest radiographs and step-2 is application for a primary screening with an LSCT.

We have also studied the basic, technical, and epidemiologica problems incidental to the introduction of a new modality in mass screening; namely, estimation of the exposure dose of LSCT, evaluation of diagnostic efficacy of LSCT, risk-benefit analysis and cost-effectiveness analysis of the LSCT system, development of a computer aided diagnosis(CAD) system for screening of lung cancer, and construction of a network-based LSCT system, etc. (Fig.14).

We consider that the LSCT can promote early detection of peripheral lung cancers and the benefits of LSCT will exceed the risk for Japanese over 40 years of age for males and over 45 years of age for females.

Publications:

Tateno, Y., Iinuma, T., Matsumoto, T.,et al; Sin-Iryo,10: 28-32,1990 (in Japanese)

Nisizawa, K., Kawai, K., Matsumoto, T., et al; Estimation of the exposure and a risk benefit analysis for a CT system designed for a lung cancer mass screening using mobile CT., Radiat Protect Dosimet, 67(2):101-108,1996

Matsumoto, T., Miyamoto, T., Suzuki, T., et al; Elsevier Science B.V.; Excerpta Medica International Congress Series 1153: Advances in the Prevention of Occupational respiratory Diseases, Proc. of the 9th Internatonal Conference on Occupational Respiratory Diseases, 485-489, 1998

Takizawa, H., Yamamoto, Fukano, G., et al; Proc. of Image Processing, part of SPIE's Medical Imaging 2000, 1(24)(SPIE vol.3979), 998-1007, 2000

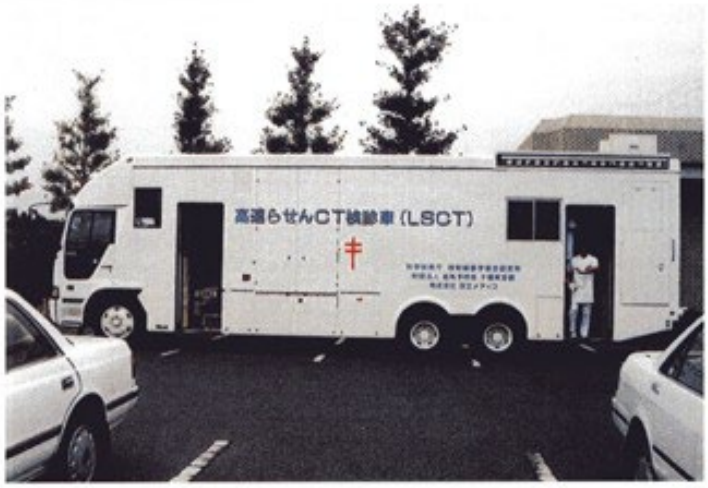

Chiba Anti-Tuberculosis Association
(Chiba : Kanto Region)

Osaka Medical Center for Cancer and
Cardiovascular Diseases (Osaka : kansai Region)

Accumulation of CT Image
at NIRS
(MO : 5.25inch)

Lung Cancer Screening
with CT at two Institutes

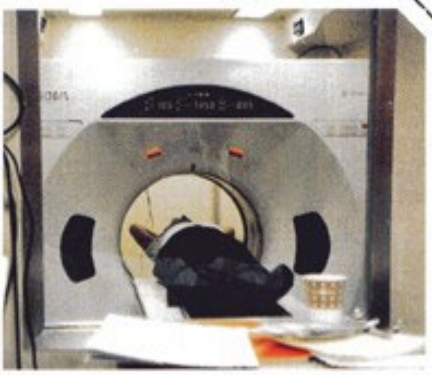

Arakawa Center Prevention Center
(Tokyo:Kanto Region)

and Hitachi Health Care Center

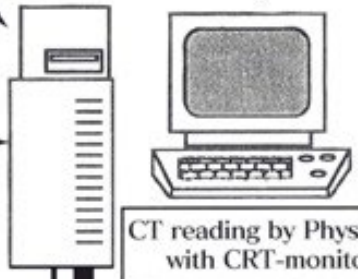

CT reading by Physician
with CRT-monitor

CAD-system (Sun Ultra2 ModeL/2200)

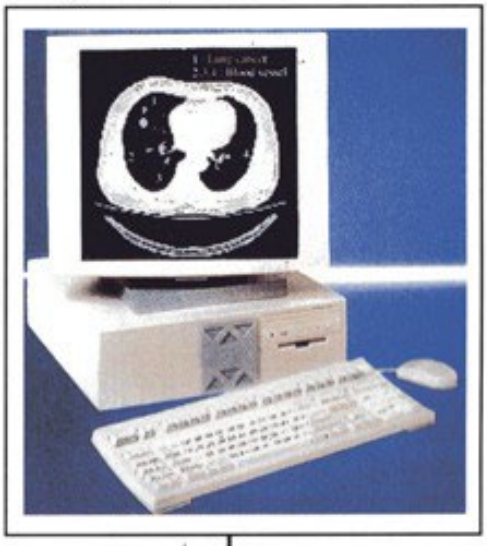

Conversion of CT
Image Format

Sending Results to
the Site of Lung
Cancer Screening

LAN

Contructed Network Reading System

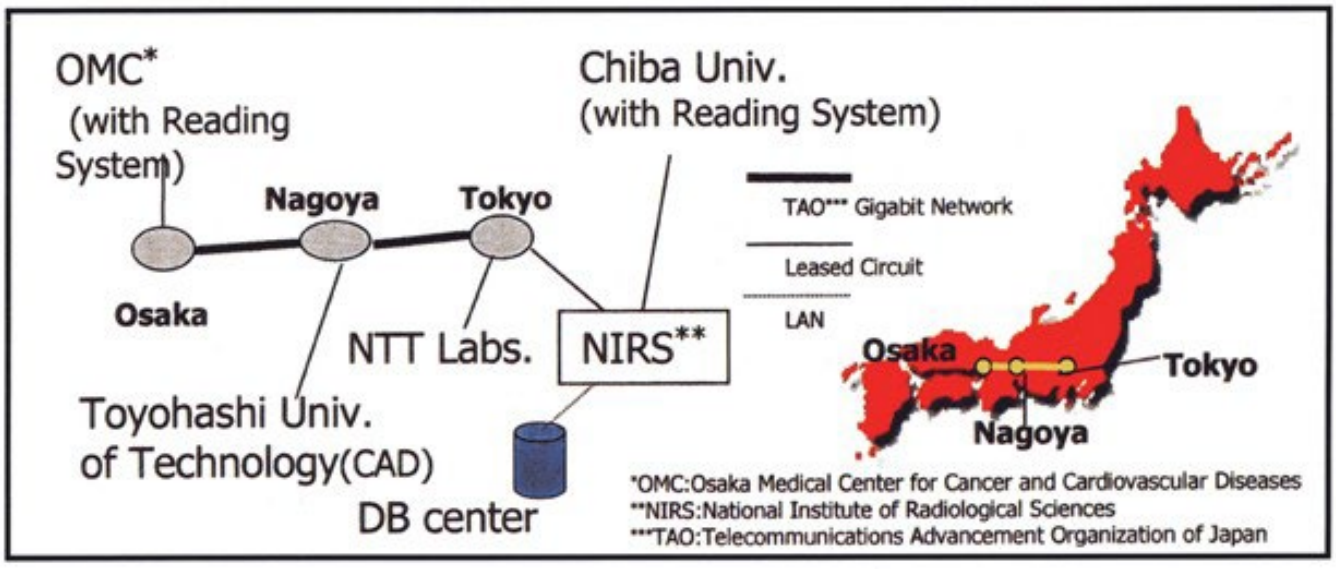

41. Clinical Application of Autoactivation PET Imaging Derived From C-12 Ion Radiotherapy.

Kyosan Yoshikawa, Takehiro Tomitani, Mitsutaka Kanazawa, Tatsuaki Kanai, Masahiro Endo, Katsumi Tamura, Masahisa Koga, Hirotoshi Katoh, Susumu Kandatsu, Jun Mizoe, Hirohiko Tsujii, Katsya. Yoshida, Kazutoshi Suzuki, Fumio Shishido and Hiroshi Fukuda.

Keywords**:** *PET, C-12 ion radiotherapy, autoactivation imaging*

Clinical application of PET imaging of auto activation derived from C-12 ion radiotherapy (HIMAC) was studied. We introduced a patient fixation system for auto activation PET measurements. Using this fixation system, we can get PET images with the same patient positioning as with patient positioning of HIMAC therapy planning CT. It is very important to perform the PET measurements under exactly the same patient positioning as in HIMAC therapy to compare RI distributions.

We performed some clinical PET measurements and got superimposed images of PET and CT planning of HIMAC therapy patients. Cases in this study were malignant melanoma of the esophagus, original lung cancer, metastatic lung cancer from colon cancer, hepatocellular carcinoma, and metastatic bone tumor from thyroid cancer. We tried two fitting methods. In the first method, fitting parameters calculated from phantom simulation studies were used for modifying PET emission images in order to make superimposed images of PET and CT planning. In the second method, the automatic multi modality image registration method (AMIR method)of the Dr. View applications was used. In the latter method, we fitted the transmission images of PET to planning CT images at the start, and then superimposed emission images on the planning CT images. Our fitting results were relatively good in both methods. It seemed that the fitting results of the AMIR method had somewhat better fitting error than the phantom parameter method. We think the reason of this was insufficiency and immaturity of the measuring system for patient setup parameters on the PET bed. We are looking at ways to solve this problem.

42. Functional Diagnosis and Evaluation of Therapeutic Effects of Cancer Using PET

Kyosan Yoshikawa, Katsumi Tamura, Yasunori Imai, Noriyo Matsuno, Masahisa Koga, Masakuni Kanai, Susumu Kandatsu, Hirohiko Tsujii, Tetsuya Suhara, Katsuya Yoshida, Kazutoshi Suzuki, Osamu Inoue, Fumio Shishido, and Hiroshi Fukuda

Keywords**:** *PET, heavy ion beam therapy, detection of recurrent lesion*

Positron emission tomography (PET) can demonstrate increased metabolic demand as visual images, and it provides alternative information for diagnosis which can be used to complement morphological observations. We studied usefulness of methionine-PET and FDG-PET to distinguish between radiation necrosis and recurrence of brain tumors after irradiation. Recurrent mass lesions of a brain tumor are usually revealed as an enhanced area in the MRI using Gd-DTPA. Some necrotic lesions caused after irradiation also show Gd-DTPA enhancement in MRI. It is often very difficult to distinguish between the two types. We studied 21 patients diagnosed with a brain tumor using C-11 methionine and FDG by PET. They had received carbon beam ion therapy and then showed some unusual findings in the brain MRI or CT study during the follow up period. They had received 16.8 GyE to 52.8 GyE beam doses. All patients were followed clinically for more than one year to five and half years until the clinical status of the patient, recurrence or radiation necrosis, was clearly known. There were six CR cases, nine recurrent cases and six radiation necrotic cases. It seemed that we could not distinguish recurrence from radiation necrosis by FDG-PET. But the population of cases was very small in the study; we need more time and cases to clarify this point. However, methionine-PET seemed able to distinguish between recurrence and radiation necrosis. When we classified our cases in two groups using a cut off value of 2.1 (TMR), sensitivity was 80 %, specificity was 70 % and accuracy was 73.3%. However, if we classified our cases in two other groups using a cut off value of 0.7 reduction ratio of methionine accumulation in the lesion which was a ratio calculated from the TMR value divided by pretreatment accumulation value, sensitivity, specificity and accuracy were 100%, 71 %, and 83.3 %, respectively. We concluded that the methionine-PET might be useful for distinguishing recurrent lesions after irradiation therapy from radiation necrotic lesions.

43. Quantitative Estimation of Brain Atrophy and Function with PET and MRI Two-dimensional Projection Images

Hinako Toyama, Reiko Saito, Koji Uemura, Kenji Ishii, Michio Senda and Akihiko Uchiyama

Keywords**:** *brain atrophy, PET, MRI, corticobasal degeneration*

The purpose of this paper is to estimate the brain atrophy and the decline in brain function objectively and quantitatively.

Two-dimensional projection images of PET and MRI were made from the 3D transaxial images by using the mollweide method which keeps the area of the brain surface. The sulcus is extracted automatically by means of K-means clustering the correlation image between MRI and CBF (FDG) PET images. the rate of atrophy is calculated from the ratio of the extracted sulcus to the area of 2D-brain-surface of MRI. the cerebral function (such as blood flow or glucose metabolic rate), is calculated from the cerebral cortex area except the sulcus in the PET image, and then the relationship between atrophy and function is evaluated.

This method is applied to two groups, the young and the aged normal subjects, then the relationship between the age and the rate of atrophy or the cerebral blood flow is investigated. This method is also applied to two groups of the normal control and the corticobasal degeneration patients, the relationship between the disease and the rate of atrophy or the functional disorder is investigated.

Significantly higher values of brain atrophy and lower values of CBF were obtained for aged group and the larger SDs were shown for CBF in young group and for brain atrophy in aged group. Almost same values of brain atrophy rate were estimated by using both images of CBF and glucose metabolism images.

A new method was proposed to estimate quantitatively and objectively the brain atrophy and function from PET and MRI. This method was evaluated in the normal subjects and in patients with corticobasal degeneration.

44. Determination of ^{32}P in Urine for Early Dose Estimation of Three Victims in the JCO Criticality Accident

Yoshikazu Nishimura, Hiroshi Takeda, Kiriko Miyamoto, Yoshito Watanabe, Fuyuki Kouno, Noriko Kuroda, Hee Sun Kim and Masae Yukawa

***Keywords*:** *JCO, early dose estimation, P-32, urine*

On September 30th, 1999, a criticality accident occurred at a uranium conversion facility in Tokai-mura, Ibaraki, Japan. Three workers, who were severely exposed to neutrons and gamma-rays, were transferred to the National Institute of Radiological Sciences for medical treatment. The doses were estimated preliminarily by prodromal symptoms, lymphocyte counting, chromosomal analysis, and ^{24}Na activity in blood. For apparent dose estimation, biological materials such as blood, hair and urine were analyzed by measuring neutron-induced radionuclides**.** We measured the beta emitters induced by neutron activation in the biological samples in order to obtain as much information as possible from the irradiated individuals, and we detected ^{32}P in urine samples. ^{32}P generated by thermal neutron activation of stable phosphorous in the whole-body should be excreted into the urine. As yet, definite methods for the estimation of the neutron dose by measurement of ^{32}P in urine have not been established. Urine requires a less invasive sampling procedure, and it may possibly provide a convenient means of measuring neutron dose immediately after exposure. Table 3 shows the concentration of ^{32}P in urine from 5 h to 20 h after the accident and the relative concentration ratios for the three workers, together with the ^{24}Na concentrations in blood corrected to the time of the accident. The concentration ratios of ^{32}P in urine of three workers showed a similar tendency to the concentration ratios of ^{24}Na in the blood. Therefore the radioactivity of ^{32}P in urine could be used to determine the neutron exposure dose. Collecting blood is not only sometimes difficult to carry out, but also puts physical burdens on patients at a crucial time. Urine can be collected easily, and it may provide a convenient means of measuring neutron dose immediately after the exposure. We obtained similar urinary data from measurements of ^{32}P with a liquid scintillation counter. If ^{32}P in urine can be detected rapidly and easily, it could become a good indicator for estimating the neutron dose.

Table 3. Concentration of ^{32}P in urine on the first day after the accident, and relative concentration ratio for the workers.

	^{32}P in Urine		^{24}Na in Blood[a]	
	Concentration[b] (Bq/ml)	Ratio[c]	Concentration[b] (Bq/ml)	Ratio[c]
Worker A	20.2	6.1	169.0	7.4
Worker B	12.2	3.7	91.3	4.0
Worker C	3.3	1	22.8	1

[a] ^{24}Na activities in blood were measured with Ge gamma-ray spectrometer.

[b] Concentrations were corrected to the time of the accident.

[c] Ratios indicate relative values of the concentrations to worker C.

45. Determination of 32P Concentration in Hair of Three Victims in JCO Criticality Accident and Estimation of the Fast Neutron Fluence on Body Surfaces

Masae Yukawa, Hiroshi Takeda, Kiriko Miyamoto, Yoshito Watanabe, Shoichi Fuma, Yoshikazu Nishimura, Fuminori Soga, Nobuhito Ishigure, Yutaka Noda and Makoto Akashi

Keywords: 32P, hair, neutron fluence, criticality accident, beta-ray counting

32P is generated by fast neutrons of 2.5MeV and over in sulfur with an (n, p) reaction, as well as by thermal neutron activation of stable phosphorous (n,). Human hair contains a higher amount of sulfur, approximately 5% in chemical abundance, than other human tissues, and the distribution in hair is almost uniform. Additionally, hair contains little phosphorus. Since the neutron activation cross sections of sulfur and phosphorus are essentially the same, most of the 32P activity present in the hair is derived from fast neutron capture by sulfur. Therefore, hair samples have been used for estimation of the fast neutron dose on body surface. When hair samples are collected from different positions of the body, the distribution of neutron fluence on the body surface can be estimated. We determined 32P and S in the hair of three workers severely exposed to neutrons in the JCO criticality accident to estimate fast neutron dose to their body surfaces.

In this work, head and pubis hair samples of workers A and B who were heavily exposed in the vicinity of the precipitation tank were analyzed by beta-ray counting, as 32P is a beta-emitter. Hair samples of worker C who was in a room next to the precipitation tank had an obvious contamination with fissions products such as 91Sr, 91Y and 140Ba. Therefore, determination of 32P in his hair samples was not carried out.

Concentrations of neutron-induced 32P in the hair were measured with a low background -ray spectrometer (Pico ; Fuji Electric Co, Japan) and a liquid scintillation counter. The Pico is composed of a gas flow type GM tube and plastic scintillator with an anticoincidence system to achieve low background counting. Weight of each hair sample was less than 1g, and the hair was cut into small pieces so it could be put into a counting vessel. The activities of 32P were counted in the regions of the corresponding energy. Concentrations of 32P were determined by comparing the activities to the reference standard, an NIST standard radioactive solution. Stable sulfur was determined by ICP-AES method after wet digestion with ultra-pure HNO3 and a microwave digester.

Concentrations of 32P in the hair are shown in Table 4. Pubic hair of workers A and B had higher concentrations than scalp hair. Neutron doses to the body surface for workers A and B were estimated using Maruyama's equation (Daf/a =2.92X10-2/S, Daf: rad, a: activity of 32P, S: concentration of sulfur) and were: worker A, 7.9Gy; worker B, 4.2Gy.

The results show that workers A and B received higher doses of irradiation to the frontal side of their body trunk than to the head.

Table 4. Concentrations of 32P and stable S in hair

(Radioactivity of 32P was decay-collected to Sep. 30, 1999.)

	Worker A		Worker B	
	^{32}P (Bq/g)	Stable S(μg/g.dry)	^{32}P(Bq/g)	Stable S(μg/g.dry)
Head right side	3.9 ± 0.3	43850	2.3 ± 0.1	37800
Head left side	4.5 ± 0.2			
Pubic hair	19.8 ± 0.5		8.8 ± 0.2	

46. Tokai-mura Criticality Accident: Whole Body Distributions of ^{45}Ca and ^{32}P in Bone of the Victims Exposed to High-Dose Neutron Irradiation

Yoshito Watanabe, Masae Yukawa, Kiriko Miyamoto, Hiroshi Takeda, Yoshikazu Nishimura, Makoto Akashi, Toshiyasu Hirama, Hisamasa Joshima and Fuyuki Kouno

Keywords**:** *Tokai-mura criticality accident, neutrons, bone, ^{45}Ca, ^{32}P*

In the criticality accident in Tokai-mura on 30 September 1999, two workers received especially high dose of neutrons and -rays over their bodies. We found evidence indicating the inhomogeneous exposures of neutrons to their bodies by measuring the whole body distribution of 45Ca and 32P generated in bone matrix through neutron capture reactions of 44Ca + n > 45Ca and 31P + n > 32P.

Small pieces of bone (0.5-3g wet) were taken from fourteen parts of the body after the death of the two workers. Calcium and phosphorus in the samples was purified separately for the measurements of 45Ca and 32P activities with a low-background -ray spectrometer (Pico-beta, Fuji Electric Co., Japan). There was a high positive correlation (r=0.90) between 45Ca and 32P concentrations in the bone samples of one worker (worker A). This assured us that both the analyses of 45Ca and 32P were suitable for the estimation of thermal neutron fluence entering bone.

In worker A, the concentration of 45Ca varied widely among the different parts of the body (Fig.15). The highest concentration was observed in the right side of the anterior rib and the iliac bone. The bones in the trunk and thighbone showed higher concentrations of 45Ca. On the other hand, the lower and upper ends of his body, such as the frontal bone, finger bone and toe bone had lower concentrations. In the comparison between the right and left parts in the anterior rib and the iliac bone, the right showed much higher concentrations than the left. This suggested that the worker received a higher dose of neutrons at the frontal right position around the waist and chest, and that the dose decreased with the distance from the central part of the body.

In the other worker (worker B), there was only a small variation of 45Ca concentration among the parts of the body. The concentration in the ribs was lower, and the concentrations in the frontal bone, finger bone, iliac bone and thighbone was higher. He seemed to have gotten higher doses of irradiation in the face, hands and waist.

The 45Ca concentration ratio of worker B to worker A in the iliac bone was about 0.5. The value agreed with the worker B / worker A ratio of the estimated average doses for the whole body from lymphocyte number, chromosome abbreviation and 24Na activity in the blood. This suggested that the dose to the abdomen should contribute mainly to the estimation of the average dose from the parameters in the blood.

The analyses of 45Ca and 32P in bone gave us valuable information for the estimation of the dose received by particular organs, which were critical for the health conditions of the workers.

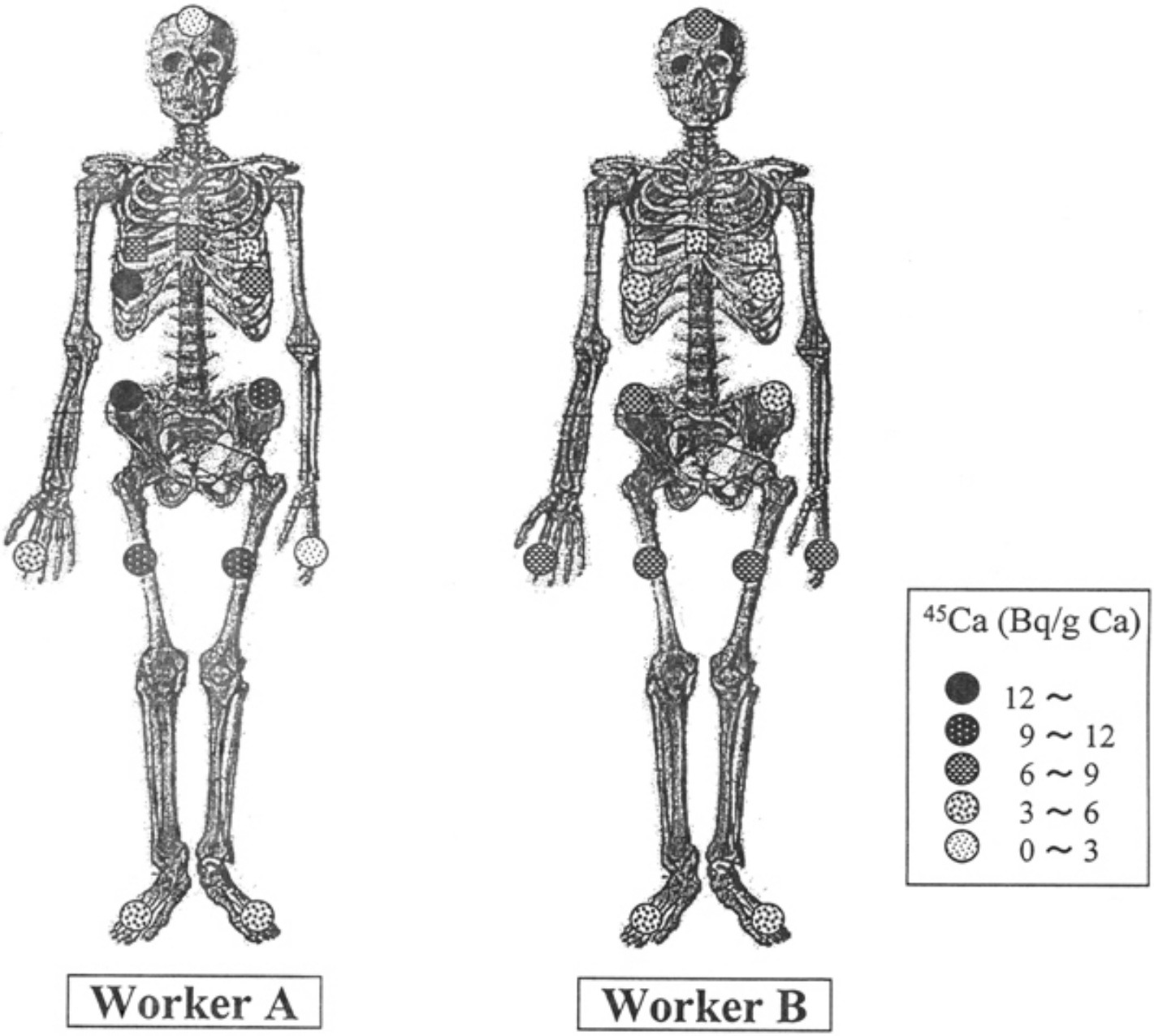

Fig.15. ^{45}Ca concentrations in bone samples from fourteen parts in the bodies of worker A (left) and B (right). Circles indicate the concentration levels in the samples from anterior parts, and squares indicate the levels from posterior parts. Activities are normalized to the date of the accident.

47. A Quality Assurance Aspect of IAEA-RCA Reference Asian Man Project (Phase 2): Ingestion and Organ Content of Trace Elements of Importance in Radiological Protection

Hisao Kawamura, Kunio Shiraishi, Masae Yukawa, G. Venkatesh Iyenger1, Robert M. Parr1 and H. S. Dang2 (1International Atomic Energy Agency, Vienna; 2Bhabha Atomic Research Centre, Mumbai)

Keywords: radiological protection, Reference Asian Man Project, IAEA

The current CRP was initiated by the IAEA in 1995 within the framework of the Regional Co-operative Act program to establish representative data in Asian countries, namely Bangladesh, China, India, Indonesia, Japan, Korea, Pakistan, the Philippines and Vietnam. The objective is to measure trace elements of radiological significance such as Cs, I, Sr, Th and U (known as the first priority elements), and other trace elements of secondary importance, in staple foods and total diets, and in tissues such as thyroid, bone, liver and muscle. To ensure accuracy and comparability of the analytical results generated, both internal and external quality control steps were incorporated in the protocols, including the appointment of a Central Reference Laboratory (CRL), namely NIRS. In this paper, further progress of the quality assurance system for the first priority elements, i.e. Cs, I, Sr, Th and U is described.

Representative dietary intakes of the elements of interest were studied in the adult (20-50 years) populations of nine countries and food components collected in typical market places were cooked, dried, and powdered, and then combined into sets of total diet samples. The duplicate portion method was also employed in a few countries. A blender with Ti-coated blades was distributed to each laboratory for sample preparation work. Tissue samples were obtained at autopsy generally from accident victims and subjects of sudden death at forensic or police departments in five countries. The samples were dried and ground to powder before analysis.

At the CRL, ICP-MS was used for determining Sr, Cs, Th and U and ICP-AES was used for Sr, Ca, K and several elements of second priority. The samples were chemically treated in a Class 100 clean air draft chamber installed in a Class 100,000 or Class 5,000 clean room (a switch to the latter was made in May 1999). The total number of samples to be analysed by the CRL up to the end of the project in December 2000 was approximately 260 including 53 tissue samples, of which about 60 are for "10%" (see below) samples, and 200 for backup analysis including 54 from Japan. Iodine was determined by co-operating institutes (Y. Muramatsu, NIRS, Chiba; and C. Yonezawa, JAERI, Tokai) by ICP-MS and ENAA, respectively.

For internal QC, validation of the analytical methods by each participant was made using the NIST SRMs and RMs distributed. External quality assurance and quality control (QA/QC) was performed by duplicate analysis both by the participant and by the CRL of a representative selection (roughly 10%) of all the "real" samples collected by the participants. A new reference material for the CRP was prepared by the National Institute for Environmental Studies (NIES), Tsukuba under a joint project between it and NIRS. Besides the domestic collaborative analysis for certification, a subsequent international collaboration was organized by the IAEA to provide supplementary data for Cs, Sr, Th, U and I.

In general, analytical results for NIST reference materials are satisfactory, though some participants are still experiencing problems for a few elements and matrices. Some of the elements (e.g. thorium) are notoriously difficult to determine at the concentrations commonly found in diets and other biological materials.

Comparison in "10%" sample analyses between participants and the CRL was made. Our experience so far showed that most z-scores were acceptable even using 10% as the target relative SD. However, occasionally, z-scores with values of 5 or more were obtained and these are still the subject of further investigation.

Certified values for NIRS/NIES Typical Japanese Diet have been given for 14 elements and reference values for 12 elements (the first priority elements in Table 5).

In conclusion, analytical results obtained for NIST reference materials have been satisfactory. The results for Cs, Sr, Th and U in NIST SRMs obtained over a period confirmed acceptable performance by the CRL.

A CRM based on Japanese total diet was developed. The results for the 10% samples analysed by both CRL and participant laboratories as seen from their z-scores were acceptable (with occasional exceptions) even using 10% as the target relative standard deviation. The above work is expected to enhance the quality of data obtained by participant laboratories taking part in this CRP.

Should appear as a foot note for Table 1.

J. Yoshinaga and M. Morita, Certificate of Analysis, NIES/NIRS Typical Japanese Diet Certified Reference Material, NIES, Tsukuba 305-0053, Japan, April 2000.

Table 5. Some certified and reference values for NIES/NIRS Typical Japanese Diet.*

Element	Unit	Certified value	Reference value
K	%	0.550±0.015	
Ca	%	0.125±0.004	
Sr	mg/kg	4.9±0.2	
I	mg/kg		1.9
Cs	mg/kg		0.020
Th	mg/kg		0.002
U	mg/kg	0.0029±0.0004	

*) J. Yoshinaga, and M. Morita, Certificate of Analysis, NIES/NIRS Typical Japanese Diet Certified Reference Material, NIES, Tsukuba 305-0053, Japan, April 2000.

48. Contributions of 18 Food Categories to Intakes of ^{232}Th and ^{238}U in Japanese

Kunio Shiraishi, Keiko Tagami, Yasuyuki Muramastu and Masayoshi Yamamoto* (* Kanazawa Univ.)

***Keywords*:** *dietary intakes, ^{232}Th, ^{238}U, Japanese, market basket study*

Dietary intake studies have been conducted to estimate the representative values of radioactive and non-radioactive nuclides from the viewpoints of radiation protection for Japanese. Assessments of radiation dose from ^{232}Th and ^{238}U are important because both nuclides are the parent nuclides in decay series. Dietary nuclide intakes are estimated by several methods. Market basket studies and duplicate portion studies are two representative ways. Although duplicate portion studies offer the greatest degree of reality compared to other methods, market basket studies are advantageous regarding identification of what kinds of food are critical foods for radionuclide intakes. In the report, a market basket study using 18 food categories was conducted to clarify the food pathways of ^{232}Th and ^{238}U in Japanese subjects. A total of 336 foodstuffs equivalent to a total wet-weight of 120 kg was used.

During 1994-1995, foodstuffs were bought from markets in the vicinity of Mito, Ibaraki Prefecture. Statistical consumption data of 1989-1991 (MHW 1993) was used for collection of the food samples. Food categories, daily intakes, and the number of foodstuffs used in the present study are shown in Table 6. The purchased foodstuffs, were divided into the18 categories a follows: 1) rice; 2) cereals, excluding rice; 3) nuts and seeds; 4) potatoes; 5) sugars and confectionaries; 6) fats and oils; 7) bean products; 8) fruits; 9) green vegetables; 10) other vegetables; 11) mushrooms; 12) seaweeds; 13) seasonings and beverages; 14) fishes and shellfishes; 15) meats; 16) eggs; 17) milk and milk products; and 18) cooked meals. Each food group was homogenized and was freeze-dried. An aliquot of sample was taken and completely decomposed with a mixture of nitric acid, perchloric acid, and hydrofluoric acid. The sample solution was measured with inductively coupled plasma mass spectrometry. For ^{238}U and ^{232}Th, concentrations (μBq per g-fresh) and daily intakes (mBq per person) of the 18 food categories are shown in Table 6. Food categories having higher ^{238}U contents were found to be as follows: seaweeds 1140 μBq; fishes and shellfishes 37 Bq; nuts and seeds 11 Bq; bean products 8.6 Bq; and cooked meals 7.3 μBq. Big contributors to the daily ^{238}U intake in Japanese were as follows: seaweeds (50%); fishes and shellfishes (26%); and bean products (4.3%). For ^{232}Th, higher contents were found as follows: seaweeds 28 μBq; fishes and shellfishes 13 μBq; nuts and seeds 8.2 μBq; green vegetables 3.9 μBq; cooked meals 3.5 μBq; and bean products 2.9 μBq. Big contributors to the daily ^{232}Th intake were as follows: fishes and shellfishes (44%); green vegetables (11 %); bean products (7.4%); and seaweeds (6.0%). For both nuclides, marine food products were big contributors, while minor contributors were oil and fats, eggs, and cooked meals. Daily intakes of ^{232}Th and ^{238}U in Japanese were estimated to be 2.7 mBq and 14 mBq per person from the intakes of the 18 categories,

respectively. Annual effective doses (Sv/y) were estimated from these experimental results with dose coefficients (Sv/Bq) of the International Commission on Radiological Protection Publication 61 (ICRP 1994) as 2.2×10^{-7} for ^{232}Th and 2.2×10^{-7} for ^{238}U in Japanese.

In conclusion, big contributors to Japanese dietary ^{232}Th and ^{238}U intakes were found to be marine products. Dietary intake studies using eighteen or more food categories should be effective for constructing the critical pathway. Furthermore, foodstuffs in the big contributor groups and foodstuffs having high contents of the nuclides should be analyzed in detail to find individual critical foods in the food chain.

Publication:

Shiraishi, K., Tagami, K., Muramatsu, Y. and Yamamoto, M.: Health Phys., 78, 28-36, 2000.

Table 6. Actitity concentrations and daily intakes of ^{238}U and ^{232}Th in 18 food categories for Jpanese.

Food category	Food intake[b] (g per person per day)	Concentration of ^{238}U[b] Mean	SD	Concentration of ^{232}Th[b] Mean	SD	Daily intake of ^{238}U[c]	Daily intake of ^{232}Th[c]
Rice	198.3	0.98	0.08	0.460	0.066	0.194	0.0912
Cereals excluding rice	88.3	3.85	0.27	0.134	0.256	0.340	0.119
Nuts and seeds	1.5	10.8	1.1	8.16	2.92	0.016	0.0122
Potatoes	66.5	4.89	0.62	1.76	0.53	0.325	0.117
Sugars and confectionaries	31.9	6.26	0.27	1.63	0.02	0.120	0.0519
Fats and oils	17.9	0.45	0.06	0.139	0.029	0.0081	0.0025
Bean products	68.4	8.64	0.29	2.92	0.19	0.591	0.200
Fruits	121.7	0.44	0.12	0.384	0.005	0.053	0.0468
Green vegetables	77.2	6.13	1.26	3.89	1.30	0.473	0.300
Other vegetables	167.0	2.48	0.20	0.898	0.121	0.414	0.150
Mushrooms	10.2	2.80	0.15	2.33	0.52	0.029	0.0239
Seaweeds	5.9	1140	4	27.8	1.6	6.87	0.164
Seasons & beverages	134.0	2.73	0.25	0.895	0.121	0.366	0.120
Fishes & shellfishes	96.1	37.1	2.9	12.5	1.2	3.57	1.20
Meats	74.3	2.49	0.06	0.404	0.019	0.185	0.0300
Eggs	42.9	0.58	0.14	0.239	0.013	0.025	0.0102
Milk & milk products	129.1	0.63	0.14	0.158	0.011	0.081	0.0203
Cooked meals	14.9	7.30	0.27	3.47	0.17	0.109	0.0518
Total intake estimated	1346.2	-	-	-	-	13.8	2.71

a Daily food intakes of fresh weight per person (MHW1993).

b Mean and SD for three analysee (μBq per g-fresh weight).

c Millibecquerels per person per day

49. A Review Epidemiological Study for Health Monitoring of Potential Risk from Radiation Exposure near Nuclear Power Plants in Japan

Yasuhiko Yoshimoto and Shinji Yoshinaga

Keywords**:** *Epidemiological study, Potential risk of the public, Radiation exposure, Nuclear power plants, Radiological emergency*

An apparent increase of leukemia risk occasionally raises public concern about radiation exposure in countries where nuclear power plants (NPPs) are located, although the facilities operate normally. Certainly, on the other hand, a reactor plant accident poses a threat to increased thyroid cancer risk in children due to radioiodine uptake mainly from fallout contaminated fresh milk. At the end of 1998, there were 52 NPPs operating in Japan. One important issue in radiation epidemiology is how to clarify scientific, social, and political controversies about the potential public health risk from radiation exposure for people living near NPPs if nuclear energy is to be a necessary energy source in Japanese society. A review epidemiological study was conducted for public health monitoring of potential risk of radiation exposure near the NPPs in Japan with respect to two points: routine releases of radioactive effluents from NPPs and consequence of a NPP accident.

Our goal in this issue is not hanging onto very small potential risks or seizing one positive aspect to prove no risk at the time of normal operation. It is a challenge to provide 'evidence-based epidemiological translations' for the Japanese public to recognize what potential risk NPPs pose for our society. In the not too distant future, we expect to use national health statistics and realistic estimates of routine radiation concentration from NPPs in a geographic information system. It is very rare that a large number of the public are involved in a serious nuclear accident. A justification for the adopted implementation for decontamination is sometimes to be determined through not only radiological assessment of the environment, but also epidemiological assessment of long-term public health consequences. Further continuous efforts should be done to ensure that no major public health impact from the fallout after the Chernobyl accident is to be observed except the predicted further increase in thyroid cancer risk. It will give us useful findings to reduce risks of the public after radiological emergency.

Publication:

Yoshimoto, Y. and Yoshinaga, S. 10th International Congress of the IRPA, P-2a-62, 2000.

50. Estimation of Internal Dose by Blood Analysis for Exposure to Tritium in Various Chemical Forms

Hiroshi Takeda, Kiriko Miyamoto, Shoichi Fuma, Kei Yanagisawa, Nobuyoshi Ishii and Noriko Kuroda

Keywords**:** *tritium, dose estimation, bioassay, blood, urine, rat*

Tritium is released mainly as tritiated water (HTO) or as gaseous tritium (HT) from nuclear facilities into the environment. Differing from gaseous tritium, tritiated water easily enters plants and animals and is partly incorporated into their organic constituents. Human exposure to environmental tritium arises in both forms of tritiated water and organic tritium through the ingestion of water and food contaminated with tritium. Various tritiated compounds are produced and used for medical and biological studies. The workers engaged in these industrial and research tasks will be accidentally exposed to these tritiated compounds. To estimate radiation dose from the exposure to tritium, urine bioassay has usually been performed. However, it is not expected to accurately estimate internal doses for the exposure to organic tritium.

The purpose of the present study is to develop a method applicable to internal dose estimation after exposure to tritium in various chemical forms. In rats exposed to tritiated water or some tritiated organic compounds by a single ingestion, the concentrations of total tritium and organically bound tritium (OBT) in blood and in various internal organs were determined at various time intervals after ingestion. The concentrations of total tritium in urine were also periodically determined. The results showed that the concentrations of total tritium in blood were a little higher than those in most internal organs for all tritiated compounds examined in this study. On the other hand, the concentrations of total tritium in urine were usually lower than those in the majority of the internal organs for most of the period after the ingestion, except a very early period after ingestion of tritiated water when the concentration was highest in blood.

When the cumulative doses to blood and internal organs for 100 days after ingestion of various tritiated compounds were compared, the doses to blood were almost the same as the highest doses to internal organs (Table 7). This indicated that blood analysis would be useful to estimate the maximum internal doses after exposure to tritium in various chemical forms. It was also found from the analysis of blood that the concentration ratio of OBT to total tritium in blood could be used to deduce the circumstances of the exposure. The concentration ratios after ingestion of tritiated water were very low, 0.05 on the first day and 1.0 on the 20th day, while the ratios after ingestion of tritiated organic compounds were 0.4 to 1.6 on the first day and 1.3 to 3.3 on the

20th day. Thus, the ratios were dependent on the chemical form of tritium at exposure and on the time interval after the exposure. It was, therefore, suggested that blood analyses might be used not only for estimating the maximum internal doses, but also for inferring the chemical form of tritium at exposure and the elapsed time after exposure. Although these results were obtained from animal experiments, it could be expected that a bioassay method applicable to human exposure from various tritiated compounds

could be developed by comparative study of the metabolic turnover rate between humans and rats.

Table 7. Radiation doses to blood and internal organs of rats for 100 days after a single ingestion of tritiated water or some tritiated organic compounds.

	Cumulative dose (mGy)a for 100 days after a single ingestion					
	^{3}H-water	^{3}H-leucine	^{3}H-lysine	^{3}H-glycine	^{3}H-glucose	^{3}H-thymidine
Blood Internal organs	15 12-31	39 21-39	81 39-80	39 24-32	17 14-17	24 16-24

a) : The cumulative doses were calculated assuming that the same amount of radioactivity (37 kBq) per g of body weight was ingested for all the tritiated compounds.

51. Bioassay for Neutron-Dose Estimations of Three Patients in the JCO Criticality Accident in Tokai-mura by Measuring β-ray Emitters with a Liquid Scintillation Counter

Hiroshi Takeda, Kiriko Miyamoto, Shoichi Fuma, Noriko Kuroda, Masae Yukawa, Yoshikazu Nishimura, Yoshihito Watanabe, Hee Sun Kim and Makoto Akashi

Keywords**:** *bioassay, dose distribution, hair, JCO criticality accident, urine,* ^{32}P

The measurement of -emitters in biological samples (hair and urine) from three patients in the JCO criticality accident was performed to assess the neutron dose to individuals. In the body of patients exposed to the nuclear excursion, various -emitters, such as 32P, 31Si, 35S, 36Cl and 45Ca, should have been induced by neutron activation. They are all derived from bioelements (S, P, Cl, Ca) of high chemical abundance in the human body, except for H, C, O and N. Among them, 32P has mostly been of concern because of the relatively high activation probability and the availability for dosimetry in the criticality accident. For determining -emitters in biological samples from the patients, we used a liquid scintillation counter (Tri-Carb 2200, Packard Co.), as a practical reference machine of a low-background -ray spectrometer (Pico-TM ; Fuji Electric Co.).

For the measurement, hair samples were cut into small pieces and urine samples were freeze-dried. To obtain a homogeneous solution for a reproducible measurement of these samples, a tissue solubilizer (Soluene-350, Packard Co.) was used. Soluene-350 is such a strong organic base that Hionic-Fluor (Packard Co.) was also used as a cocktail tailored for samples solubilized in strong alkaline media. For colored samples after solubilization, bleaching was done by the addition of a small amount of 30% hydrogen peroxide. For measuring 32P, which has a maximum beta energy of 1700 KeV, the discriminator window was set for the range of 50 KeV to 1700 KeV. A correction for quenching was carried out by using non-radioactive hair and urine samples, and also by using the NIST (National Institute of Science and Technology, U.S.A) standard 32P solution, whose concentration was specified. Signif-icant quenching did not occur until more than 0.2 gm of hair and 1.0 gm of freeze-dried urine was dissolved in a counting vial. Almost the same results as those with Pico- were obtained.

Fig. 16 shows the daily urinary excretion of 32P in three patients, as obtained by liquid scintillation counting. The 32P excretion curves of urine were tried to analyze by the least-squares method, which were comparable with the equation used in the biokinetic model of 32P recommended by ICRP. Among the three patients, the total activities of 32P excreted daily in urine were different, and the activities were correlated with the individual provisional mean doses estimated from blood 24Na measurement, and so on.

32P is produced by fast-neutron activation of stable sulfur in hair, as well as by the thermal-neutron activation of stable phosphorus. Since the neutron-activation cross sections of sulfur (approximately 5% in hair as chemical abundance) and phosphorus (approximately 0.1% in hair as chemical abundance) are

essentially the same, most of the 32P activity present in hair should be derived from fast-neutron capture by sulfur. Therefore, hair samples have been used to estimate the fluence of fast neutrons with energies in excess of 2.5 MeV at body locations where the hair was sampled. The counting rates measured until six weeks after the irradiation showed that the hair sample contained some radioisotopes of trace bioelements. They were inferred as 36Cl, 45Ca and 89Sr based on their abundances and neutron cross sections. Although a liquid scintillation counter is not advantageous for -ray energy spectrometry, it can be used to estimate the initial radioactivity level after exposure to neutrons.

In the unfortunate event of future criticality accidents, the dose distribution as well as the total mean dose should be considered in establishing a prognosis for any irradiated individual and in evaluating the dose-effect relationship. Efforts should be made to collect samples from as many locations as possible to establish dose-distribution estimates. As limited available samples, finger and toe nails or wool in clothing as well as hair samples should be considered. By using these samples, simpler and faster procedures for performing dose distribution estimates should be developed.

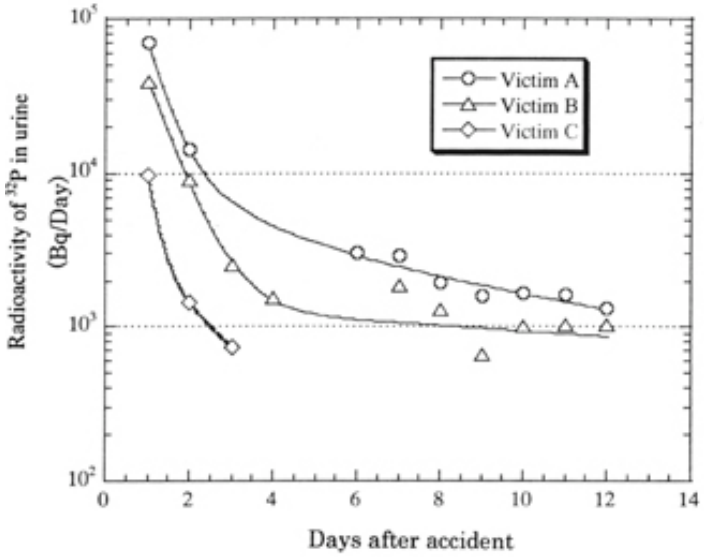

Fig. 16 Time variations in the ^{32}P activities excreted daily in the urine of three patients measured with a liquid scintillation counter, and normalized to the time of the accident.

52. Ecologically Responsive Phenomena of the Aquatic Microcosm System to Ultra Violet C

Kiriko Tanaka-Miyamoto, Hiroshi Takeda, Shoichi Fuma, Nobuyoshi Ishii, Kei Yanagisawa, Yoshikazu Inoue, Chitose Ishii, Kazunori Sugai and Zen-ichiro Kawabata* (*Kyoto Univ.)

***Keywords*:** *aquatic microcosm, ecological assessment, Escherichia coli, Euglena gracilis, model ecosystem, Tetrahymena thermophila, ultra violet C*

It is necessary to establish a reasonable method to evaluate the ecological effects of any ecological toxicants on microbial communities in the environment, since various microorganisms play a big role in the life support system of human beings. In this study an aquatic microcosm system was adopted as a model ecosystem for accumulating basic data on ecologically responsive phenomena of the microbial communities, rather than on biologically responsive phenomena of single species. This microcosm is one of the simplest biological communities, which can demonstrate indirect effects on species caused by an ecological stress. It consists of three species of microorganisms in a small container like a test tube or a small plastic bottle, and the interactions among the three species have been well investigated. The three are flagellate algae *Euglena gracilis* as a producer which has chloroplast for photosynthesis, ciliated protozoa *Tetrahymena thermophila* B as a consumer which grazes bacteria, and bacteria *Escherichia coli* DH5
αas a decomposer which decomposes metabolites and dead bodies of the other two species. The three species can survive by exchanging materials with each other in the closed container with limited nutrients when the microcosm is first started, and their population densities can be kept in a steady state for a long time, usually for more than a year.
During the past few years the authors have reported data on the impact of acidification, manganese and gadolinium on the population of the aquatic microcosm in its growth stage and the steady state. In the present paper, effects of ultra violet C on the population of the aquatic microcosm in the early steady state were investigated.
An experiment was carried out as follows: Each microorganism was preincubated following the literature method of Kawabata et al. Then the three species were inoculated into a culture medium (0.05 % proteose peptone in a half strength of modified Taub and Dollar's solution) in plastic bottles and incubated under 2500 lx and 12-12 h LD light regime at 25Åé. On the 56th day after composition, the microcosm was exposed to 1 kerg/mm^2, 10 kerg/mm^2, 50 kerg/mm^2 and 100 kerg/mm^2 of ultra violet C (wave length: 254nm). Population densities of each organism were determined at various time intervals after exposure. The population density of *T. thermophila* was counted microscopically, that of *E. coli* was measured by counting colonies formed in the broth-agar medium, and that of *Eu. gracilis* was measured by the plate culture method.
Fig.17 shows variation of the population densities of the three species in the microcosm. When the microcosm was exposed to 1 kerg/mm^2 of ultra violet C, only the population density of *E. coli* soon decreased and then recovered to the same level as that of control within 3 days, but all three species

were affected when the microcosm was exposed to 10 kerg/mm^2. In the case of the exposure to 10 kerg/mm^2, population density of *T*. *thermophila* decreased soon after the exposure and recovered within 4 days. This is an indirect effect of ultra violet C
on *T*. *thermophila* since *T*. *thermophila* followed the time course variation of the population density of *E. coli* as the food for *T*. *thermophila*. Just after the exposure, population density of *E. coli* decreased soon and recovered within 2 days, while that of *T*. *thermophila* did not decrease on the day of exposure, but then decreased on the next day and recovered on the fourth day. In both cases of 50 kerg/mm^2 and 100 kerg/mm^2, *Eu. gracilis* and *T*. *thermophila* probably experienced a direct effect of ultra violet C, since they showed the same sudden disappearance when they were exposed to ultra violet C in a single species medium not in the microcosm system. However the effect of ultra violet C seems to be moderated by the microcosm system itself, as population density of *Eu. gracilis* recovered from 7 to 13 days after the exposure. In the case of exposure to a single species not in the microcosm system, *Eu. gracilis* did not recover at all after exposures of high doses (50 kerg/mm^2 and 100 kerg/mm^2). This moderation effect of the microcosm system was considered to be caused by the effective absorption activity of ultra violet C with the microcosm medium solution. A variety of chemical compounds derived from metabolism of the three species were capable of effectively absorbing ultra violet C.

The present study demonstrated indirect effects of ultra violet C on one species through other species. It also showed that the microcosm system itself worked to protect the microorganisms in the microcosm system from the impact of ultra violet C.

Publication:

*Kawabata, Z., et al.: J. Protozool. Res., **5**, 23-26, 1995.*

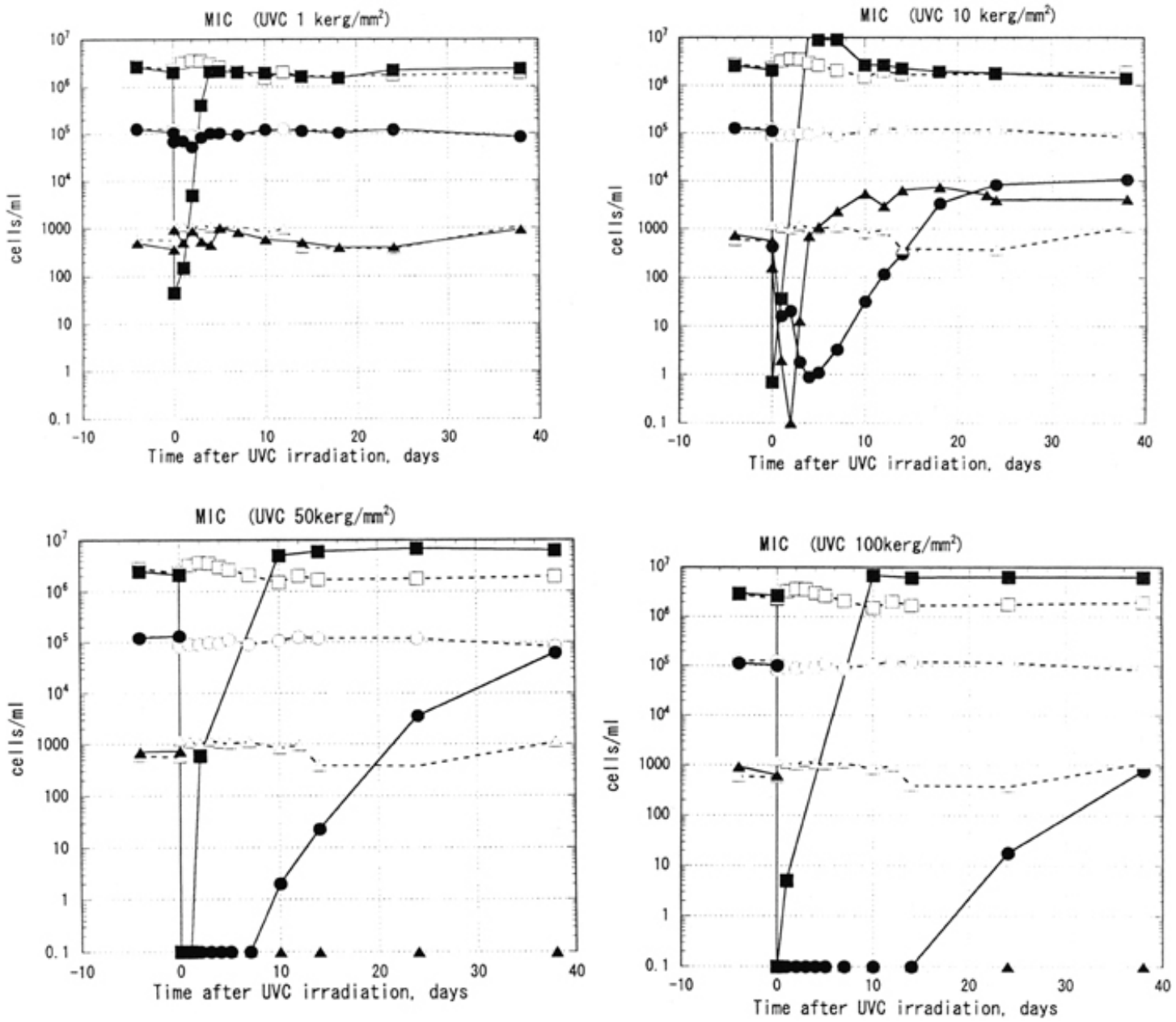

Fig.17 Population densities of three microorganisms in the microcosm exposed to ultra violet C on the 56 th day after inoculation.

53. Determination of Uranium Isotopes by ICP-MS in Soil Core Samples Collected around the Reconversion Facilities

Satoshi Yoshida, Yasuyuki Muramatsu and Keiko Tagami

***Keywords*:** *JCO criticality accident, uranium, ^{235}U, ^{238}U, isotope ratio, soil, ICP-MS*

Naturally occurring ^{235}U and ^{238}U are long-lived isotopes, and the $^{235}U/^{238}U$ abundance ratio is the same everywhere, 0.00725 in atom ratio, regardless of sampling location, rock type, and degree of weathering. Hence any deviation from the natural ratio attests to a soil affected by human activity, with the well-known exception of the Oklo reactor. After the 1999 criticality accident in Tokai-mura, we collected surface soil and plant samples around the uranium conversion building in JCO and observed the higher $^{235}U/^{238}U$ atom ratios than the natural ratio. However, we could not conclude whether the main source of the enriched U was the criticality accident or not. In the present study, U isotopes were determined with ICP-MS for seven soil core samples collected on the JCO grounds, in order to evaluate the isotope composition of excess U in soils.

In the framework of studies on environmental effects of the criticality accident, three soil core samples were collected at open areas beside the uranium conversion building (S9, S12A, S12B) and the other four soil cores were collected at deciduous forests (S6, JF1, JF2, JF3). Samples were cut every 1 to 5 cm depth using a spatula on site. After removing stones, the soil samples were oven-dried at 80 ^{o}C until of constant weight, and then ground into powder. The samples from organic layers of the forests were oven-dried and pulverized with a blender. Samples (usually 0.1 g) were digested with HNO_3, HF and $HClO_4$. Quadrupole-ICP-MS (Yokogawa PMS- 2000) or high resolution-ICP-MS (Finnigan MAT ELEMENT) was used for the analysis of ^{235}U and ^{238}U. Standard reference materials such as GSJ-JB-1a (basalt) were used to validate the analytical procedure.

The $^{235}U/^{238}U$ ratios were higher than the natural ratio in most samples. The highest ratio observed was 0.0262. Although vertical profiles of the $^{235}U/^{238}U$ ratio differed among the soil cores, the ratios tended to be high at the surface and decreased with depth. The U concentration also changed with depth. The percentages of ^{235}U in the excess U, estimated from the positive correlation between U concentration and the $^{235}U/^{238}U$ ratio in soil samples, were less than 4 % by mass (mostly 1 - 3 %), and were much lower than the enrichment of the U used in the uranium conversion building at the time of the criticality accident (18.8 %) (see Fig. 18). These findings indicate that enriched U had been released before the criticality accident during the U processing at JCO in connection with the reconversion of light water reactor fuel. Since the range of the U concentrations found was comparable to the range of uncontaminated Japanese surface soils, the amount of U added to the soil was judged negligible from a radiation protection viewpoint.

Publications:

Yoshida, S., Muramatsu, Y., Tagami, K., Uchida, S., Ban-nai, T., Yonehara, H. and Sahoo, S.:
J. Environ. Radioactivity, 50, 161-172, 2000.
Yoshida, S., Muramatsu, Y. and Tagami, K.: *Environ. Sci. Technol.* (in press).

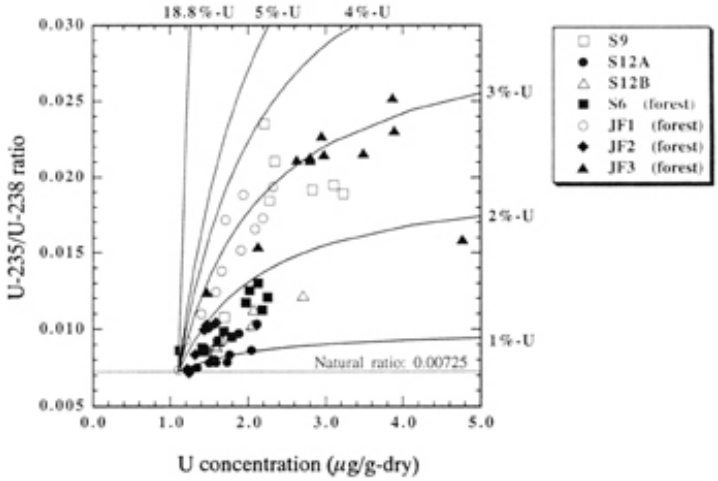

Fig.18. Relationships between U concentration and $^{235}U/^{238}U$ ratio in soil core samples. Curves: calculated mixing curves of the enriched U with certain enrichments (percentage of ^{235}U by mass) and natural soil with 1.1 g/g (dry wt) of U.

54. Measurement of Technetium-99 in Marshall Islands Soil Samples by ICP-MS

Keiko Tagami and Shigeo Uchida

***Keywords*:** *technetium-99, Marshall Islands, ICP-MS, soil samples*

In order to improve our understanding of the behavior of ^{99}Tc in the environment and to develop appropriate waste storage/disposal options, it is essential that we obtain more reliable information on the distributions and fate of ^{99}Tc in the environment. Generally it is difficult to obtain information from a global fallout area due to the extremely low ^{99}Tc concentrations. However, there are several contaminated sites where elevated levels of ^{99}Tc are expected because of inputs from nuclear facilities and/or nuclear weapons test programs. One of the sites is the northern Marshall Islands where the United States carried out over 60 nuclear test detonations during the 1950's. There is little or no information available on the levels of ^{99}Tc contamination in and around the atolls. In this study, soil samples collected from various sites in the Marshall Islands were used as the basis for developing a refined analytical method for determination of ^{99}Tc by ICP-MS.

The following three Tc extraction techniques were examined: (M1) acid leaching of Tc from incinerated soil; (M2) acid leaching of Tc from raw dry soil; and (M3) Tc volatilization from incinerated soil using a combustion apparatus. The chemical recovery was measured by counting ^{95m}Tc in the sample with a NaI (Tl) scintillation counter (Aloka, ARC-380) and comparing the result with standard solutions. The ^{99}Tc content of the sample solution was then determined by ICP-MS (Yokogawa, PMS-2000) with 180 s counting time at mass 99.

Total chemical recoveries of Tc for extraction techniques M1, M2 and M3 were 49.6 - 98.5%, 39.7 - 76.4% and 7.6 - 16.9%, respectively. The low recoveries obtained using the combustion apparatus (M3 extraction method) appeared to show that Tc is not very efficiently volatilized from Marshall Islands soils due to the high carbonate contents.

The concentrations of ^{99}Tc in the seven soil samples collected from the Marshall Islands are listed in Table 8 as determined by M1 and M2. These measurements represent the first analyses of ^{99}Tc in environmental samples collected from former U.S. test sites in the Marshall Islands. The concentrations of ^{99}Tc ranged from 0.1 to 1.1 mBq g^{-1} dry weight. In order to provide a preliminary assessment of the levels and spatial variability of ^{99}Tc in soils we also measured ^{137}Cs activity concentrations by gamma-spectrometry. Cesium-137 was used as a comparative indicator of the source term of ^{99}Tc, because the fission yields from ^{235}U and ^{239}Pu are about the same (ca. 6%) for the two isotopes, and the behavior and distribution of ^{137}Cs in the environment is reasonably well understood. It is interesting to note that the ^{99}Tc concentrations in the three soil samples taken from Bikini Island (94BB, 95BB_1 and 95BB_2) were all very similar, within the range of the uncertainties of the measurements (i.e., 0.73 - 1.11 mBq g^{-1}). These three ^{99}Tc values were consistent with similar levels of ^{137}Cs observed in the same samples. Using a reference date of 1954 the ^{99}Tc /^{137}Cs activity ratios in Bikini surface soils ranged from 0.7 - 1.1 x 10^{-4} or around 50 - 70% of the theoretical fission yield production ratio of 1.4 x 10^{-4}.

Publication

Tagami, K., Uchida, S., Hamilton, T. and Robison, W.: *Appl. Radiat. Isot.* **53**, 75-79, 2000.

Table 8. ^{99}Tc and ^{137}Cs activity concentrations and activity ratios of ^{99}Tc/^{137}Cs in Marshall Islands soil samples.

Sample code	Location	n	^{99}Tc (mBq g^{-1})	^{137}Cs (mBq g^{-1})	Activity Ratio (^{99}Tc/^{137}Cs)
92RR	Rongelap Island (*Rongelap Atoll*)	3	0.29 ± 0.10	2159 ± 11	(1.3 ± 0.5) x 10−4
94EP	Lujor Island (*Enewetak Atoll*)	3	0.46 ± 0.08	464 ± 4	(9.9 ± 1.7) x 10−4
95EY	Runit Island (*Enewetak Atoll*)	6	0.10 ± 0.02	112 ± 2	(8.7 ± 2.2) x 10−4
96EO	Aej Island (*Enewetak Atoll*)	3	0.60 ± 0.15	1059 ± 7	(5.6 ± 1.4) x 10−4
94BB	Bikini Island (*Bikini Atoll*)	7	0.93 ± 0.14	10094 ± 20	(9.3 ± 1.4) x 10−5
95BB_1	Bikini Island (*Bikini Atoll*)	7	0.73 ± 0.14	10058 ± 20	(7.3 ± 1.4) x 10−5
95BB_2	Bikini Island (*Bikini Atoll*)	3	1.11 ± 0.23	10128 ± 21	(1.1 ± 0.2) x 10−4

(Note) ±: 1 sigma statistical error for ^{99}Tc and activity ratio and counting error for ^{137}Cs.
Reference date for ^{137}Cs activities is 1 March 1954.

55. Radon and Its Progeny in Office Buildings

Shinji Tokonami, Masahide Furukawa and Yuji Yamada

Keywords*: *radon, office buildings, dose assessment

It is well known that the inhalation of radon progeny gives large radiation dose to general public. Indoor radon surveys have been carried out in many countries. For more accurate dose assessment, it is important to understand the level and behavior after taking human activities into account. In order to investigate the behavior of radon and its progeny in occupational environments, measurements were made in actual office buildings. Long-term measurements with passive radon detectors have been conducted over five years at five sites. Continuous measurements were also done at two sites every season. The measurements were made for a week. From results of the continuous measurements, it can be recognized that their concentrations varied with time drastically based on the working hours.

Radon concentrations have been measured with passive radon detectors in several typical office buildings over five years in Tokyo. Since long-term measurement with passive radon detectors is often used for radon surveys in dwellings, the same procedure was also adopted in this survey. A passive radon detector using an electrostatic collection method was placed at each site. The prototype of the passive detector was developed by T. Iida *et al*., and the device manufactured by Aloka Co., Ltd was used here. The air exchange rate of the device was set to 0.67 h^{-1} so as to minimize the entry of thoron (^{220}Rn) into the device. After radon gas goes inside of the device through a membrane filter, ^{218}Po atoms are formed. Since most of them are positively charged, they can be collected on a negative electrode using an electric field. The collection efficiency of ^{218}Po atoms depends on humidity in the device. A desiccant of P_2O_5 is placed in the device so as to maintain high sensitivity. A solid-state nuclear track detector is placed on the electrode to detect alpha particles emitted from radon progeny. Although cellulose nitrate (CN) films (LR115, Type 2) used to be mounted as the detecting material, the quality of the CN film was not stable and large uncertainty in the experimental results was found in our preliminary tests. Therefore, The CN films were replaced with CR-39 detectors (commercial name: BARYOTRAK) because the CR-39 detectors have a very low background and high reproducibility. The detectable range of alpha particles is wide, both alpha particles of 6.0 MeV for ^{218}Po and those of 7.7 MeV for ^{214}Po can be detected. The CR-39 detector and desiccant in each device were replaced every two months. After two months exposure, the CR-39 is chemically etched for 24 h in a 6N NaOH solution at 60Åé. The number of alpha tracks is counted using an optical microscope with 100 magnification.

For continuous measurement, two instruments were used. One is commercially called ALPHAGUARD. It can measure radon concentration continuously together with three meteorological parameters, temperature, relative humidity and air pressure. The other is used to measure the equilibrium equivalent radon concentration (EERC) using the Pylon AB-5 and

AEP-47 as the sampling head. The conversion factor is experimentally determined at an adequate flow rate (1 L/min here). It can provide the EERC continuously every 60 min. The continuous measurements were carried out at two sites for a week every season.

Table 9 shows the average radon concentration at each site based on the long-term measurement with the passive radon detector. The concentrations seemed to be consistently constant at each site. Although seasonal variations of the concentration were analyzed, no significant difference was found. However, the radon concentrations were somewhat higher than expected after taking the result of the latest indoor radon survey (15.5 Bq/m^3 as the annual mean) into account. Actually, the radon concentration should be determined with the human activities for more accurate dose assessment. In these office buildings, air conditioning was automatically supplied during the working hours (normally 9 a.m. to 5 p.m., Monday to Friday). When taking the airtight construction of these buildings into account, the radon concentration might be considerably enhanced when the air conditioning was off. While the air conditioning was on, on the other hand, ventilation would reduce the indoor radon level. In order to verify these hypotheses, radon and its progeny concentrations were continuously measured for a week at two office buildings together with the long-term measurement. Figure 19 shows the time variation of the concentration for a week in winter on the 6^{th} floor at site A. The building had 8 floors above ground. While people were working, the concentrations were low. After work, the concentrations rose steadily because the air conditioning was stopped.

Once the air conditioning began to work in the morning, the concentration level went down again. This pattern seemed to reflect activities in a week, and the same pattern was also found in summer. From this measurement, average radon concentrations throughout the day and during working hours were estimated to be 59.6 Bq/m^3 and 30.7 Bq/m^3, respectively; 44.5 Bq/m^3 was the average EERC throughout the day and 16.2 Bq/m^3 was that during working hours. The equilibrium factors were estimated to be 0.75 (throughout the day) and 0.60 (during working hours). There were large differences in their concentrations between the two when taking the ratios. On the other hand, there was a minor difference in the equilibrium factor. Other continuous measurements were made on the 10^{th} floor at site B in summer. The building had 44 floors above ground and accommodated a lot of office workers. The continuous measurement gave 32.9 Bq/m^3 as the average radon concentration throughout the day and

10.4 Bq/m^3 as that during working hours; 15.6 Bq/m^3 was the average equilibrium equivalent radon concentration (EERC) and 4.4 Bq/m^3 was that during working hours. Evaluating the results as the equilibrium factor (F), they were 0.47 (throughout the day) and 0.42 (during working hours). These equilibrium factors seemed to be typical for an indoor environment. In terms of the differences between the two, the same conclusion could be drawn as that in the measurements at site A. Table 10 summarizes the physical parameters related to dose assessment at the two sites.

It is obvious that the radiation doses in occupational environments might be overestimated if the radon concentrations are obtained with ordinary passive radon detectors in long-term surveys. More data

should be accumulated so as to evaluate the concentration using suitable modeling of the behavior of radon and its progeny in an occupational environment.

It is obvious that the radiation doses in occupational environments might be overestimated if the radon concentrations are obtained with ordinary passive radon detectors in long-term surveys. More data should be accumulated so as to evaluate the concentration using suitable modeling of the behavior of radon and its progeny in an occupational environment.

Publication

Tokonami, S., *et al*.: *Healthy Buildings 2000*, 3, 81-84, 2000.

Table 9. Annual average radon concentrations obtained with the passive radon detectors.

Year	1995	1996	1997	1998	Remarks
Site A	59.2	60.7	69.8	59.0	6^{th} floor
Site B	22.6	25.7	29.6	30.4	10^{th} floor
Site C	28.4	31.8	35.0	31.9	1^{st} floor
Site D	19.9	19.3	23.5	18.8	2^{nd} floor
Site E	37.3	44.1	50.1	37.3	10^{th} floor

unit: Bq/m^3

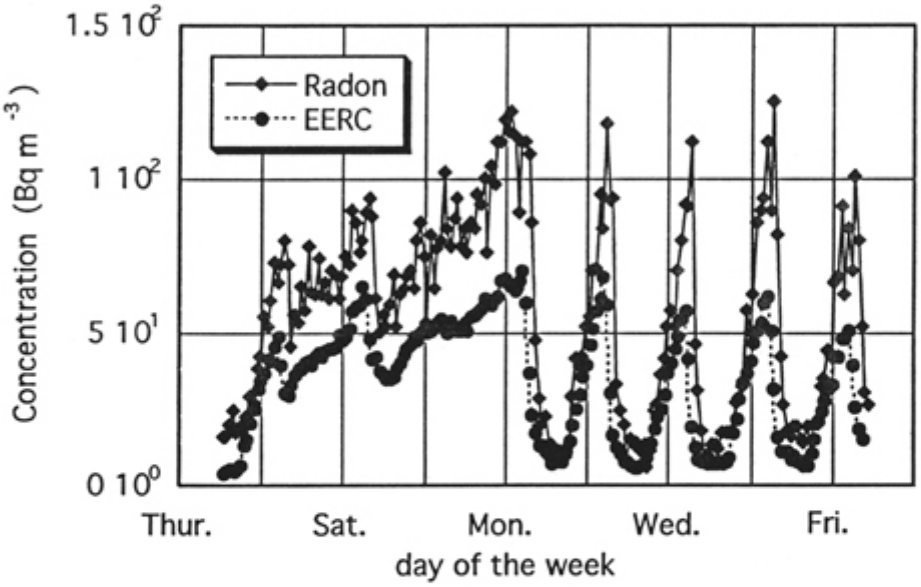

Fig. 19. An example of the time variation of radon and its progeny concentrations in a week (Nov., 1998).

Table 10. Physical parameters related to dose assessment at two sites.

	Rn conc. throughout the day	Rn conc. during working hours	EERC throughout the day	EERC during working hours	F throughout the day	F during working hours
Site A	59.6	30.7	44.5	16.2	0.75	0.60
Site B	32.9	10.4	15.6	4.4	0.47	0.42

unit: Bq/m^3

56. Dose Evaluation and Effective Dose Estimation for Multi-Detector CT

Kanae Nishizawa, Masaki Matsumoto, Kazuo Iwai[1], Ayako Tonari [2], Takashi Yoshida[2], Makoto Takayama[2] ([1] Nihon Univ., [2] Kyorin Univ.)

Keywords*: *Patient dose, multi-detector CT, effective dose, medical exposure

Computed tomography (CT) has devolved remarkably though device improvement and advancement of peripherals, including the computer. In 1999, multi detector-row CT (MDCT) appeared and made high-speed scanning possible. However, utility of clinical MDCT applications has not been gauged. Since CT examinations need a comparatively high dose, it is necessary to evaluate patient exposure prior to the introduction of the MDCT.

The CT scanners used for the measurements were Somatom Plus 4 (Siemens Medical System, Germany), Aquilion/M (Toshiba Medical, Japan) and QX/i (GE, USA). The dose measurements were carried out under routine operating conditions. An anthropomorphic phantom (Rando; Alderson Research Lab. USA, 163cm stature and 53kg weight) was used as the model for a Japanese adult. Two types of glass encapsulated thermo luminescence radiation dosimeters (TLDs) were used for the measurements of the organ or tissue doses in/on the phantom. They were UD-170A (BeO) and UD-110S ($CaSO_4$: Tm) (Panasonic, Japan). The UD-170A type TLDs were calibrated within the direct beam field while the UD-110S tips were calibrated outside the field with the tissue equivalent phantom. The exposure at each position in the phantom where the TLD was placed was determined with an ionization chamber traceable to the Japanese National Standard of the Electrotechnical Laboratory in Tsukuba, Japan. Dose measurements were performed in the organs or tissues in a phantom to which tissue weighting factors (W_T) were assigned by the 1990 Recommendation of the International Commission on Radiological Protection for whole pulmonary (about 37cm axial scan) as the chest scan and the abdomen-pelvis scan (about 38cm axial scan) with normal conditions, as used in hospitals for routine examinations.

The effective doses were in the range of 9.4-28mSv for the chest examination and 13-34 mSv for the abdomen-pelvis (Table11). The average surface doses varied from 14 to 25mGy for the chest examination and 20-37mGy for the abdomen-pelvis. In the chest examination, the organ or tissue doses and the effective dose showed large differences depending on CT equipment. Plausible reasons were significant differences in table speed and beam width and existence of beam overlapping. In the abdomen-pelvis examination, overlapping of beams was also found in the one apparatus.

The advantages of MDCT in clinical uses are that multiple slice data can be obtained by one scanning with multiple detectors and a thin slice image can be taken rapidly during one breath stop. As for CT, it has been conventionally thought that higher radiation exposure is delivered to the patient, compared with other X-ray diagnosis techniques.

Since MDCT uses multi-detector rows at the same time, it was expected that exposure dose could be smaller in contrast to the conventional system and the reconstruction of the scan could be done with a low radiation dosage with keeping the same image quality of the conventional CT. However, the exposed doses differed very much according to scanning method and technical conditions and it seems that dose

reduction by MDCT has not been realized yet.

Table 11. Effective dose and surface dose with multi-detector CT systems.

	Scan position		CT systems A	B	C	Average
Effective dose (mSv)	Chest	Male	12.52	9.41	27.9	16.61
		Female	12.53	9.43	27.9	16.62
	Abdomen-Pelvis	Male	23.4	13.15	15.26	17.27
		Female	27.7	15.96	16.89	20.2
Surface dose (mGy)	Chest		17.67	15.50	42.7	25.3
	Abdomen		-	23.6	23.9	23.8
	Pelvis		36.6	20.8	23.9	27.1

57. Elution Behavior of Tc and Re through a Tc-selective Chromatographic Resin Column

Shigeo Uchida and Keiko Tagami

***Keywords*:** *technetium, rhenium, yield tracer, ICP-MS, elution behavior*

Technetium-99 has been determined in environmental samples to understand the behavior of Tc in the environment. To measure ^{99}Tc in environmental samples, a chemical separation and purification of the nuclide from interfering elements is required, because the concentration in the environment is very low. There are several yield tracers for ^{99}Tc measurement, such as ^{95m}Tc, ^{99m}Tc, ^{97}Tc and Re. From a practical point of view, Re is a convenient yield monitor because it is cheap and has no interference on ^{99}Tc counting by ICP-MS. In this study, we performed tracer experiments to compare the elution behavior of Tc and Re through a Tc- selective chromatographic resin (TEVA resin) column under various conditions. Two hundred and fifty mL of pure water or tap water were adjusted to 0.1 M HNO_3 with conc. HNO_3. The solution spiked with ^{99}Tc and Re was passed through the column. Next, the column was washed with 40 mL of 1, 2, 4 or 8M HNO_3. Finally, Tc and Re retained in the column were stripped with 10 mL (5 mL x 2) of 12M HNO_3. The loading solutions and the nitric acid solutions were allowed to drain completely and the eluate was collected into polyethylene vials for the measurement of ^{99}Tc and Re by ICP-MS.

The elution behaviors of Tc and Re are listed in Table 12. The recovery was defined as the ratio of the amount of the nuclide in each fraction to that in the sample solution. There was no difference in each nuclide's behavior between pure water and tap water. When the solution was introduced into the column, Re was extracted onto the resin together with Tc. Then the column was washed with 8 mL of 1, 2, 4 or 8M HNO_3 for 5 times (total 40 mL). When 1M HNO_3 was used, Re remained on the resin as well as Tc did. With 2M HNO_3, Re was gradually removed and it was found in the third 8 mL wash fraction but Tc was not found in the eluates. When solutions of higher nitric acid concentrations than 4M HNO_3 were used, Re was removed from the resin easily and was found in the first 8 mL.

Since the distribution coefficient of Re between the resin and nitric acid solution was almost half the value of that of Tc over a wide range of nitric acid concentrations from 0.1M to 8M HNO_3, Re could be removed with less than 40 mL of 2M HNO_3. Thus, when the TEVA resin is applied for Re separation, less than 1M HNO_3 should be used for washing the column to avoid Re losses. For stripping, as seen in Table 12, with 8 mL of 8M HNO_3 both Tc and Re can be completely removed from the resin.

From the results, it was concluded that the TEVA resin showed high selectivity for Re, similar to that for Tc. When concentrations of nitric acid solutions of 1M and 8M were used for washing and stripping, respectively, the elution behaviors of Tc and Re were the same. This indicated that Re could be used as a yield tracer for Tc in environmental water samples.

Table 12. Recoveries of ^{99}Tc and Re in wash and strip solutions when nitric acid concentrations for wash were 1, 2, 4 and 8M. The sample solutions were pure water and tap water.

Pure water	Volume (mL)	Tc-99				Re-185			
		1M	2M	4M	8M	1M	2M	4M	8M
Load*	250	0.00	0.00	0.00	0.00	0.00	0.00	0.00	0.00
Wash-1	8	0.01	0.01	0.01	0.98	0.00	0.00	1.00	0.98
Wash-2	8	0.00	0.00	1.00	0.00	0.00	0.00	0.00	0.00
Wash-3	8	0.00	0.00	0.00	–	0.00	0.10	0.00	–
Wash-4	8	0.01	0.00	0.00	–	0.00	0.50	0.00	–
Wash-5	8	0.00	0.01	–	–	0.00	0.39	–	–
Strip-1**	5	1.00	1.04	0.01	0.01	0.98	0.04	0.00	0.00
Strip-2**	5	0.02	–	–	–	0.00	–	–	–
Tap water	Volume (mL)	Tc-99				Re-185			
		1M	2M	4M	8M	1M	2M	4M	8M
Load*	250	0.00	0.00	0.00	0.00	0.00	0.00	0.00	0.00
Wash-1	8	0.00	0.00	0.03	0.98	0.00	0.00	1.00	1.00
Wash-2	8	0.00	0.00	0.95	0.00	0.00	0.00	0.00	0.00
Wash-3	8	0.00	0.00	0.00	–	0.00	0.10	0.00	–
Wash-4	8	0.00	0.00	–	–	0.00	0.45	–	–
Wash-5	8	0.00	0.00	–	–	0.00	0.39	–	–
Strip-1**	5	0.95	1.03	0.01	0.01	1.05	0.06	0.00	0.00
Strip-2**	5	0.01	0.01	0.01	0.01	0.00	0.00	0.00	0.00

(Notes) *: The acidity of the loading solution was 0.1M HNO_3. **: The 12M HNO_3 was used as strip solution.

–: Not measured.

58. Fate of Two Important Radionuclides in the Coastal Seas of Japan and Resultant Dose from Intake through Fishery Products

Teruhisa Watabe, Mitsue Matsuba and Setsuko Yokosuka

***Keywords*:** *^{137}Cs, ^{90}Sr, radioactivity survey data, mathematical model, coastal sea, residence time, depth of mixing, effective dose commitment, collective effective dose commitment, fishery products*

The fate of two important radionuclides, ^{137}Cs and ^{90}Sr, in the sea was investigated by analyzing radioactivity survey data, which had been collected since the 1960's. A simplified mathematical model was introduced to determine the relationship between the flux of the fallout radionuclides at the surface of the sea and their concentrations in seawater, and the parameter values determining the fate of radionuclides, namely the residence time and the depth of mixing of the radionuclides in the sea, were derived for three regions of the coastal sea of Japan by a regression analysis as reported previously in NIRS Annual Reports. The residence time ranged from 5.3 y to 6.8 y and from 2.8 y to 5.7 y among the three regions in terms of effective half-life respectively for ^{137}Cs and ^{90}Sr, whereas the respective depth of mixing ranged from 46.6 m to 85.3 m and from 24.1 m to 44.1 m. It is likely that the effective half-lives observed in the present study were comparable to that of tritium observed in the early 1970's. This might reveal that both the radionuclides substantially dispersed in a manner comparable to the general water mass flow. The mathematical formulation of the fate of the radionuclides allows estimation of their time-integrated concentrations in seawater to infinity, which is basic information for assessments of dose to members of the public due to the consumption of fishery products. When a hypothetical release of ^{137}Cs and ^{90}Sr into the sea by unit deposition density (1MBq/km^2) happens, resulting effective dose commitment of a member of the critical group would correspond to 2.6 X 10^{-3} Sv to 4.1 X 10^{-3} Sv and 2.4 X 10^{-4} Sv to 6.3 X 10^{-4} Sv for ^{137}Cs and ^{90}Sr, respectively. The corresponding collective effective dose commitment could be determined, on the other hand, to be 8.9 X 10^{-4} to 4.5 X 10^{-3} manSv and 5.8 X 10^{-5} to 1.5 X 10^{-4} manSv, with total catch quantity for each region being taken into account. A release of ^{137}Cs into the sea would result in an internal exposure of the population approximately one order of magnitude higher than that of ^{90}Sr, although the time-integrated concentrations were not so greatly different between two radionuclides. This difference could be attributed entirely to the parameter values of the concentration factor of the radionuclides in marine organisms adopted. The consumption of fish obviously played an important role in the delivery of ^{137}Cs from seawater to the human body, whereas more than 80 % of the total was delivered for ^{90}Sr by consumption of sea weeds, which accounted for just approximately 6 % of the total consumption of fishery products on a weight basis. The results obtained in the present study will provide probable dose perspectives for an assessment of radiological impacts of the release of the radionuclides in liquid effluents from nuclear facilities.

Publication:

Watabe, T., Matsuba, M and Yokosuka, S.: *Proc. 10th Int. Cong. of Int. Radiat. Prot. Assoc*., P-4-244, 2000.

59. Cellular Response in Normal Human Cells Exposed to Chronically Low-dose Radiation in Heavy Ion Radiation Field

Masao Suzuki, Yukio Uchihori, Ryonfa Lee[1], Chisa Ohira[1], Chizuru Yamaguchi, Kumie Nojima, Hideyuki Majima, Hisashi Kitamura, Tatsumi Koi, Masashi Takada, Nakahiro Yasuda, Yoko Yamaguchi[2], Hiroshi Yamaguchi and Kazunobu Fujitaka ([1] Frontier Research Center; [2] School of Dentisty, Nihon University)

Keywords**:** *cellular response, low-dose radiation, heavy ion radiation field*

We have been studying cellular responses in normal human fibroblasts exposed to chronically low- dose radiation in a heavy ion radiation field. Cells were cultured in a CO_2 incubator, which was set in the irradiation room of heavy ions in the HIMAC. The life-span of the exposed cells was reduced to 70-94% of non-exposed control cells. This life-span reduction is opposite to that by gamma rays reported previously. Furthermore, the shortening speed of telomere length in exposed cells was much higher than that in non-exposed cells at the 26^{th} passage (at 155 days after stating experiment). There is evidence that chronic exposure to low-dose radiation in a heavy ion radiation field promotes life-span reduction in either cellular or molecular levels. On the contrary, there was no observation that radiosensitivity of the cells with low-dose accumulation changed for acute irradiation of X-rays during exposures up to 182 days after starting the experiment. These findings indicate that different biological responses occur in different biological endpoints due to the chronic low-dose irradiation in the heavy ion radiation field. We have now begun to examine genomic instability in both mutation induction and choromosome aberration.

60. Radiobiological Effectiveness of Different HZE Beams on Cells

Yoshiya Furusawa, Mizuho Aoki, Hideki Matsumoto[1], Akihisa Takahashi[2], Tetsuya Kawata[3], Kerry George[3] and Marco Durante[4] ([1]Fukui Med Univ, [2]Nara Med Univ, [3]Johnson Space Center, [4]Univ Fedellico II.)

***Keywords*:** *HZE beam, LET, RBE, cell killing, chromosome aberration*

A method to estimate cell killing induced by accelerated heavy ions as a function of ion species and LETs was considered from LET-RBE spectra for V79 cells. The cells were exposed to ^{3}He-, ^{12}C-, ^{20}Ne-, ^{28}Si-, ^{40}Ar- and ^{56}Fe-ion beams at HIMAC and the Medical Cyclotron at NIRS, RRC at RIKEN, and AGS at BNL with an LET ranging over approximately 10-4000 keV/ μm under aerobic conditions. Cell-survival curves were fitted by equations from the linear-quadratic model to obtain survival parameters, and the RBE values were analyzed as a function of LET. The RBE increased with LET, reaching a maximum at around 200 keV/ μm, then decreased with a further increase in LET. Clear splits of the LET-RBE spectrum were found among ion species. The LET- RBE spectra were fitted by a newly contrived equation that included three parameters. The parameters indicate the LET that gives the maximum RBE, a related value for the maximum RBE, and the width of the RBE peak. The parameters can also be defined as functions of atomic mass numbers of the accelerated ions. At a given LET, the RBE value for lighter ions was higher than that for heavier ions at lower LET. The position of the maximum RBE shifted to higher LET values for heavier ions, and the width of the peak of RBE increased with the atomic mass number of the irradiated ions.

High-LET radiation-induced aberrations in prematurely condensed G_2 chromosomes of human fibroblasts were studied. To determine the number of initial chromatid breaks induced by low- or high-LET irradiations, and to compare the kinetics of chromatid break rejoining for radiations of different quality, exponentially growing human fibroblast cells AG1522 were irradiated with gamma-rays, and carbon-, silicon- and iron-ions. Chromosomes were prematurely condensed using calyculin A. Chromatid breaks and exchanges in G_2 cells were scored. PCC were collected after several post-irradiation incubation times, ranging from 5 to 600 min. The kinetics of the chromatid break rejoining following low- or high-LET irradiation consisted of two exponential components representing a rapid and a slow time constant. Chromatid breaks decreased rapidly during the first 10min after exposure, then continued to decrease at a slower rate. The rejoining kinetics were similar for exposure to each type of radiation. Chromatid exchanges were also formed quickly. Compared to low-LET radiation, isochromatid breaks were produced more frequently and the proportion of unrejoined breaks was higher for high-LET radiation.

Compared with gamma-rays, isochromatid breaks were observed more frequently in high-LET irradiated samples, suggesting that an increase in isochromatid breaks is a signature of high- LET radiation exposure.

The new method for chemical-induced premature chromosome condensation combined with fluorescence *in situ* hybridization (FISH) was used to analyze chromosomal damage in peripheral blood mononuclear lymphocytes of patients undergoing radiation treatment for esophageal cancer with high-energy X-rays or accelerated carbon ions at NIRS. The total number of aberrant cells correlated with radiation field size, but no correlation was found for acute toxicity. A high frequency of complex-type exchanges was also recorded. This aberration type presented a high individual variability, and correlated well with the acute morbidity.

Cytogenetic analysis by interphase chromosome painting is proposed as a useful tool for monitoring normal tissue effects during radiotherapy.

Publications:

1) Furusawa, Y., et al.: Radiat Res 154: 485-96, 2000.
2) Furusawa, Y.: In; Exploring Future Research Strate- gies in Space Radiation Sciences. Iryoukagakusha, pp.104-109, Tokyo. 2000.
3) Aoki, M. et al.: J. Radiat. Res. 41: 163-75, 2000.
4) Durante, M., et al.: Int. J. Radiat. Oncol. Biol. Phys. 47: 793-8, 2000.
5) Kawata, T., et al.: Int. J. Radiat. Biol. 76: 929-37, 2000.
6) Matsumoto, H., et al.: Int. J. Radiat. Biol. 76: 1649-57 2000.
7) Takahashi, A., et al.: Int. J. Radiat. Oncol. Biol. Phys. 47: 489-94, 2000.
8) Takahashi, A., et al.: Int. J. Radiat. Biol.76: 335-41, 2000.
9) Yamada, S., et al.: Cancer Lett. 150: 215-21, 2000.
10) George, K., et al.: Int. J. Radiat. Biol. 77: 175-83, 2001.
11) Kawata, T., et al.: Int. J. Radiat. Biol. 77: 165-74, 2001.
12) Shigematsu, N., et al.: Int. J. Mol. Med. 7: 509-513, 2001.

61. Development of Radiation Monitors and Detectors for Cosmic Rays or These Secondary Particles in Space Environment and High Altitude

Yukio Uchihori, Hisashi Kitamura, Toshisuke Kashiwagi[*] and Kazunobu Fujitaka ([*] Kanagawa University)

***Keywords*:** *space radiation monitor, detector, cosmic rays, high altitude*

A mobile radiation monitor with a silicon detector which was developed in a collaboration between Bulgaria Solar-Terrestrial Influences Laboratory and NIRS was calibrated with protons, light ions and heavy ion beams in the cyclotron and HIMAC facilities. The response function of the monitor was gotten with these calibrations. This mobile monitor was used to measure the radiation environment in airplanes at high altitude.

Artificial diamond detectors were developed in a collaboration between Kanagawa University and NIRS. The diamond detector attracts notice because of its equivalency with human tissue. Its energy resolution corresponded to that of silicon detectors.

Publication:

Dachev, Ts., Tomov, B., Matviichuk, Yu., Dimitrov, Pl., Lemaire, J., Gregoire, Gh., Cyamukungu, M., Schmitz, H., Fujitaka, K., Uchihori, Y., Kitamura, H., Reitz, G., Beaujean, R., Petrov, V., Shurshakov, V., Benghin, V.: *Adv. Space Res.*, in press.

62. Effective Dose Equivalent on the Ninth Shuttle-Mir mission (STS-91)

Hiroshi Yasuda, Tatsuto Komiyama* and Kazunobu Fujitaka (* National Space Development Agency of Japan)

***Keywords*:** *space radiation, effective dose equivalent, Shuttle-Mir mission, organ and tissue doses, low Earth orbit*

Organ and tissue doses and effective dose equivalent were measured using a life-size human phantom in the 9^{th} Shuttle-Mir Mission (STS-91), a 9.8-day spaceflight at a low Earth orbit (about 400 km in altitude and 51.65^{o}C in inclination). The doses were measured at 59 positions by a combination of thermoluminescent dosemeters of Mg_2SiO_4:Tb (TDMS) and plastic nuclear track detectors (PNTD). In correction of efficiency change of TDMS, it was assumed that reduction of efficiency is predominantly attributed to HZE particles with energy greater than 100 MeV amu^{-1}. A conservative calibration curve was chosen for LET determination from PNTD track-formation sensitivities. The organ and tissue absorbed doses during the mission ranged from 1.7 to 2.7 mGy, varying by a factor of 1.6. The dose equivalent ranged from 3.4 to 5.2 mSv with a variation factor of 1.5 on the basis of the Q-LET relationship in the 1990 recommendation of the ICRP. The effective quality factor (Q_e) varied from 1.7 to 2.4. The dose equivalents at several radiation-sensitive organs, such as the stomach, lung, gonad and breast, were not significantly different from the skin dose equivalent (H_{skin}). The effective dose equivalent was evaluated as 4.1 mSv; this value was about 90 % of the H_{skin}.

Publications:

1) Yasuda, H., Badhwar, G.D., Komiyama, T. and Fujitaka, K.: *Radiat. Res.* 154, 705-713, 2000.
2) Yasuda, H. and Fujitaka, K.: *Radiat. Prot. Dosim*. 87, 115-120,2000.
3) Yasuda, H. and Fujitaka, K.: *Radiat. Meas.* 32, 355-360, 2000.

63. Molecular Dynamics Simulation of a DNA Containing a Single Strand Break

Hiroshi Yamaguchi, Joerg-Gerald Siebers[1], Akira Furukawa, Nobumasa Otagiri[2] and Roman Osman[3] ([1] RIKEN; [2] Univ. of Tokyo; [3] Mount Sinai School of Medicine)

***Keywords*:** *DNA damage, single strand break (ssb, SSB), molecular dynamics, computer simulation, essential dynamics*

Molecular dynamics (MD) simulations were performed for a dodecamer DNA containing a single strand break (SSB), which the authors assumed to be the simplest type of SSB: it had two ends, 3'-OH deoxyribose and 5'-OH phosphate. Molecular force field parameters of the 5'-OH phosphate region were newly evaluated using the *ab initio* program package *GAMESS* at the HF/6-31G level, while the force field of the 3'-OH end of deoxyribose has been well defined within the database.

To study possible sequence dependence of SSB, four dodecamers of the same sequence containing a SSB in a different position, (1) G8-C9, (2) G16-C17, (3) A18-A19 and (4) T6-T7, were considered. TIP3 water and counter ions (Na^+) in a box were added and minimization and heating up to 300 K and production run up to a time of 1ns were carried out by *AMBER 4.1*.

Root Mean Square Distances (RMSDs, not shown here) showed that all cases were stabilized after 200 ps. This work is the first successful MD calculation for DNA containing a SSB. As seen in snapshots of conformations of DNA at the time of 1 ns (Fig.20), conformational changes were surprisingly small.

A detailed analysis, by the program *Dials and Windows,* of the equilibrated average structure supported this findings. Among inter-base pair parameters, *Rise*, *Twist* may adjust local conformation at the site of a SSB such that the SSB does not drive the DNA structure into overall corruption. This finding may be supported by the calculations of stacking force between base pairs by Sarai *et al*.. Their calculations suggested that only the stacking force between base pairs could form the double helix DNA structure, that is, no so much change would be expected for the present type of SSB.

However, dynamical properties calculated using the essential dynamics, where the program *WHATIF* was applied, showed some noticeable difference between DNA containing a SSB and normal DNA, and among DNAs that had a SSB in a different position. This difference may be a signal for recognition of this type of break by a repair enzyme. Study along this working hypothesis is in progress by the authors.

As mentioned in various reports, SSB produced by ionizing radiations may well be far more complex than presently thought, and non-specific in position as well as in chemical forms. However, if molecular structure of the SSB can be specified, the authors believe that this approach may work for radiation induced SSB and disclose molecular behavior of the SSB, and hence provide useful insight about possible mechanisms of the repair process by repair enzymes.

Publication:

Yamaguchi, H. *et al*.: *Radiat. Prot. Dosim*. in press.

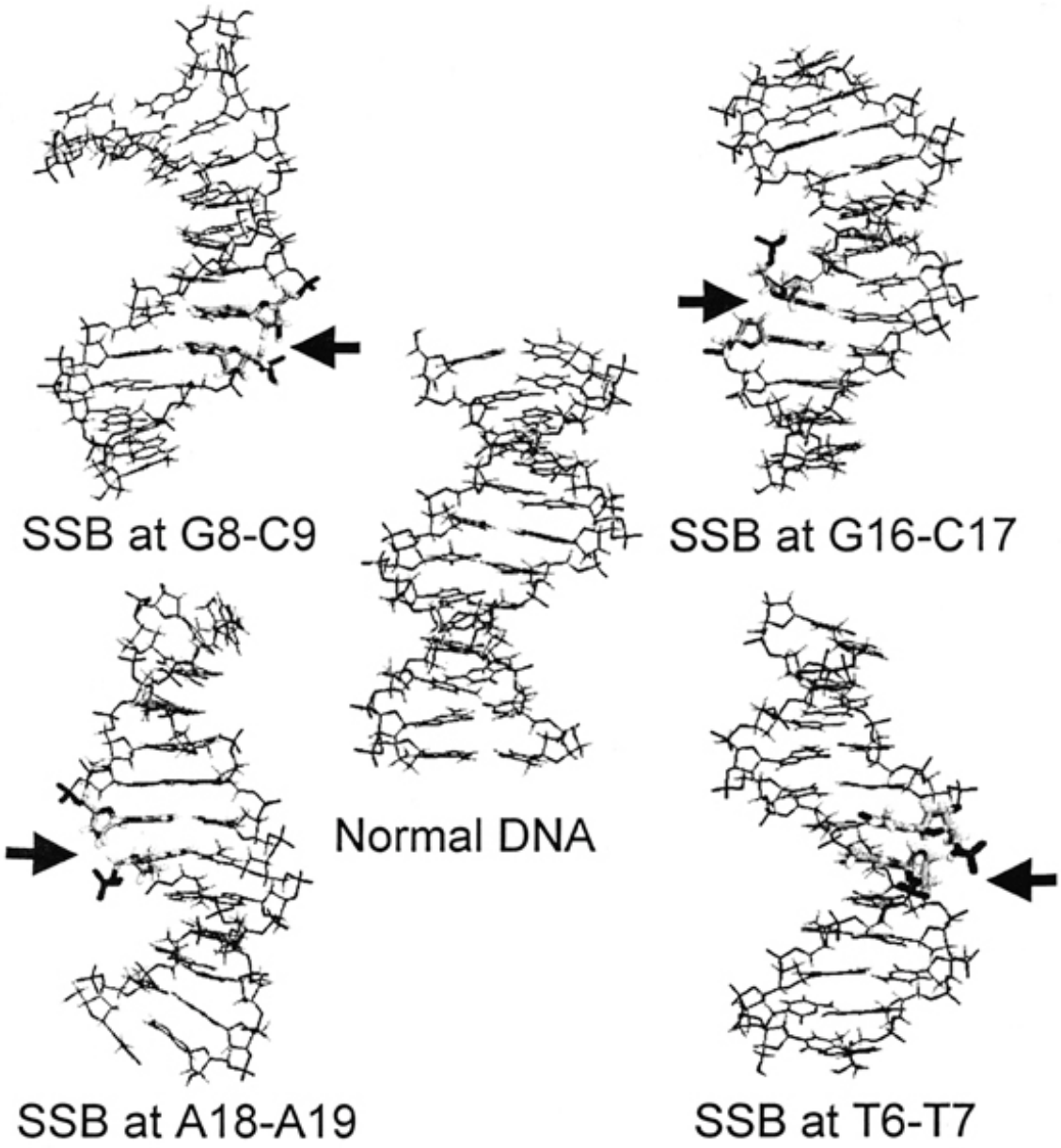

Fig.20. Snapshots of normal and SSB-containing DNA structures taken at simulation time lns. The positions of SSB sites are indicated by arrows.

Preface

It is my great pleasure to publish the Annual Report, NIRS 2000. This report contains all of the accomplishments of NIRS, which includes rsearch and investigations, medical practice, training and technology assistance that NIRS performed during fiscal year 2000 (from April 2000 to March 2001).
This is NIRS's last year as a national research institute under the direct auspices of the Science and Technology Agency of Japan as well as the end of the 20th century. As a part of the national administrative reform, the Sciene and Technology Agency merged with the Ministry of Educaion, Culture and Sport to form the Ministry of Education, Culture, Sports, Scinece and Technology(MEXT) as of January 6, 2001. Then, as of April 1, 2001, NIRS was reborn as an independent corporative body, "dokuritsu gyousei houjin" in Japaese. The name of the Institute remains the same in both Japanese and English. In praparing for the reform, tremendous efforts were made by all staff members of NIRS, spending much time. It is my pleasure to report that 266 original articles were published in scientific journals and 569 oral presentations were made during this busy year. Details of those research acitvities are summarized in this volume for those interested. I would like to mention a few topical issues among them.
Clinical trials of heavy-ion radiotherapy for cancer have been performed for 7 years. In total, 946 cancer patients were registered by March, 2001. Promising results were obtained with good local control and rare side effects. This therapy may prove to be particularly useful for heads and neck cancers, lung caicinomas, bone and soft tissue malignanacies, prostate carcinomas and uterine cervical cancers. Detailed results were reported at the Net Work Panel of Heavy Ion Radiotheraoy held in August, 2000 and March, 2001, which are open to the public. A certain amount of progress was made in the application process as a "highly advanced medical procedure".
Research activities on radiation-sensitive genes and gene-expression profiles were remarkably promoted. Further progress is expected in the year 2001. The installed PIXE machine made it possible to implement irradiation experiments with micron-level radiation beams. The radon research building was completed at the end of the year 2000, which will promote radon research tremendously.
After a criticality accident occurred at the JCO uranium processing plant in Tokai village, NIRS has been involved in various activities related to the accident, including medical treatment, monitoring environments, care of inhabitants who suffered from anxiety, etc. A comprehensive report on the activites and involvement of NIRS has been published.
The annual environment seminar dealt with "Environmental monitoring and radiation- dose estimates of the criticality accident at a uranium processing plant". An international

symposium on medical trearments of 3 heavily exposed workers at the criticality accident was held in December, 2000. An NIRS symposium on the "New Development of Molecular Imaging" was held to commemorte the opening of the diagnostic imaging research building. Those as well as many other meetings served for the close communication of researchers from both inside and outside of NIRS.
As an annual event, many people who had served NIRS for many years as scientists and administrative staff left the institute after having reached the retirement age. I would lilke to express my sincere gratitude with respect for their great efforts and contributions to the progress of science and technology.
I would like to finish this note with heartfelt thanks for the cooperation and advice during fiscal year 2000. I also ask for continuous support of the research activities to be perfoemed in accordance with the mid-term 5-year action plan starting from April, 2001.

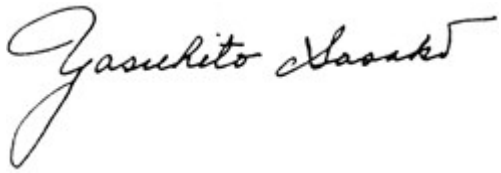

Yasuhito Sasaki, M. D., Ph. D.
President